University of Sarajevo
Faculty of Science and Mathematics
Department of Physics

Diploma thesis:

Neutrino mean free paths in proto-neutron stars

Author:
Haris Đapo

Mentor: Prof.Dr. Jochen Wambach
Co-mentor: Prof.Dr. Kenan Suruliz

January 2004

Acknowledgments

This thesis represents the nine months work, which was done at th NHQ (Nuclei, Hadrons and Quarks) group at TUD (Technische Universität Darmstadt). I would like to thank Prof. Dr. Jochen Wambach for making this thesis possible. His extraordinary experience was crucial in determining the way in which the work should progress. I would also like to thank him for valuable advice on how things should be done.

I would like to thank the DAAD and especially Dr. Suad Jakirlić for giving me the opportunity and the means to start this work in Darmstad.

I would like to thank Prof. Dr. Kenan Suruliz for helping me complete this thesis as well as constructive critic that made this thesis what it is.

I would also like to thank the entire NHQ group at TUD, who welcomed me, helped me with my thesis both in a scientific way as well as with numerical problems that appeared during the work, and especially Prof. Dr. Robert Roth for having the patience with the load of sometimes probably silly questions. Finally, I would like to thank my family for supporting me trough my education and my entire life.

Contents

1 Introduction

The core collapse supernovae are spectacular events, which are being studied, by using numerical simulations, since more than three decades. Despite the huge amount of physics involved in these catastrophic explosions, a sort of "standard model" has been emerging in the last years: the inner Iron core of a massive star overcomes its hydro dynamical stability limit (the Chandrasekhar mass) and collapses, raising its density up to many times the nuclear density; this anomalous density produces an elastic bounce of the core, which results in a shockwave. The wave propagates through the star, loses energy in dissociating nuclei and producing neutrinos and finally stalls at ~ 200 km from the centre of the star (this means that the so-called "prompt" mechanism, in which a star would explode just from this shock wave, unavoidably fails). However, ν_e and $\bar{\nu}_e$ are absorbed on the nucleons liberated by the shock; such processes supply new energy to the wave, which is revived, ~ 500 ms after the bounce (this energy transfer is known as "neutrino heating"). The reinforced shock can propagate within the stellar matter and expel the external layers into the space (this is the so-called "delayed" mechanism). After the explosion the star loses energy, mainly by neutrino emission, and cools down, forming a neutron star or a black hole. However in this picture there still remains many unanswered questions, many of which relate to neutrinos, nuclear matter and the relationship between the two.

The structure of this thesis is as follows. In this chapter we present the surrounding in which, and the some of the conditions under which, subsequent processes will take place. Also we present the large number of experiments capable of shedding some light at this largely unexplored topic. This was in part our motivation to consider this topic since so many experiments could in the near future, with some luck, collect an unprecedented amount of data about supernova.

In the second chapter we introduce and derive most of the quantities relating to the neutrino interaction with the medium. There we will also establish necessary framework for the conditions of equilibrium for the medium in which processes take place.

In the third chapter we introduce the nuclear potential and its effect on the quantities, which are important for our study. There we also consider some of the more direct changes that the strong interaction introduces to the cross section.

In the fourth chapter we introduce an approximation with whose aid we study the effects of the strong interaction on the neutrinos in medium that exists. There we connect the parameters that we calculated in the third chapter with the cross section and mean free path which we calculated in the second chapter to get the final result.

In the fifth chapter we present the result for several cases as well as a comparison between the various approximations used. We also explain to the best of our abilities how the features one can observe in the results relate to the some of the characteristics of the expressions that we had in the previous chapters.

The last chapter presents the summary of the thesis, some comments about shortcomings of our work and an outlook on how to repair them in the future. Also several appendices have been added for the sake of elaborating on some of the derivations that were necessary in the course of the thesis.

1.1 Core collapse supernova

A supernova represents the end stage of evolution of massive stars. Stars evolve peacefully and quasistatically for millions of years, passing trough recognizable stages of development, until they finally run out of nuclear fuel and can no longer support themselves. When this happens, the core of the star collapses under its own weight in less than a second. In the final stages of the collapse, the stars are expected to radiate nearly all of their binding energy in the form of the neutrinos (and antineutrinos) of different flavours.

During nearly all of the lifetime of a star, the heat given off by the sequence of nuclear fusion reactions creates a thermal pressure, which counteracts the gravitational attraction. However once these reactions create an iron core, namely iron isotope ^{56}Fe, further fusion, because of the properties of that isotope (it is the most strongly bound of all nuclei), would instead of releasing energy absorb it. At that point the star has an onion-like structure. In its layers - products of earlier fusions can be found. So one can find, directly above the iron core, a layer of silicon and sulphur, and beyond that there are shells of oxygen, neon, carbon and helium. The outer envelope is mostly hydrogen.

It is only the largest stars that produce fusion elements all the way to the iron. Most stars like the Sun do not produce an iron core. Such small stars that end their fusion somewhere between hydrogen and iron settle into a white dwarf, a burned-out star supported against gravity by the degeneracy pressure of electrons.

These very massive stars, the lower limit is thought to be of order eight solar masses, after developing an iron core, collapse under its own weight.

1.2 Proto-neutron star

A proto-neutron star is formed in the aftermath of the gravitational collapse of the core of a massive star. Its evolution precedes trough several distinct stages, which may have various outcomes, as shown schematically in Fig. 1.1[1]

1. Immediately following core bounce and the passage of a shock through the outer proto-neutron star's mantle, the star contains an unshocked, low entropy core, $(0.5 - 0.7)\ M_{\odot}$, in which neutrinos are trapped. This is surrounded by a low density, high entropy mantle that is both accreting matter falling through the shock and rapidly losing

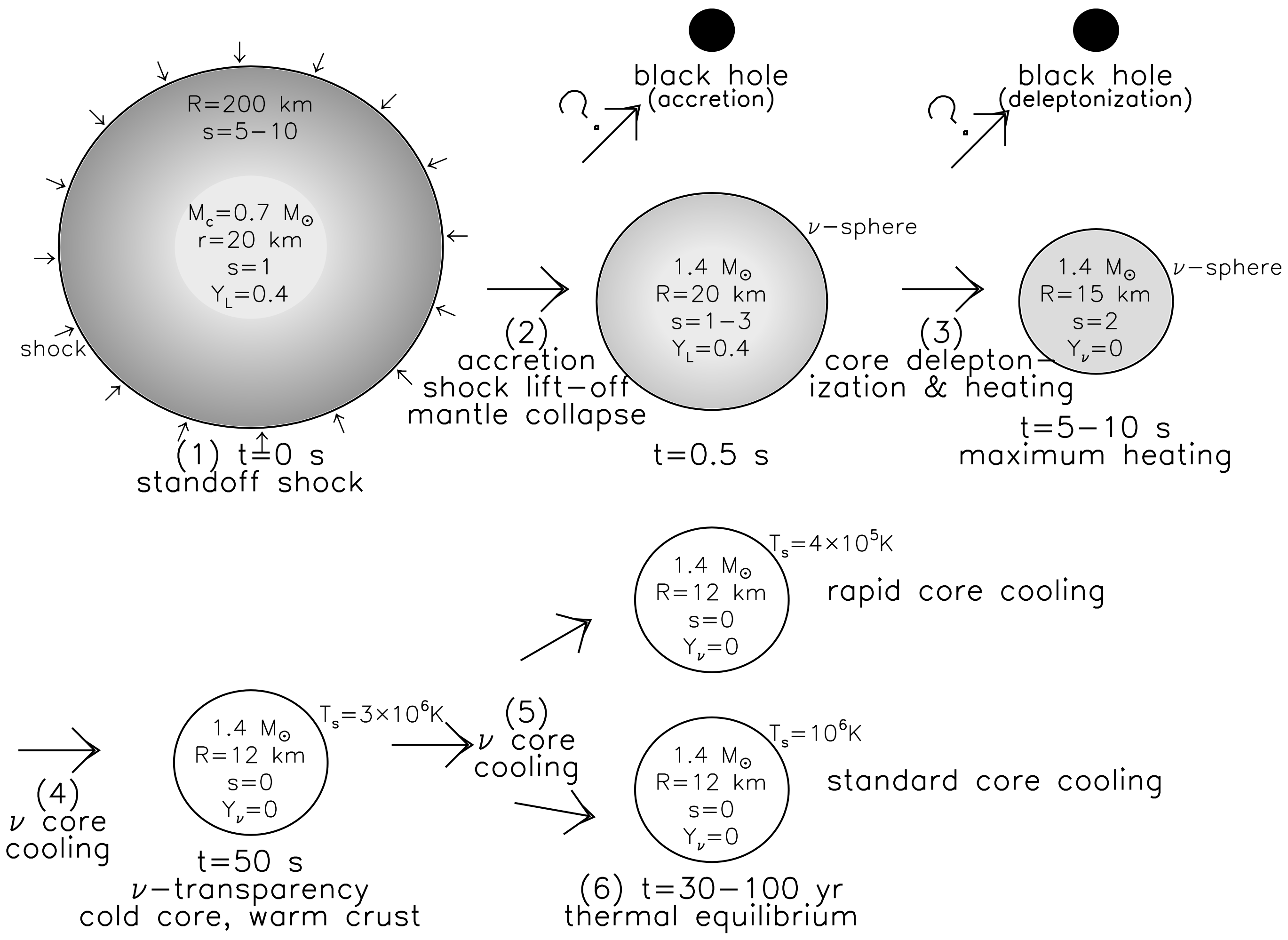

Figure 1.1: Main stages of evolution of a neutron star. Numbers in parentheses refer to the stages discussed in the text [1].

energy due to beta decays and neutrino emission. The shock is momentary stationary prior to an eventual explosion.

2. On a timescale of about 0.5 s, accretion becomes much less important as the supernova explodes and the shock lifts off the stellar envelope. Extensive neutrino losses and deleptonization of mantle lead to the loss of lepton pressure and to collapse of the mantle on the same timescale. Neutrino diffusion times from the core are too long to significantly alter the core during this stage. If enough accretion occurs, and the initial core was large enough, the mass of hot, lepton-rich matter could exceed the maximum mass that is stable, in which case the star would collapse to form a black hole. In this case, neutrino emission would effectively cease, since the event horizon is believed to form outside the neutrino photosphere.

3. This stage is dominated by neutrino diffusion causing deleptonization and heating of the core. Neutrino-nucleon absorption reactions set the diffusion timescales to about 10-15 s. The maximum entropy per baryon reached in the core is about 2 (in units of the Boltzmann's constant). When the core deleptonizes, the threshold for the appearance of strangeness, in the form of hyperons, a Bose kaon condensate, or quarks will be reduced. If one (or more) of these additional components is present, the equation of state will soften, leading to the decrease in the maximum mass. There is, therefore, the possibility that a black hole could form at this later time.

4. Following deleptonisation, the star has high entropy, so that thermally produced neutrino pairs of all flavours are abundant, and thermal diffusion and cooling of the hot neutron star takes place. Because the entropy is higher at the beginning of cooling than it is at the beginning of deleptonization, the neutrino mean free paths are smaller and the timescales longer. In approximately 50 s, as the average neutrino energy decreases, it becomes essentially transparent to neutrinos and the core achieves a cold, catalysed configuration. The loss of thermal energy leads to a small increase in the threshold density for the appearance of strange matter, so that, in the absence of further accretion, it is unlikely that a black hole could form during this or later phases.

5. Following the onset of neutrino transparency, the core continues to cool by neutrino emission, but the star's crust cools less because of its lower neutrino emissive. The crust acts as an insulating blanket that prevents the star attaining complete thermal equilibrium and keeps the surface relatively warm ($T \approx 3 \times 10^6$ K) for up to 100 y. This timescale is primary sensitive to the neutron star's radius and the thermal conductivity of mantle.

6. Ultimately, the star achieves thermal equilibrium when the energy stored in the crust is depleted. The temperature to which the surface now cools is determined by the rate of neutrino emission in the star's core. If this rate is large, the surface temperature will become relatively small, and the photon luminosity may become virtually undetectable from the Earth. This will be the case if direct Urca (beta decay) process can occur, which happens if the nuclear symmetry energy is large or if hyperons, a Bose condensate, or quarks are present. Somewhat higher surface temperatures occur if superfluidity in the core cuts off the direct Urca rate below the superfluid's critical temperature. A relatively high surface temperature will persist if the Urca process can

only occur indirectly with the participation of spectator nucleon- the so-called standard cooling scenario.

1.3 Neutrino sphere and shockwave

A supernova explosion releases $\sim 2 \div 4 \times 10^{53}$ ergs of gravitational binding energy. The kinetic energy of the expelled matter is lower by about two orders of magnitude and the energy emitted in electromagnetic radiation and gravitational waves is even less; then the bulk of the energy is released in the form of neutrinos [2].

A first ν_e burst is emitted during the infall stage of the collapse ("infall burst"), since the high density of matter makes the electron capture by proton

$$e^- + p \to \nu_e + n \tag{1.1}$$

very efficient. However, this neutrino emission does not continue indefinitely, since at density $\sim 10^{12}$ g cm^{-3} the neutrinos are trapped in stellar core and go into equilibrium with matter via the inverse process:

$$\nu_e + n \to e^- + p. \tag{1.2}$$

Immediately after the bounce, also neutrinos of other flavours are beginning to be produced, via nucleonic bremsstrahlung and pair annihilation processes as:

$$e^+ + e^- \to \nu_x + \bar{\nu}_x \tag{1.3}$$

The neutrinos are trapped in a region (the "neutrinosphere") whose size is different for different neutrino flavours. Neutrino produced at a distance from the centre larger than the neutrinosphere radius can freely escape to infinity, while neutrinos produced within this sphere remain trapped. Electron neutrinos and antineutrinos interact with matter via neutral and charged current processes, while nonelectron neutrinos and antineutrinos interact only via neutral current. Therefore, the ν_x are less tightly coupled with matter than ν_e and $\bar{\nu}_e$ and a higher matter density is needed to trap them. Moreover, since the matter is richer in neutrons than protons, the ν_e are more strongly coupled than the $\bar{\nu}_e$. As a result, the neutrinosphere radius is maximum for ν_e and amounts to ~ 70 km for ν_e, to ~ 50 km for $\bar{\nu}_e$ and to ~ 30 km for ν_x. The larger the neutrinosphere radius, the lower the mean neutrino energy (a deeper neutrinosphere corresponds to a higher temperature); so, the neutrino mean energies are expected to be:

$$\langle E_{\nu_e} \rangle \approx 10 \div 13 \text{ MeV}; \tag{1.4}$$

$$\langle E_{\bar{\nu}_e} \rangle \approx 14 \div 17 \text{ MeV}; \tag{1.5}$$

$$\langle E_{\nu_x} \rangle \approx 22 \div 27 \text{ MeV}; \tag{1.6}$$

When the shock crosses the ν_e neutrinosphere, an intense burst of ν_e is produced, since the efficiency of the (1.1) process is abruptly enhanced by large number of protons liberated

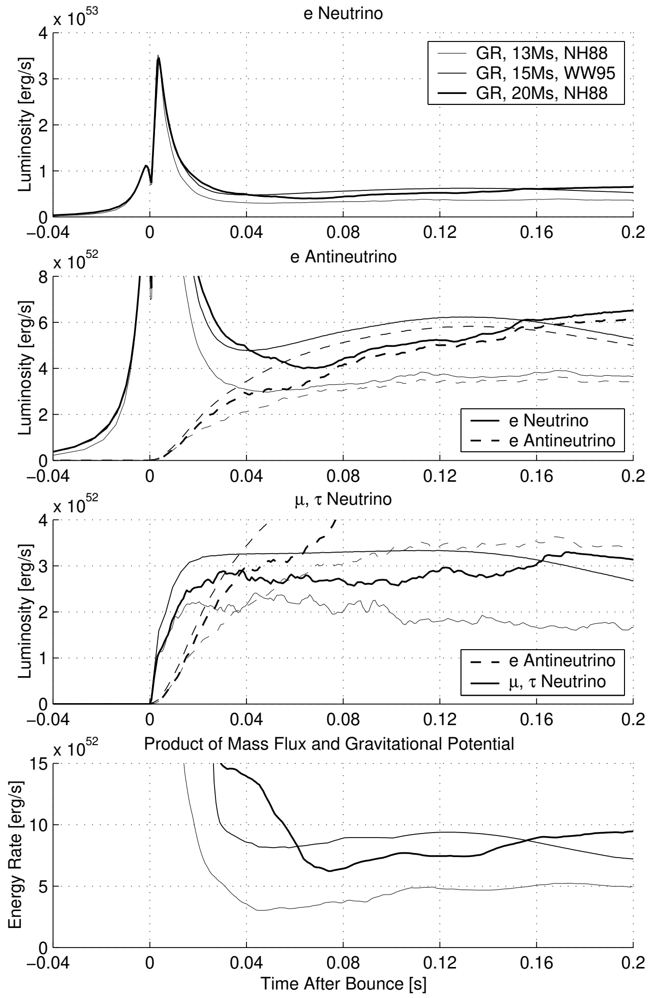

Figure 1.2: Luminosities for all kind, of neutrinos as functions of time after the bounce (first three graphs). Three different curves are shown in every graph, each corresponding to a different explosion model. The last graph shows the energy production rate, closely similar to the neutrino luminosities (from [2])

by the shock ("neutronization burst"). The infall and neutronization burst are very rapid ($\sim$ 10 Ms); the ν_e energy is $\sim$ 10 MeV and the total released energy is $\lesssim 10^{52}$ erg.

After the neutronization stage, the ν_e luminosity rapidly decreases, while the luminosity of other flavour neutrinos increase. The neutrinos are now produced mainly via the (1.3) process and the higher rate of ν_e, $\bar{\nu}_e$ production is compensated by the large couplings of these neutrinos with matter. As a result, at the end of the neutrino diffusion inside the mantle the energy is practically equally distributed between the neutrino flavours ($\sim 5 \times 10^{52}$ ergs for each neutrino type). This final stage ("cooling") requires $\sim$ 10 s and takes away $> 99\%$ of the gravitational energy of the star.

Fig 1.2. shows an example of the neutrino luminosities as a function of time after bounce. Note the ν_e neutronization peak, the sharp rise (tenths of ms) of all flavours luminosities and the much longer trailing edge of all neutrino signals. The general features of neutrino spectra and luminosities are rather similar in various simulations; some of them (average $\bar{\nu}_e$ energy, duration of the burst, energy emitted in $\bar{\nu}_e$ etc.) were also confirmed by the observation of SN1987A neutrinos.

1.4 Experimental status

The detection of supernova neutrinos requires their conversion into a charged lepton or the emission of some other particle (essentially $\gamma's$ or neutrons) which can be efficiently observed. An "ideal" reaction should be sensitive to all flavours of neutrinos and preserve all information on neutrino energy spectrum, timing, direction and type; however, usually only a part of this information can be derived by single process and then combined observation by detectors based on different technologies is fundamental to obtain a comprehensive picture of the neutrino burst properties [2].

Reactions that can possibly be used in the neutrino detection fall in one of four main categories.

Charged currents on nucleons; these processes are useful only for ν_e and $\bar{\nu}_e$ because the ν_x energies are under the threshold for charged leptons (μ and τ) production. However since target materials containing free neutrons are not available one is for the practical purposes only left with the inverse-beta reaction.

$$\bar{\nu}_e + p \rightarrow e^+ + n. \tag{1.7}$$

Elastic scattering on electrons; this reaction is possible in principle for all kind of neutrinos; however, ν_e and $\bar{\nu}_e$ interact with electron via charged (with different couplings) and neutral currents, while ν_x interact only via neutral currents.

Charged currents on nuclei; again, only ν_e and $\bar{\nu}_e$ can interact via charged current reactions.

Neutral currents on nuclei are sensitive to all neutrino species, which makes them very important, because the detection of ν_x is the most challenging goal of the supernova neutrino detectors.

Supernova has several characteristics to which we need to model the detectors of the neutrinos coming from them. First of all supernovae are very rear events: the expected rate of galactic stellar collapses is one in 20 to 40 years (note that this is a, so to say, "unlucky" number: the rate is too low to give a good chance of success to an experiment with an operating life ~ 10 years and, at the same time, the rate is too high to make a real time detection of a supernova neutrino burst a hopeless dream). Second, the supernova neutrinos have energies of tens of MeV or less, with low cross sections. And finally, a supernova has (or at least can have) a bright optical flare and releases radiation in other forms then neutrinos.

Such characteristics of a supernova and supernova neutrinos give us several desired properties of supernova neutrino detectors.

1. the detector should have as high as possible active material mass (preferably material should be cheap, robust and possibly non-polluting);

2. the detector must be located underground, to reduce the cosmic ray induced background, and possibly in a low radioactivity environment;

3. the detector should have a very high duty cycle (in principle it should be always active) and an operating life of at least ~ 10 years;

4. the detector must be equipped with electronics and acquisition system well suited to perform real time neutrino detection. The energy threshold should not exceed ~ 10 MeV.

Detector Type	Material	Energy	Time	Point	Flavour
Scintillator	C_nH_{2n}	y	y	n	$\bar{\nu}_e$
Water Čerenkov	H_2O	y	y	y	$\bar{\nu}_e$
Heavy water	D_2O	NC:n CC:y	y y	n y	all ν_e
Long string	H_2O	n	y	n	$\bar{\nu}_e$
Liquid Argon	Ar	y	y	n	ν_e
High-Z	Pb,Fe	y	y	n	all
Radio-chemical	Cl,I,Ga	n	n	n	ν_e

Table 1.1: Summary of types of supernova neutrino detectors

We now turn to the presentation of actual detectors, some of which have already ended and some of which are yet to be built. Note that most of these detectors were built having in mind also other physics goals, as the detection of solar and atmospheric neutrinos, the search for magnetic monopoles and proton decay, the observation of high cosmic rays etc.

The **LVD** (**L**arge **V**olume **D**etector) experiment is presently the largest operating liquid scintillation detector in the world. This detector is located in the Hall "A" of the Laboratory Nazionali del Gran Sasso (LNGS), in central Italy. After many years of operation with ~ 600 ton of liquid scintillator, LVD has recently reached its final active mass of $\approx 10^3$ ton.

The **MACRO** (**M**onopole **A**strophysics and **C**osmic **R**ay **O**bservatory) experiment, also located in the LNGS (Hall "B") which ended in December 2000. It had 570 ton of active mass.

A third scintillation detector, the **Baksan** observatory equipped with 200 ton (fiducial volume) of liquid scintillator, has been searching for galactic stellar collapse since more than 20 years. During 1987 this detector recorded a 5 event burst, which was generally attributed to neutrinos from SN1987.

The **KamLAND** is a liquid scintillation detector located in the Kamioka mine (Japan). It has a an active volume of ≈ 1000 ton, surrounded by an external buffer of mineral oil and liquid scintillator, used as veto for radioactivity and cosmic ray muons.

The **Borexino** is also a liquid scintillator detector, with a multi-shielding structure, which has an internal fiducial volume of 300 ton. It should go on-line soon in the LNGS (Hall "C").

Super-Kamiokande (**SK**) detector is a 50 kton Čerenkov experiment located in the Kamioka mine (Japan). This detector has a fiducial volume for supernova neutrinos of 32 kton.

SNO (**S**udbury **N**eutrino **O**bservatory) is a large heavy water Čerenkov detector, located in the Creighton mine (Canada). The experiment is based on 1000 ton of D_2O, surrounded by an external shield of 5000 ton of light water (the inner 1400 ton of water can also be used for supernova neutrino detection). The simultaneous presence of heavy and light water makes SNO a very promising experiment for detecting supernova neutrinos, since it has a good sensitivity to neutrinos of all flavours.

Icarus (**I**maging of **C**osmic **A**nd **R**are **U**nderground **S**ignals) is a modular Liquid Argon projection chamber, with a sensitive mass of 600 ton. It is located in LNGS (Hall "C").

HENTs (**H**igh **E**nergy **N**eutrino **T**elescopes), **AMANDA** (future upgrade **Ice-Cube**),
Baikal, **NESTOR** and **ANTARES**, are arrays of hundreds of optical modules, deployed in long strings ($\sim$ km) in deep sea or Antarctic ice. These detectors look at energetic cosmic ray muons and have an energy threshold in the GeV range; however, they have some sensitivity to a galactic supernova explosion because of collective effect, the excess of single counting rates produced in all optical modules by stream of thousands of low energy positrons concentrated in a short time. A supernova trigger based on this idea is active in **AMANDA**.

There are several ideas for future projects. We will mention only a few most interesting and promising here. **UNO** is a project for a large scale water Čerenkov detector. The idea is to reach a total mass of 650 kton of water. **LANNDD** is a proposal of a 70 kton magnetized Liquid Argon tracking detector. Two projects based on low-cost high-Z (NaCl,Fe and Pb) materials are also planed. Those are **SNBO** and **OMNIS** with mass of $\sim 10^4$ ton. Other projects also include a possible **Super-Kamiokande** upgrade called

Detector	Type	Mass (kton)	Location	No. of events at 8.5 kpc	Status
SK	Water Čerenkov	32	Japan	7000	running
SNO	Heavy water	1.4(D_2O) 1(H_2O)	Canada	300 450	running
LVD	Scintillator	1	Italy	200	running
KamLAND	Scintillator	1	Japan	300	running
Borexino	Scintillator	0.3	Italy	100	soon
Baksan	Scintillator	0.33	Russia	50	running
AMANDA	Long string	$\sim$ 0.4/PMT	South Pole	N/A	running
Icarus	Liquid Argon	2.4	Italy	200	running
OMNIS	Pb	2-3	USA	>1000	proposed
LANNDD	Liquid Argon	70	USA	6000	proposed
UNO	Water Čerenkov	600	USA	>100 000	proposed
Hyper-K	Water Čerenkov	1000	Japan	>100 000	proposed

Table 1.2: Summary of current and future supernova neutrino detectors

Hyper-Kamiokande which should have a total mass of 1000 kton of water.

2 Neutrino interactions

The weak interaction is one of the four fundamental forces in nature. Like the other three - strong, electromagnetic and gravitation - it plays a key role in many astrophysical processes. This can be nicely illustrated by the observation that new insights into the nature of the weak interaction usually were closely followed by the recognition of their importance in some astrophysical context. Shortly after Pauli postulated the existence of the neutrino and Fermi developed the first theory of weak interaction, Gamow and Schoenberg speculated about the possible role of neutrinos in stellar evolution and proposed their production in the star as an important source for stellar energy losses. The development of universal V-A theory led Pontecorvo to realize that the bremsstrahlung radiation of neutrino pairs by electrons would be very effective stellar energy loss mechanism. Just after the discovery of neutral weak current it was recognized that this interaction would result in sizable elastic scattering cross section between neutrinos and nucleons, leading to neutrino trapping during the core collapse of massive star in a type II supernova [1].

The unified model of electroweak interaction allows derivation of accurate cross section for weak processes among elementary particles [3].

2.1 Processes considered

Processes mediated by the weak interaction in stars can be classified as leptonic (all interacting particles are leptons) and semileptonic (leptons interact with hadrons via the weak interaction). The calculation of semileptonic processes (i.e. neutrino-nucleon reactions, neutrino capture, etc.) is what we are interested in. More specifically we are interested in only two types of processes, scattering of neutrino on nucleons and absorption of neutrino on neutrons. It should be noted that due to the fact that the momentum of particles, which we have in our mixture, are small compared to masses of vector bosons (Z and $W^{\pm}$), it is sufficient to consider the semileptonic processes of interest in the lowest-order approximation in the weak interaction. This observation comes from the characteristics of the environment in which these processes are taking place. The relevant interaction Lagrangian will not be the full electroweak Lagrangian,

[1] Classification of supernova by type comes from their spectral and total luminosity characteristics. Type II is attributed to the core collapse of massive stars which produces a neutron star or possibly a black hole.

but instead we will have an old Fermi-like weak Lagrangian, which can be written in terms of current-current interactions as [4]:

$$\mathcal{L}_{int}^{cc} = \frac{G_F C}{\sqrt{2}} l_\mu j_W^\mu \quad \text{for} \quad \nu_l + B_2 \to l + B_4 \tag{2.1}$$

$$\mathcal{L}_{int}^{nc} = \frac{G_F}{\sqrt{2}} l_\mu^\nu j_Z^\mu \quad \text{for} \quad \nu_l + B_2 \to \nu_l + B_4 \tag{2.2}$$

where $G_F = 1.166 \times 10^{-11}\text{MeV}^{-2}$ is Fermi weak coupling constant, and the Cabibbo factor $C = \cos\theta_c$ for change of strangeness $\Delta S = 0$ and $C = \sin\theta_c$ for $\Delta S = 1$. Since in processes that we are considering there will be no strangeness change and since $\cos\theta_c$ is close to 1 we will use an approximation in which for $\Delta S = 0$ we have $C = 1$. Lagrangian (2.1) is that of charged current interaction which are transmitted by W-boson and (2.2) is that of neutral current interactions transmitted by Z-boson. The lepton and baryon weak charged currents are

$$l_\mu = \bar{\psi}_l \gamma_\mu (1 - \gamma_5) \psi_\nu, \tag{2.3}$$

$$j_W^\mu = \bar{\psi}_4 \gamma^\mu (g_V - g_A \gamma_5) \psi_2. \tag{2.4}$$

Similarly, the lepton and baryon neutral currents are

$$l_\mu^\nu = \bar{\psi}_\nu \gamma_\mu (1 - \gamma_5) \psi_\nu, \tag{2.5}$$

$$j_Z^\mu = \bar{\psi}_2 \gamma^\mu (c_V - c_A \gamma_5) \psi_2, \tag{2.6}$$

where 2 and 4 are the baryon initial and final state labels, respectively (these are identical for neutral current reaction). Other particle labels and four-momenta are as shown in Fig. 2.1(left) for charged current reaction and Fig. 2.1(right) for neutral current reaction. The vector and axial-vector coupling constants g_V and g_A for charged current and c_V and c_A for neutral current are listed in Table 2.1 [5] for particles of interest.

ψ_l, ψ_ν, ψ_2 and ψ_4 are quantized fields of leptons, neutrinos, incoming baryons and outgoing baryons. Since they all are fermions they can be described in terms of quantized Dirac fields. We expand them in terms of complete set of plane wave states

$$\psi(x) = \sum_{sp} \left(\frac{m}{VE_p}\right)^{\frac{1}{2}} c_s(\vec{p}) u_s(\vec{p}) e^{-ipx} \tag{2.7}$$

where $c_s(\vec{p})$ is creation operator and $u_s(\vec{p})$ is spinor of a particle with spin s and four-momenta p. The normalization in this case is in a box of volume V, but as usual whenever needed we will take the limit $V \to \infty$.

In the following sections we will, in addition to the momenta and energies listed in figure (2.1), use also several "transfer" variables. So we define transferred momentum as $\vec{q} = \vec{k}_i - \vec{k}_f = \vec{p}_i - \vec{p}_f$. The transferred energy is $q_0 = \epsilon_i - \epsilon_f = E_i - E_f$. Since ϵ_f ranges between 0 and ∞ the limits of q_0 are $-\infty$ and ϵ_i

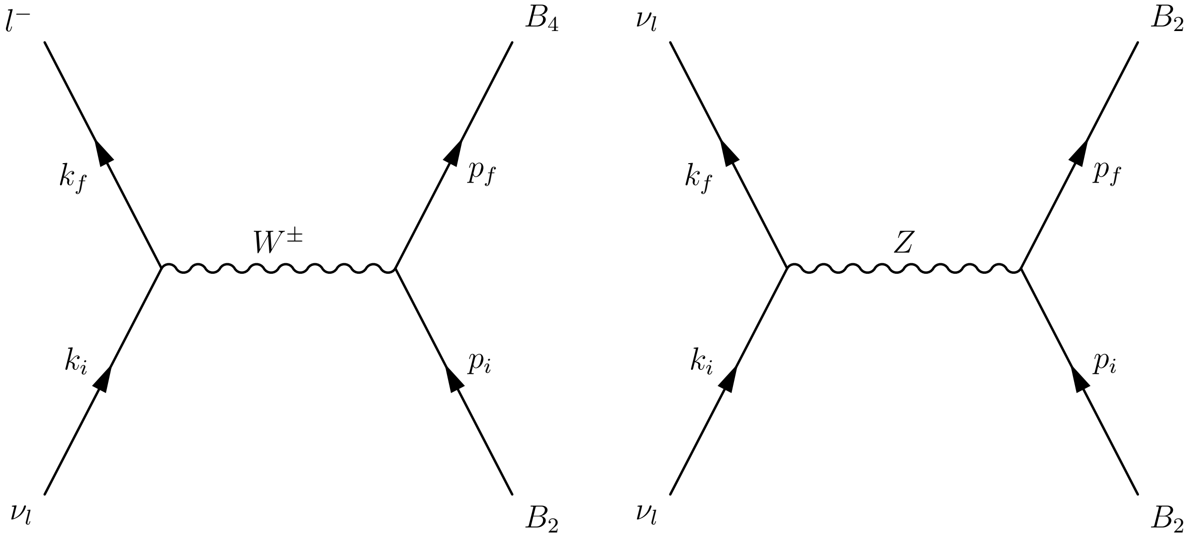

Figure 2.1: This figure shows two Faynmman graphs, one for absorption (left) and one for scattering (right)

Reaction	Vector(V) coupling	Axial-vector(A) coupling
$\nu_l + p \rightarrow \nu_l + p$	$c_V^p = 0.04$	$c_A^p = 0.615$
$\nu_l + n \rightarrow \nu_l + n$	$c_V^n = -0.5$	$c_A^n = 0.615$
$\nu_l + n \rightarrow l^- + p$	$g_V = 1.$	$g_A = 1.23$

Table 2.1: Vector and axial-vector couplings for processes of interest.

The accurately measured beta decay lifetime of the neutron in vacuum, $n \rightarrow p + e^- + \bar{\nu}_e$, fixes the ratio of axial and vector couplings of the neutron to be $|g_A/g_V| = 1.2601 \pm 0.0025$. Studies of beta decays in nuclei, however, have suggested that a value of $|g_A/g_v| \simeq 1$ better fits the observed systematics. Such a lower value also appears to be consistent with pion-nucleus optical potentials and the systematics of Gamow-Teller resonances in nuclei. On the basis of this data one can conclude that the vacuum couplings are not necessarily equal to the same values in medium. The precise value of in-medium axial coupling, denoted by g_A^* and c_A^*, in the dense matter encountered in astrophysical phenomena is crucially important. Here we will take over these, "quenched" values from reference [5] as $g_A^* = 0.7\ g_A$ and $c_A^* = 0.7\ c_A$. Further explanation for this effect can also be found in [6].

2.2 Cross section

Now we move on to calculation of the cross section for the processes of interest. We are considering a process in which two particles with four-momenta $p_i = (E_i, \vec{p}_i)$ and $k_i = (\epsilon_i, \vec{k}_i)$, collide and produce two final states with momentum $p_f = (E_f, \vec{p}_f)$ and

$k_f = (\epsilon_f, \vec{k}_f)$. Scattering matrix can now be written for this process as [7]:

$$S_{fi} = \delta_{fi} + (2\pi)^4 \delta^4(k_i + p_i - k_f - p_f) \left(\frac{m_1}{\epsilon_V} \frac{m_3}{\epsilon_f V} \frac{M_2}{E_i V} \frac{M_4}{E_f V} \right)^{\frac{1}{2}} \mathcal{M}_{fi} \tag{2.8}$$

where m are lepton and M are hadron masses. $\mathcal{M}_{fi}$ is the invariant matrix element. With this we can calculate the transition probability per unit time as:

$$w = \frac{|S_{fi}|^2}{T}. \tag{2.9}$$

With the aid of the expression $|\delta(x)|^2 = \frac{VT}{(2\pi)^4}\delta(x)$ we can rewrite transition probability:

$$w = V(2\pi)^4 \delta^4(k_i + p_i - k_f - p_f) \left(\frac{m_1}{\epsilon_i V} \frac{m_3}{\epsilon_f V} \frac{M_2}{E_i V} \frac{M_4}{E_f V} \right) \sum_{s_i, s_f, S_i, S_f} |\mathcal{M}_{fi}|^2 . \tag{2.10}$$

Eq. (2.10)) is the transition rate to one definite state. To obtain the transition rate to a group of final states with momentum in the intervals $(\vec{p}_f, \vec{p}_f + d\vec{p}_f)$ and $(\vec{k}_f, \vec{k}_f + d\vec{k}_f)$, we must multiply w by the number of these states,

$$(1 - f(E_f)) \frac{V}{(2\pi)^3} d^3 p_f; \tag{2.11}$$

$$(1 - f(\epsilon_f)) \frac{V}{(2\pi)^3} d^3 k_f. \tag{2.12}$$

As usual $f(E)$ denotes the particle distribution function, which in thermal equilibrium is given by the Fermi-Dirac function:

$$f(E) = \frac{1}{1 + \exp\left(\frac{E-\mu}{T}\right)} \tag{2.13}$$

where E is the single particle energy, μ is the corresponding chemical potential and T is the temperature. The factor $1 - f(E)$ selects between the available and occupied particle states and would not be there if the particles were in vacuum.

To calculate the total cross section we also need the available phase space for the particle with which our incident particle interact,

$$f(E_i) \frac{V}{(2\pi)^3} d^3 p_i. \tag{2.14}$$

Here standes the factor $f(E)$ because now we are interested at occupied and not available particle states.

With our choice of normalization for the states, the volume V that we are considering contains one scattering centre, and the incident flux is v_{rel}/V where v_{rel} is the relative velocity of the colliding particles. Combining these results, we obtain the required expression for the total cross section:

$$\sigma(\epsilon_i) = \int\int\int w\frac{V}{v_{rel}}f(E_i)(1-f(E_f))(1-f(\epsilon_f))\frac{V}{(2\pi)^3}d^3p_i\frac{V}{(2\pi)^3}d^3p_f\frac{V}{(2\pi)^3}d^3k_f \quad (2.15)$$

Then the total cross section per unit volume is:

$$\begin{aligned}\frac{\sigma(\epsilon_i)}{V} &= \int\frac{m_1m_3M_2M_4}{(2\pi)^3}(1-f(\epsilon_f))d^3p_f \\ &\int\frac{d^3k_i}{(2\pi)^3}\int\frac{d^3k_f}{(2\pi)^3}(2\pi)^4\delta^4(p_i+k_i-p_f-k_f)\frac{f(E_i)(1-f(E_f))}{\epsilon_i\epsilon_f E_iE_f v_{rel}}\sum_{s_i,s_f,S_i,S_f}|\mathcal{M}_{fi}|^2,\end{aligned} \quad (2.16)$$

where the invariant matrix element is summed over final spins and averaged over the initial spins. From here we can also get the differential cross section per unit volume for outgoing leptons which scatter into a space angle $d\Omega$ with energies in the interval $(\vec{p}_f, \vec{p}_f + d\vec{p}_f)$

$$\begin{aligned}\frac{1}{V}\frac{d^3\sigma}{d^2\Omega\; d\epsilon_f} &= \frac{m_1m_3M_2M_4}{(2\pi)^3}(1-f(\epsilon_f)) \\ &\int\frac{d^3k_i}{(2\pi)^3}\int\frac{d^3k_f}{(2\pi)^3}(2\pi)^4\delta^4(p_i+k_i-p_f-k_f)\frac{f(E_i)(1-f(E_f))}{\epsilon_i\epsilon_f E_iE_f v_{rel}}\sum_{s_i,s_f,S_i,S_f}|\mathcal{M}_{fi}|^2.\end{aligned} \quad (2.17)$$

Eq.(2.16) holds in any Lorentz frame in which the colliding particles move collinearly. In such a frame the relative velocity v_{rel} is given by the expression:

$$\epsilon_iE_iv_{rel} = \left[(p_ik_i)^2 - m_1^2M_2^2\right]^{\frac{1}{2}}. \quad (2.18)$$

We now turn to the calculation of squared matrix element $\sum_{s_i,s_f,S_i,S_f}|\mathcal{M}_{fi}|^2$. First we write the invariant matrix element as a product of electroweak currents between the interacting leptons and nucleons as defined earlier by the interaction Lagrangian (here we will consider as general process as possible and only later shall we introduce the specific characteristics of each process in which we are interested):

$$\mathcal{M}_{fi} = G_F\sqrt{2}j_\mu(k_f,s_f,\,k_i,s_i)J^\mu(p_f,S_f,\,p_i,S_i), \quad (2.19)$$

where the electroweak currents are defined as, for leptons

$$j_\mu(k_f,s_f,\,k_i,s_i) = \bar{\psi}'(k_f,s_f)\gamma_\mu(1-\gamma_5).\psi(k_i,s_i) \quad (2.20)$$

Equivalently for hadrons we have:

$$J^\mu(p_f,S_f,\,p_i,S_i) = \bar{\Psi}'(p_f,S_f)\gamma^\mu(V-A\gamma_5)\Psi(p_i,S_i) \quad (2.21)$$

where V and A stand in for vector and axial-vector coupling constants depending on the process.

From here we can construct the squared matrix element as:

$$\sum_{s_i,s_f,S_i,S_f} |\mathcal{M}_{fi}|^2 = \frac{G_F}{2} L_{\mu\nu} W^{\mu\nu} \tag{2.22}$$

where $L_{\mu\nu}$ is the lepton tensor defined as:

$$L_{\mu\nu} = \sum_{s_i,s_f} j^*_\mu(k_f, s_f,\, k_i, s_i) j_\nu(k_f, s_f,\, k_i, s_i) \tag{2.23}$$

and $W^{\mu\nu}$ is hadron tensor defined as:

$$W^{\mu\nu} = \sum_{S_i,S_f} J^{*\mu}(p_f, S_f,\, p_i, S_i) J^\nu(p_f, S_f,\, p_i, S_i). \tag{2.24}$$

We will now here only quote the result for the squared matrix element, which we have calculated in more detail in the Appendix A.

$$\sum_{s_i,s_f,S_i,S_f} |\mathcal{M}_{fi}|^2 = \\ \frac{2G_F^2}{m_1 m_3 M_2 M_4} \left\{ V^2 \epsilon_i \epsilon_f M_2 M_4 (1 + \cos\theta) + A^2 \epsilon_i \epsilon_f M_2 M_4 (3 - \cos\theta) \right\}. \tag{2.25}$$

One should note that several approximations were used to obtain this result. First, since the temperature range that we are interested in is of order $\sim$ 10 MeV we can safely assume that hadrons which we are looking at, because of their mass $\sim$ 1 GeV which is far greater than temperature range ($T \ll M$), are fully nonrelativistic so the following approximation holds:

$$p_i = \begin{pmatrix} E_i \\ \vec{p}_i \end{pmatrix} \approx \begin{pmatrix} M_2 \\ 0 \end{pmatrix}, \qquad \text{and} \qquad p_f = \begin{pmatrix} E_f \\ \vec{p}_f \end{pmatrix} \approx \begin{pmatrix} M_4 \\ 0 \end{pmatrix}. \tag{2.26}$$

Second, since the chemical potentials range that we have is far grater than the mass of electron and certainly than any possible mass range for neutrinos ($m \ll \mu$) we can consider all leptons to be fully relativistic. So we have

$$k_i = \begin{pmatrix} \epsilon_i \\ \vec{k}_i \end{pmatrix} \approx \begin{pmatrix} |\vec{k}_i| \\ \vec{k}_i \end{pmatrix}, \qquad \text{and} \qquad k_f = \begin{pmatrix} \epsilon_f \\ \vec{k}_f \end{pmatrix} \approx \begin{pmatrix} |\vec{k}_f| \\ \vec{k}_f \end{pmatrix}. \tag{2.27}$$

With these approximations it is natural to use a laboratory reference frame in which, for relative velocity, we have

$$v_{rel} = \frac{|\vec{k}_i|}{\epsilon_i}. \tag{2.28}$$

Now with the aid of these results we write the differential cross section Eq.(2.17) as

$$\frac{1}{V}\frac{d^3\sigma}{d^2\Omega\, d\epsilon_f} = M_2 M_4 \frac{G_F}{8\pi^3}\epsilon_f^2(1-f(\epsilon_f))\left[V^2(1+\cos\theta)+A^2(3-\cos\theta)\right] \left[2\int\frac{d^3p_f}{(2\pi)^3}\int\frac{d^3p_i}{(2\pi)^3}(2\pi)^4\delta^4(p_i+k_i-p_f-k_f)f(E_i)(1-f(E_f))\right] \quad (2.29)$$

We have conveniently written the expression (2.29) so that the abbreviation, which we are about to introduce, is more obvious. It is a commonly introduced abbreviation [4]:

$$S(q_0,q) = 2\int\frac{d^3p_i}{(2\pi)^3}\int\frac{d^3p_f}{(2\pi)^3}(2\pi)^4\delta^4(p_i+k_i-p_f-k_f)f(E_i)(1-f(E_f)). \quad (2.30)$$

This function is called the structure or response function.

Since we have already introduced the transferred energy and we have expressed the response function with its aid we will also make the same transition in the differential cross section. Thus we can write the differential cross section as

$$\frac{1}{V}\frac{d^3\sigma(\epsilon_i)}{d^2\Omega\, dq_0} = \frac{G_F^2}{8\pi^3}\epsilon_f^2\,(1-f(E_3))\left[V^2(1+\cos\theta)+A^2(3-\cos\theta)\right]S(q_0,q). \quad (2.31)$$

It should be noted that the end step of this derivation assumes that the vector and axial-vector structure functions are equal, which is true in the case of free gas. But since we are interested in more than free gas case we will return later to this step. For that we will need to look here more deeply in to the nature of the structure function we have introduced with the formula (2.30). This will be done in the next section.

Since in the last section we are interested in the dependence of the differential cross section on the transferred energy it is useful to see which range of values is allowed for the transferred energy given the approximations. The limiting factor will be the value of angle θ or $\cos\theta$. From the definition of transferred momentum $\vec{q}=\vec{k}_i-\vec{k}_f$ it is posible to get

$$\cos\theta = \frac{\epsilon_i^2+\epsilon_f^2-q^2}{2\epsilon_i\epsilon_f}. \quad (2.32)$$

The limits are $|\cos\theta|\le 1$. From this with the aid of the relation for the transferred energy $q_0=\epsilon_f-\epsilon_i$ we get two conditions $|q_0|\le q$ and $q_0\le 2\epsilon_i-q$. Since in the most of the cases of differential cross section we choose $q=\epsilon_i$ these two condition will be one and the same condition.

Now from the differential cross section we can calculate the total cross section and mean free path. The total cross section is easily calculated simply by integrating over all of the remaining variables.

$$\frac{\sigma(\epsilon_i)}{V} = \int\frac{1}{V}\frac{d^3\sigma(\epsilon_i)}{d^2\Omega\, dq_0}d\Omega dq_0. \quad (2.33)$$

In a way this is just the reverse of the step, which was made going form (2.16) to (2.17)

The mean free path is just the inverse of the total cross section

$$\lambda = \left(\frac{\sigma(E_1)}{V}\right)^{-1}. \tag{2.34}$$

2.3 Structure and polarization function

Now we return to the structure function or the response function as it is also called because it represents the response of the medium in which process take place. In this section as in the previous we assume that we are dealing with noninteracting nonrelativistic baryons. In this section we will use somewhat different notation than in the last. So instead of denoting the energy of initial baryon with E_i we will us E_2 and instead of denoting the final state baryons with E_f we will us E_4. Also for the sake for clarity we will introduce additional labels to the Fermi-Dirac functions, which have obvious meaning.

If we look at the integral (2.30) one can notice that we can use the delta function to eliminate one of the integrals, we will perform the integral over the final state momentum p_4. If we do that we will have [4]

$$S(q_0, q) = \frac{1}{2\pi^2}\int d^3p_2\delta(q_0 + E_2 - E_4)f_2(E_2)(1 - f_4(E_4)). \tag{2.35}$$

We note that $E_4 = (\vec{p}_2 + \vec{q})^2/2M$ (although there will be occasions where we will have neutrons and protons as particles 2 and 4 the assumption of equal masses will be valid still for the case of free gas).

The function $S(q_0, q)$ is directly related to the lowest-order polarization function Π^0 (also known as the Lindhard function [8])

$$S(q_0, q) = -2\frac{\mathrm{Im}\Pi^0(q_0, q)}{1 - \exp\left(-\frac{q_0+\mu_2-\mu_4}{T}\right)}, \tag{2.36}$$

$$\Pi^0(q_0, q) = \frac{2}{(2\pi)^3}\int d^3p\left[\frac{f(E_p)\left[1 - f(E_{|\vec{p}+\vec{q}|})\right]}{q_0 + E_p - E_{|\vec{p}+\vec{q}|} + i\epsilon} - \frac{\left[1 - f(E_p)\right]f(E_{|\vec{p}+\vec{q}|})}{q_0 + E_p - E_{|\vec{p}+\vec{q}|} - i\epsilon}\right]. \tag{2.37}$$

This connection has been illustrated in more detail in Appendix C. As before $f(E)$ is the Fermi-Dirac distribution and the energy is $E_p = p^2/2M$.

The integral in the Eq.(2.35) can be performed analytically. We my rewrite the energy delta function in terms of angle between $\vec{p}_2$ and $\vec{q}$ as:

$$\delta(q_0 + E_2 - E_4) = \frac{M}{p_2 q}\delta(\cos\theta - \cos\theta_0)\Theta(p_2^2 - p_-^2), \tag{2.38}$$

where

$$\cos\theta_0 = \frac{M}{p_2 q}\left(q_0 - \frac{q^2}{2M}\right), \quad p_-^2 = \frac{M^2}{q^2}\left(q_0 - \frac{q^2}{2M}\right)^2 \tag{2.39}$$

$$\frac{(\vec{p}_2 + \vec{q})^2}{2M} = \frac{p_2^2}{2M} + q_0 \tag{2.40}$$

and $\Theta(x)$ is the Heaviside function. Substituting these results in Eq.(2.35) and performing the angular integrals we obtain

$$
\begin{aligned}
S(q_0, q) &= \frac{M}{\pi q} \int_{p_-}^{\infty} dp_2 p_2 f_2(E_2)(1 - f_4(E_4)) & (2.41)\\
&= \frac{M}{\pi q} \int_{p_-}^{\infty} dp_2\, p_2 \frac{1}{1 + \exp\left(\frac{\frac{p_2^2}{2M} - \mu_2}{T}\right)} \frac{1}{1 + \exp\left(\frac{\frac{(\vec{p}_2 + \vec{q})^2}{2M} - \mu_4}{T}\right)} & (2.42)
\end{aligned}
$$

with the substitution $x = \frac{\frac{p_2^2}{2M} - \mu_2}{T}$ we get

$$
S(q_0, q) = \frac{M^2 T}{\pi q} \int_{x_-}^{\infty} dx \frac{1}{1 + \exp(x)} \frac{1}{1 + \exp\frac{(x + (q_0 + \mu_2 - \mu_4)}{T})} \tag{2.43}
$$

where $x_- = \frac{1}{T}\left[\frac{M}{2q^2}\left(q_0 - \frac{q^2}{2M}\right)^2 - \mu_2\right]$. The integration over x can be performed by using the relation

$$
\int \frac{dx}{1 + \exp(x)} \frac{1}{1 + \exp(-x - z)} = -\frac{1}{1 - \exp(-z)} \ln \frac{1 + \exp(x)}{1 + \exp(x + z)}. \tag{2.44}
$$

Thus the free gas response function is given by

$$
S(q_0, q) = \frac{M^2 T}{\pi q} \left[\frac{z}{1 - \exp(-z)} \left(1 + \frac{\xi}{z}\right)\right] \tag{2.45}
$$

where

$$
\begin{aligned}
z &= \frac{q_0 + \mu_2 - \mu_4}{T}, & (2.46)\\
\xi_- &= \ln\left[\frac{1 + \exp\left(\frac{e_- - \mu_2}{T}\right)}{1 + \exp\left(\frac{e_- + q_0 - \mu_4}{T}\right)}\right], & (2.47)\\
e_- &= \frac{p_-^2}{2M} = \frac{1}{4} \frac{(q_0 - q^2/2M)^2}{q^2/2M}. & (2.48)
\end{aligned}
$$

This is the result we have been looking for. Later we will repeat the calculation of the response function without some of the assumptions we have made here, such as equal nucleon masses and others. This calculation will then tour out to be just a subcase of that calculation.

2.4 β-equilibrium

For stars in which the strongly interacting particles are only baryons the composition is determined by the requirements of charge neutrality and equilibrium under the weak processes. If we consider a general process with baryons B_2 and B_4 and a lepton l and its corresponding neutrino ν_l we have [1]

$$B_2 \rightarrow B_4 + l + \bar{\nu}_l; \quad B_4 + l \rightarrow B_2 + \nu_l \tag{2.49}$$

If the neutrinos have left the system these two conditions give

$$\sum_i \left(n_{B_i}^{(+)} + n_{l_i}^{(+)}\right) = \sum_i \left(n_{B_i}^{(-)} + n_{l_i}^{(-)}\right), \tag{2.50}$$

$$\mu_i = b_i \mu_n - q_i \mu_l. \tag{2.51}$$

In eqautions (2.50) and (2.51), n denotes the number density and the superscripts $(\pm)$ on n signify positive or negative charge. The symbol μ_i refers to the chemical potential of baryon i, b_i is its baryon number and q_i is its charge. The chemical potential of neutron is denoted μ_n.

If the neutrinos are trapped in the system second condition (beta equilibrium) is altered to

$$\mu_i = b_i \mu_n - q_i(\mu_l - \mu_{\nu_l}), \tag{2.52}$$

where μ_{ν_l} is the chemical potential of the neutrino. Because of trapping, the number of leptons per baryon of each flavour of neutrino, $l = e$ and μ,

$$Y_{L_l} = Y_l + Y_{\nu_l} \tag{2.53}$$

is conserved on dynamical time scales. Gravitational collapse calculations of the white-dwarf core of massive stars indicate that at the onset of trapping, the electron lepton number $Y_{L_e} = Y_e + Y_{\nu_e} \simeq 0.4$, the precise value depending on the efficiency of electron capture reactions during the initial collapse stage. Also, because no muons are present when neutrinos become trapped, the constraint $Y_{L_\mu} = Y_\mu + Y_{\nu_\mu} = 0$ can be imposed. We fix Y_{L_l} at these values in calculations for neutrino trapped matter.

Now that we have introduced the chemical potentials and expressed the condition of equilibrium we will connect chemical potentials with the density of medium because request for neutrality of the medium and lepton conservation both are expressed in terms of density. For now we will do that in the approximation of the free gas, and in the next chapter we will calculate the chemical potential for hadrons from nuclear potential while for the leptons we will stay with the free gas approximation.

From statistical physics we know that the chemical potential of fermions at zero temperature is equal to the Fermi energy of that fermion. Depending on what approximation we have there will be two cases, that of nonrelativistic fermions $\epsilon_F = \frac{p_F^2}{2M}$ and the case of fully relativistic fermions $\epsilon_F = p_F$, where the p_F is the Fermi momentum. Also from statistical physics we know the connection between the Fermi momentum and density for these two cases.

$$p_F = \left(3\pi^2 \rho\right)^{1/3} \tag{2.54}$$

for the case of nonrelativistic fermions and

$$p_F = \left(\frac{6\pi^2}{g}\rho\right)^{\frac{1}{3}} \tag{2.55}$$

for the case of fully relativistic fermions, where g is degeneracy parameter.

For us the nonrelativistic fermions are hadrons, proton and neutron, because of their large mass, as was mentioned before. So for the chemical potential of hadrons in the case of free gas at zero temperature we have

$$\mu = \frac{(3\pi^2\rho)^{\frac{2}{3}}}{2M} \tag{2.56}$$

And the fully relativistic fermions are leptons, electron and neutrino, because of their small mass. So for the chemical potential of leptons in the case of zero temperature we have

$$\mu = \left(\frac{6\pi^2}{g}\rho\right)^{\frac{1}{3}} \tag{2.57}$$

We also need to discus how to calculate the chemical potential at finite temperature. This can be done if we use the Fermi-Dirac distribution expression for calculation of density at finite temperature

$$\rho = \frac{1}{\pi^2}\int_0^\infty p^2 dp \frac{1}{1+\exp{(E-\mu)/T}} \tag{2.58}$$

One can notice we have already performed the angular integration. From this expression we can, starting from zero temperature chemical potential, by iteration find the chemical potential that fits given density for that temperature.

3 EOS and Migdal parameters

The significant influence of nuclear forces on neutron star structure is by now established by a large body of theoretical and observational evidence. In absence of these forces the maximal possible mass of neutron stars composed of noninteracting neutrons is ~ 0.7 M$_\odot$. Since most observed neutron star masses are above 1.3 M$_\odot$, they must be supported against gravitational collapse by pressure originating from nuclear forces.

Shortly after discovery of pulsars, calculation of the equation of state (EOS) of neutron matter with realistic models of two-nucleon interaction, obtained by fitting the nucleon-nucleon scattering data then available, were carried out using the lowest order constrained variation method. The result demonstrated that nuclear forces increase the mass limit of stable neutron stars beyond 1.4 M$_\odot$.

3.1 EOS

Nuclear effective Hamiltonian consists of the kinetic energy and effective interaction [9],

$$H = K + V; \qquad K = \sum_i \frac{\vec{p}_i^2}{2M}, \qquad V = \sum_{i<j} v_{ij}. \tag{3.1}$$

Here i and j are indices of individual nucleons. It will be natural to assume the effective interaction v_{ij} to be translationally invariant, except for the density dependence mentioned below. We consider the effective interaction having the following form

$$v_{12} = v_{12}^{(C)} + v_{12}^{(TN)} + v_{12}^{(DD)}; \tag{3.2}$$

In the momentum space these potentials are given as follows [10]:

$$v_{12}^{(C)}(q) = \left(\frac{f}{m_1}\right)^2 \left[\sum_n \left(t_n + t_n^s \vec{\sigma}_1 \cdot \vec{\sigma}_2 + t_n^t \vec{\tau}_1 \cdot \vec{\tau}_2 + t_n^{st} \vec{\sigma}_1 \cdot \vec{\sigma}_2 \vec{\tau}_1 \cdot \vec{\tau}_2\right)\right] \frac{m_n^2}{q^2 + m_n^2} \tag{3.3}$$

$$v_{12}^{(TN)}(q) = -\left(\frac{f}{m_1}\right)^2 \frac{\vec{\tau}_1 \cdot \vec{\tau}_2}{3} \left(3\vec{\sigma}_1 \cdot \vec{q}\vec{\sigma}_2 \cdot \vec{q} - \vec{\sigma}_1 \cdot \vec{\sigma}_2 q^2\right) \left(\frac{1}{m_1^2 + q^2} - \frac{0.89}{m_2^2 + q^2}\right) \tag{3.4}$$

$$v_{12}^{(DD)}(q) = \left[\alpha_1 \hat{\rho}^{\lambda_1} \frac{\mu_1^2}{q^2 + \mu_1^2} + \alpha_2 \hat{\rho}^{\lambda_2} \frac{\mu_2^2}{q^2 + \mu_2^2} (\vec{\tau}_1 \cdot \vec{\tau}_2) + \alpha_3 \hat{\rho}^{\lambda_3} \frac{\mu_3^2}{q^2 + \mu_3^2}\right] \tag{3.5}$$

The $v_{12}^{(C)}$ is interaction based on a Yukawa fit to the Brueckner G-matrix, with long-range part identical to a one-pion-exchange potential (OPEP). Tensor interaction $v_{12}^{(TN)}$ was taken to have the same form, fit to the Reid soft-core G-matrix elements, but instead of three-term Yukawa which we had in the central part for tensor interaction only two-term Yukawa was needed [10]. We also introduced the density-dependent part $v_{12}^{(DD)}$ in the same Yukawa form, but with density constants in front of them [11].

The σ and τ are as usual Pauli matrices, and $f = 0.97$. The subscript n corresponds to the parameter attached to the Yukawa force (e.g. range of interaction), and t_n are the coefficients. With the aid of saturation density ρ_0 we defined $\hat{\rho} = \frac{\rho}{\rho_0}$ which is dimensionless density dependent quantity.

The saturation of density and energy is a basic property of nuclei. In developing effective interactions adaptive to many nuclei, it is required to reproduce the saturation property. However, the non-relativistic G-matrix calculations fail to reproduce the saturation at the right density and energy [10]. Therefore it would not be appropriate to use the G-matrix calculation for Hartree-Fock calculations without any modifications. The M3Y interaction gives no saturation point within the Hartree-Fock theory, unless density-dependence is taken into account explicitly.

We start from the potential taken over from reference [10]. We have fitted the density dependent part of this interaction so to reproduce some basic properties of nuclear matter at saturation point. In the unpolarized uniform nuclear matter, matrix elements of $v_{12}^{(TN)}$ between Hartree-Fock states vanish [9]. Therefore $v_{12}^{(C)} + v_{12}^{(DD)}$ determine the properties at saturation point. The range parameters for the Yukawa force are $m_1 = 0.7\ \mathrm{fm}^{-1}$, $m_2 = 2.5\ \mathrm{fm}^{-1}$ and $m_3 = 4\ \mathrm{fm}^{-1}$ for the central and tensor part and where $\mu_1 = 1.42\ \mathrm{fm}^{-1}$, $\mu_2 = 1.42\ \mathrm{fm}^{-1}$ and $\mu_3 = 2.5\ \mathrm{fm}^{-1}$ for the density dependent part ([9] and [11]).

Basic characteristics of nuclear effective interaction can be discussed via properties of the infinite nuclear matter; in particular, properties at and around the saturation point. In the Hartree-Fock theory of nuclear matter, the single particle wave functions can be taken to be the plane waves,

$$\phi_{\vec{k}\sigma\tau}(\vec{r}) = \frac{1}{\sqrt{\Omega}} e^{i\vec{k}\cdot\vec{r}} \chi_\sigma \chi_\tau. \tag{3.6}$$

Here $\chi_\sigma(\chi_\tau)$ denotes the spin (isospin) wave-function, and Ω indicates the volume of the system, for which we will take the $\Omega \to \infty$ limit. The single particle energy for this state is defined as

$$\epsilon(\vec{k}\sigma\tau) = \frac{\vec{k}^2}{2M} + \frac{\Omega}{(2\pi)^3} \sum_{\sigma_2\tau_2} \int_{k_2 \le k_{F_{\tau_2\sigma_2}}} d^3k_2 \left\langle \vec{k}\sigma\tau, \vec{k}_2\sigma_2\tau_2 |v_{12}| \ \vec{k}\sigma\tau, \vec{k}_2\sigma_2\tau_2 \right\rangle. \tag{3.7}$$

Energy of the nuclear matter is expressed by function of densities depending on the spin and the isospin, $\rho_{\tau\sigma}$ $(\tau = p, n; \sigma =\uparrow, \downarrow)$. The density variables can be converted to total density

$$\rho = \sum_{\sigma\tau} \rho_{\sigma\tau} \tag{3.8}$$

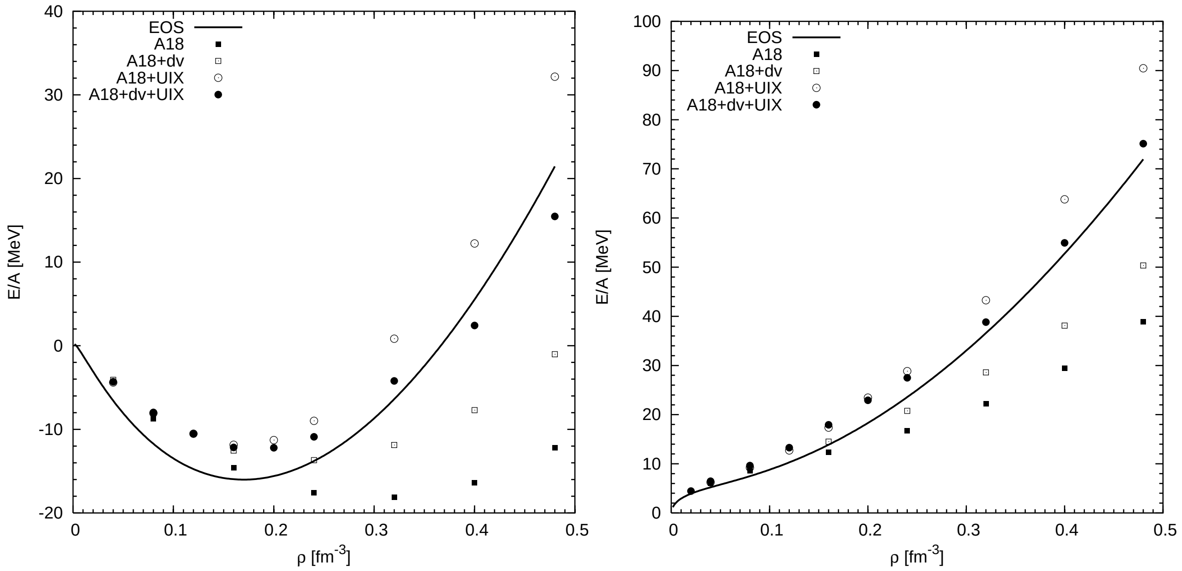

Figure 3.1: EOS for symmetric nuclear matter (left panel) and for neutron nuclear matter (right panel). For comparison we have listed the values of Argon potential and several of its corrections taken from [12]

and the spin- and isospin-asymmetry parameters

$$\eta_s = \frac{\sum_{\sigma\tau} \sigma \rho_{\sigma\tau}}{\rho} = \frac{\rho_{p\uparrow} - \rho_{p\downarrow} + \rho_{n\uparrow} - \rho_{n\downarrow}}{\rho} \tag{3.9}$$

$$\eta_t = \frac{\sum_{\sigma\tau} \tau \rho_{\sigma\tau}}{\rho} = \frac{\rho_{p\uparrow} + \rho_{p\downarrow} - \rho_{n\uparrow} - \rho_{n\downarrow}}{\rho} \tag{3.10}$$

$$\eta_{st} = \frac{\sum_{\sigma\tau} \sigma\tau \rho_{\sigma\tau}}{\rho} = \frac{\rho_{p\uparrow} - \rho_{p\downarrow} - \rho_{n\uparrow} + \rho_{n\downarrow}}{\rho} \tag{3.11}$$

where $\sigma(\tau)$ in the summation takes values ± 1,corresponding to $\sigma = \uparrow, \downarrow$ $(\tau = p, n)$. By assuming that the single particle states are occupied up to the Fermi momentum, the density is related to the Fermi momentum for each spin and isospin,

$$\rho_{\tau\sigma} = \frac{1}{6\pi^2} k^3_{F_{\tau\sigma}}. \tag{3.12}$$

Here we also define several other Fermi momenta that we will be needed later

$$k_{F_p} = \left(3\pi^2(\rho_{p_\uparrow} + \rho_{p_\downarrow})\right)^{\frac{1}{3}} \tag{3.13}$$

$$k_{F_n} = \left(3\pi^2(\rho_{n_\uparrow} + \rho_{n_\downarrow})\right)^{\frac{1}{3}} \tag{3.14}$$

$$k_F = \left(\frac{3}{2}\pi^2 \rho\right)^{\frac{1}{3}} \tag{3.15}$$

with obvious meanings as proton Fermi momentum k_{F_p}, neutron Fermi momentum k_{F_n} and total Fermi momentum k_F.

The total energy of nuclear matter is given by

$$
\begin{aligned}
E &= \frac{\Omega}{(2\pi)^3}\sum_{\sigma_1\tau_1}\int_{k_1\le k_{F_{\tau_1\sigma_1}}} d^3k_1 \frac{\vec{k}_1^2}{2M} \\
&+ \frac{\Omega^2}{2(2\pi)^6}\sum_{\sigma_1\sigma_2\tau_1\tau_2}\int_{k_1\le k_{F_{\tau_1\sigma_1}}} d^3k_1 \int_{k_2\le k_{F_{\tau_2\sigma_2}}} d^3k_2 \left\langle \vec{k}_1\sigma_1\tau_1, \vec{k}_2\sigma_2\tau_2 | v_{12} | \vec{k}_1\sigma_1\tau_1, \vec{k}_2\sigma_2\tau_2 \right\rangle .
\end{aligned}
\tag{3.16}
$$

As already pointed out, only $v_{12}^{(C)}+v_{12}^{(DD)}$ contributes to the energy of the isotropic nuclear matter. In Appendix B, several formulas on the Hartree-Fock energy of the nuclear matter are derived for interactions expressed in form of Eq.(3.2), with general and typical $\frac{m^2}{q^2+m^2}$.

In the spin-saturated symmetric matter, we have $\eta_s = \eta_t = \eta_{st} = 0$, which indicates $k_{F_{p\uparrow}} = k_{F_{p\downarrow}} = k_{F_{n\uparrow}} = k_{F_{n\downarrow}}$ and $\rho_{p\uparrow} = \rho_{p\downarrow} = \rho_{n\uparrow} = \rho_{n\downarrow} = \rho/4$. The lowest energy for a given ρ normally occurs along this line. The saturation point is obtained by minimizing the energy per nucleon $\mathcal{E} = E/A$,

$$
\left.\frac{\partial \mathcal{E}}{\partial \rho}\right|_{sat.} = 0, \tag{3.17}
$$

which yields the saturation density ρ_0 (equivalently, k_{F_0}) and energy $\mathcal{E}_0$.

The curvature at the saturation point with respect to ρ is proportional to the incompressibility,

$$
\mathcal{K} = k_F^2 \left.\frac{\partial^2 \mathcal{E}}{\partial k_F^2}\right|_{sat.} = 9\rho^2 \left.\frac{\partial^2 \mathcal{E}}{\partial \rho^2}\right|_{sat.} . \tag{3.18}
$$

The volume asymmetry energy corresponds to the curvature of $\mathcal{E}$ with respect to η_t,

$$
a_t = \frac{1}{2} \left.\frac{\partial^2 \mathcal{E}}{\partial \eta_t^2}\right|_{sat.} . \tag{3.19}
$$

For the experimental values of these properties of nuclear matter one can find the following values in the literature ([13] and [14]). For the actual value of saturation density, which is most commonly denoted ρ_0 (the notation which we will also use), one can find

$$
\rho_0 = 0.16 \pm 0.02 \text{ fm}^{-3} \tag{3.20}
$$

To illustrate how high this density is compared to the densities that we can usually meet one can calculate the mass of a neutron gas at such density contained in a volume of 1 cm^3. The mass of such an object would be $\simeq 3 \cdot 10^{11}$ kg.

The actual value of the energy per nucleon at saturation density, which in symmetric matter represents the lowest energy, is

$$
\mathcal{E} = \frac{E}{A} = -15.6 \pm 0.2 \text{ MeV} \tag{3.21}
$$

The incompressibility at the same density is

$$K \approx 220 \pm 30 \text{ MeV}. \tag{3.22}$$

The asymmetry energy is

$$a_t \approx 30 \text{ MeV}. \tag{3.23}$$

n	t_n	t_n^s	t_n^t	t_n^{st}
1	0	0	0	$\frac{1}{3}$
2	-4.24	0.66	2.17	1.41
3	3.33	-0.53	-1.69	-1.11

i	α_i [fm^2]	λ_i
1	-507.17	0.1404
2	-83.22	0.1404
3	1187.7732	0.5

Table 3.1: Table of the coefficients for the nuclear potential ([9] and [11])

Now that we have introduced the effective nuclear interaction we discus some of the consequences it will have on the particles and later what effect will these changes have on the response function and cross section. First consequence is that particle mass will effectively change so we introduce the concept of effective masses for each particle species. The effective mass M^*_τ is defined by [15]

$$\frac{\partial \epsilon(\vec{k}\tau)}{\partial k} = \frac{k_{F_\tau}}{M^*_\tau}. \tag{3.24}$$

Second direct consequence will be on the chemical potential. Obviously this change will only affect the chemical potential of protons and neutrons directly. A more general formula for the calculation of the chemical potential is given by

$$\mu_\tau = \frac{\partial E}{\partial \rho_\tau}. \tag{3.25}$$

Obviously this more general expression that can be used to derive the case of free gas if we take the potential part of energy to be zero. One other note has to be made here is that for the β-equilibrium, since the chemical potential of the protons and neutrons is changed that will also indirectly, because of the requirements of the β-equilibrium, change the chemical potentials of other participating particles.

In the same manner that we introduced the chemical potential we introduce the single particle potential

$$U_\tau = \frac{\partial V}{\partial \rho_\tau}. \tag{3.26}$$

where V denotes the potential part of the total energy. With these definitions the connection between the chemical and the single particle potential can be established

$$\mu_\tau = \frac{k^2_{F_\tau}}{2M_\tau} + U_\tau \tag{3.27}$$

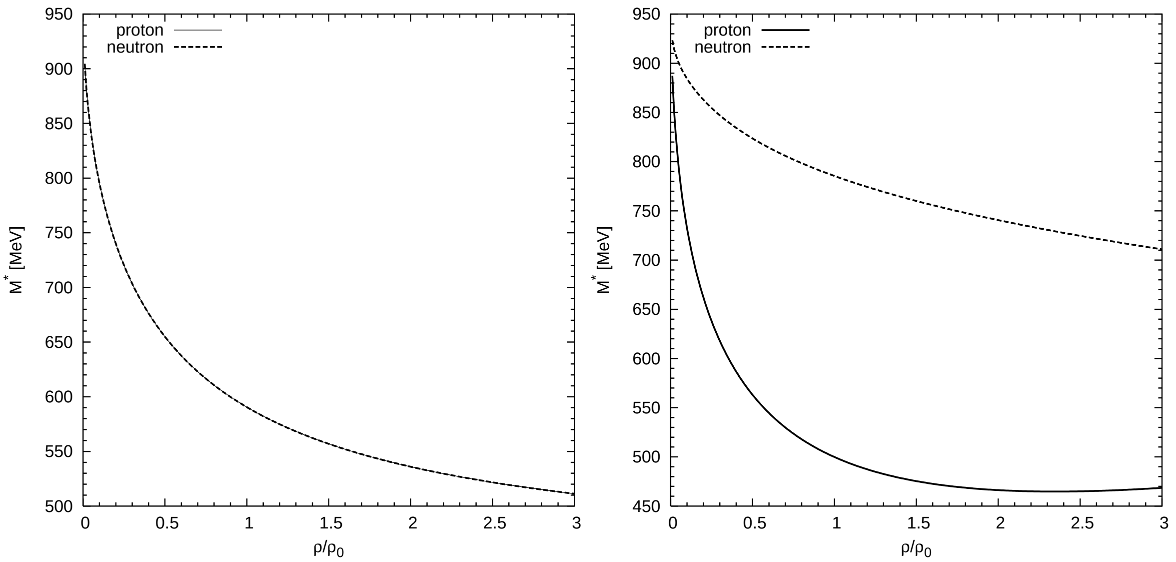

Figure 3.2: Effective mass of the nucleons for symmetric nuclear matter (left panel) and for neutron nuclear matter (right panel)

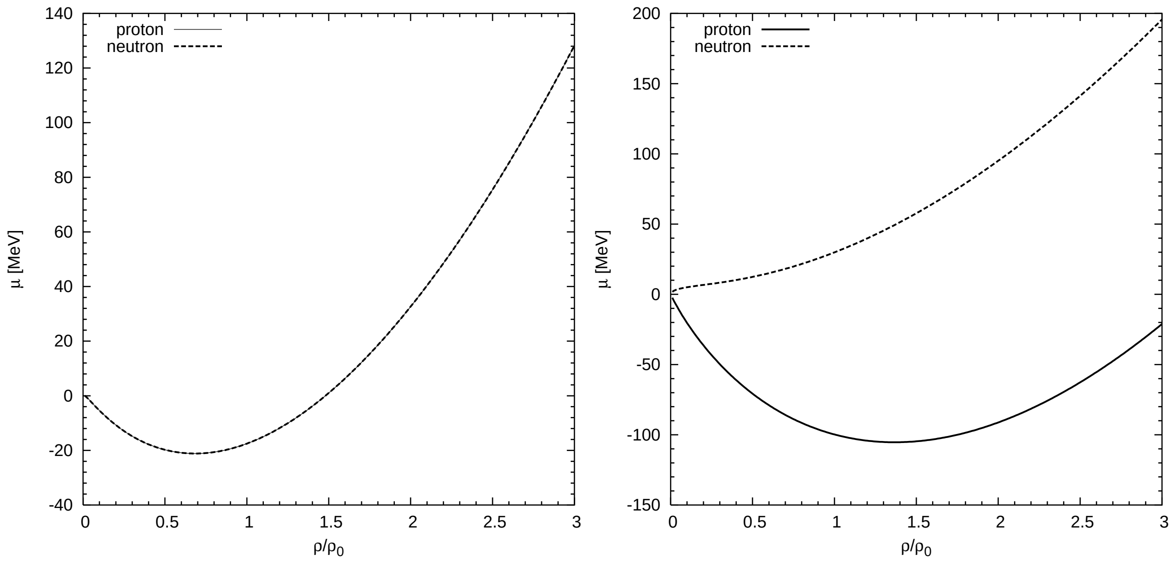

Figure 3.3: Chemical potential of particles for symmetric nuclear matter (left panel) and for neutron nuclear matter (right panel)

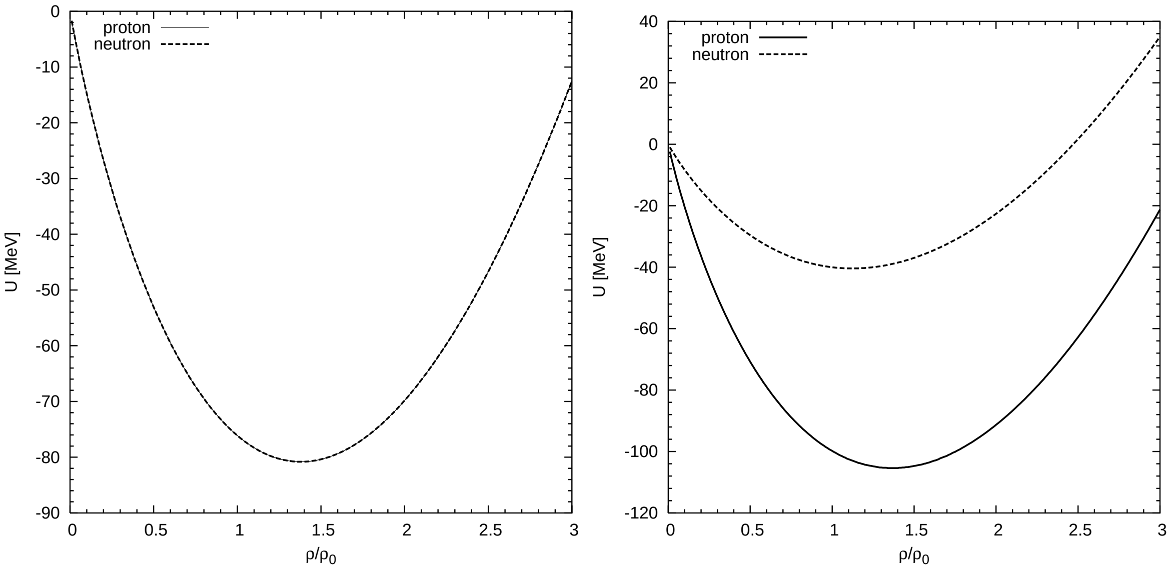

Figure 3.4: Single particle potential for symmetric nuclear matter (left panel) and for neutron nuclear matter (right panel). Variable U here denotes single particle potential of a particular particle species, proton or neutron, which means that the spin degree of freedom has been summed over.

3.2 Landau and Migdal parameters

A simple and instructive description of the residual interaction in homogeneous infinite nuclear matter is given by the Landau interaction developed in context of Fermi-liquid theory. Starting from the full density matrix in (relative) momentum space $\tilde{\rho}(\vec{k}\sigma\tau\sigma'\tau')$, the various densities are defined as [16]

$$\begin{aligned}
\tilde{\rho}_{00}(\vec{k}) &= \sum_{\sigma}\sum_{\tau}\tilde{\rho}(\vec{k}\sigma\tau\sigma\tau), & (3.28)\\
\tilde{\rho}_{1t_3}(\vec{k}) &= \sum_{\sigma}\sum_{\tau\tau'}\tilde{\rho}(\vec{k}\sigma\tau\sigma\tau')\tau^{t_3}_{\tau\tau'}, & (3.29)\\
\tilde{s}_{00}(\vec{k}) &= \sum_{\sigma\sigma'}\sum_{\tau}\tilde{\rho}(\vec{k}\sigma\tau\sigma'\tau)\sigma_{\sigma\sigma'}, & (3.30)\\
\tilde{s}_{1t_3}(\vec{k}) &= \sum_{\sigma\sigma'}\sum_{\tau\tau'}\tilde{\rho}(\vec{k}\sigma\tau\sigma'\tau')\sigma_{\sigma\sigma'}\tau^{t_3}_{\tau\tau'}. & (3.31)
\end{aligned}$$

Where the $\tilde{\rho}(\vec{k}\sigma\tau\sigma'\tau')$ is density matrix defined as in [16] and various references there in. The quantities $\sigma_{\sigma\sigma'}$ and $\tau^{t_3}_{\tau\tau'}$ are matrix elements of the Pauli matrices in spin and isospin space. The Landau-Migdal interaction is defined as

$$\begin{aligned}
\tilde{V}(\vec{k}_1\sigma_1\tau_1\sigma_1'\tau_1';\vec{k}_2\sigma_2\tau_2\sigma_2'\tau_2') &= \frac{\delta^2\mathcal{V}}{\delta\tilde{\rho}(\vec{k}_1\sigma_1\tau_1\sigma_1'\tau_1')\delta\tilde{\rho}(\vec{k}_2\sigma_2\tau_2\sigma_2'\tau_2')}\\
&= \tilde{f}(\vec{k}_1,\vec{k}_2)+\tilde{f}'(\vec{k}_1,\vec{k}_2)\vec{\tau}_1\cdot\vec{\tau}_2+\tilde{g}(\vec{k}_1,\vec{k}_2)\vec{\sigma}_1\cdot\vec{\sigma}_2+\tilde{g}'(\vec{k}_1,\vec{k}_2)(\vec{\sigma}_1\cdot\vec{\sigma}_2)(\vec{\tau}_1\cdot\vec{\tau}_2). \quad (3.32)
\end{aligned}$$

where $\mathcal{V}$ is the potential part of the energy per particle. The isoscalar-scalar, isovector-scalar, isoscalar-vector, and isovector-vector channels of the residual interaction are given by

$$\tilde{f}(\vec{k}_1,\vec{k}_2) = \frac{\delta^2\mathcal{V}}{\delta\tilde{\rho}_{00}(\vec{k}_1)\delta\tilde{\rho}_{00}(\vec{k}_2)}, \tag{3.33}$$

$$\tilde{f}'(\vec{k}_1,\vec{k}_2) = \frac{\delta^2\mathcal{V}}{\delta\tilde{\rho}_{1t_3}(\vec{k}_1)\delta\tilde{\rho}_{1t_3}(\vec{k}_2)}, \tag{3.34}$$

$$\tilde{g}(\vec{k}_1,\vec{k}_2) = \frac{\delta^2\mathcal{V}}{\delta\tilde{s}_{00}(\vec{k}_1)\delta\tilde{s}_{00}(\vec{k}_2)}, \tag{3.35}$$

$$\tilde{g}'(\vec{k}_1,\vec{k}_2) = \frac{\delta^2\mathcal{V}}{\delta\tilde{s}_{1t_3}(\vec{k}_1)\delta\tilde{s}_{1t_3}(\vec{k}_2)}, \tag{3.36}$$

Assuming that only states at the Fermi surface contribute, $\tilde{f},\tilde{f}',\tilde{g}$ and $\tilde{g}'$ depend on the angle θ between $\vec{k}_1$ and $\vec{k}_2$ only, and can be expanded into Legendre polynomials, e.g.

$$\tilde{f}(\vec{k}_1,\vec{k}_2) = \frac{1}{N_0}\sum_{l=0}^{\infty}\tilde{f}_l P_l(\cos\theta). \tag{3.37}$$

The coefficient $\tilde{f}_l$ is called Landau coefficient. Other Landau coefficient appear in the expansion of other channels, so we also have $\tilde{f}'_l$ in the expansion of $\tilde{f}'$, $\tilde{g}_l$ in the expansion of $\tilde{g}$ and $\tilde{g}'_l$ in the expansion of $\tilde{g}'$.

The normalization factor N_0 is the level density at the Fermi surface, for two-component system it is given by

$$N_0 = \frac{2M^*k_F}{\pi^2}. \tag{3.38}$$

Now if we apply the orthogonality relations for Legendre polynomials

$$\int_{-1}^{1} P_l(x)P_{l'}(x)dx = \frac{2}{2l+1}\delta_{ll'} \tag{3.39}$$

we get

$$\tilde{f}_l = \frac{2l+1}{2}N_0\int_{-1}^{1} d(\hat{\vec{k}}_1\cdot\hat{\vec{k}}_2)P_l(\hat{\vec{k}}_1\cdot\hat{\vec{k}}_2)\tilde{f}(\vec{k}_1,\vec{k}_2) \tag{3.40}$$

where $\hat{\vec{k}} = \vec{k}/|\vec{k}|$.

Since we are studying infinite nuclear matter we can choose pure neutron and proton states, which leads to $\tilde{\rho}_{1,\pm1} = 0$ and $\rho_t = \tilde{\rho}_{10}$ and similarly for all other densities. This means that we can keep only the diagonal elements of the density matrix so we have similarly as in the previous section

$$\rho(\vec{k}) = \rho_{p\uparrow} + \rho_{p\downarrow} + \rho_{n\uparrow} + \rho_{n\downarrow} \tag{3.41}$$

$$\rho_s(\vec{k}) = \rho_{p\uparrow} - \rho_{p\downarrow} + \rho_{n\uparrow} - \rho_{n\downarrow} \tag{3.42}$$

$$\rho_t(\vec{k}) = \rho_{p\uparrow} + \rho_{p\downarrow} - \rho_{n\uparrow} - \rho_{n\downarrow} \tag{3.43}$$

$$\rho_{st}(\vec{k}) = \rho_{p\uparrow} - \rho_{p\downarrow} - \rho_{n\uparrow} + \rho_{n\downarrow} \tag{3.44}$$

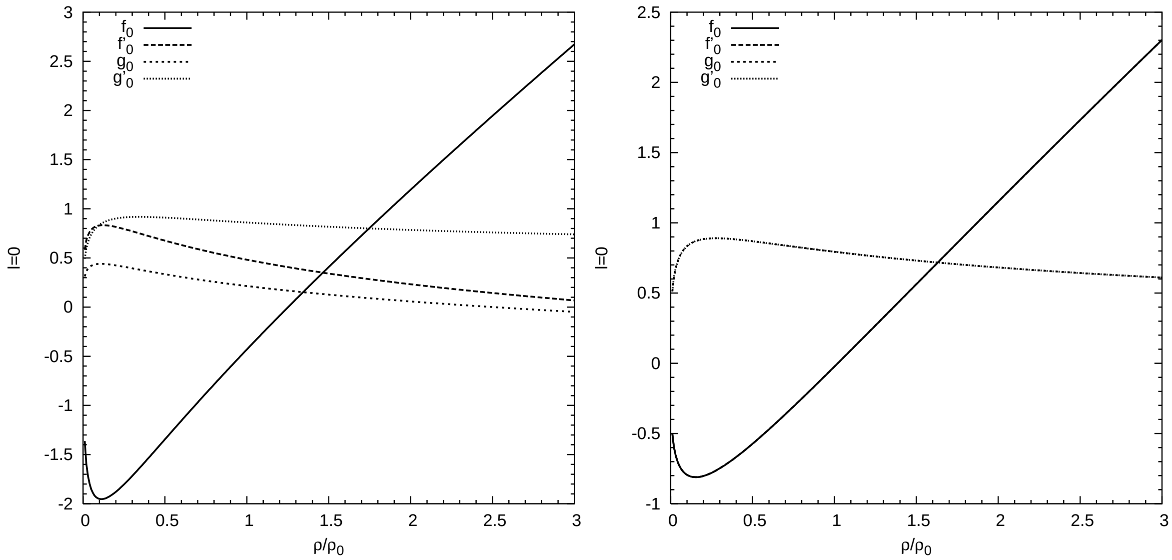

Figure 3.5: First Landau parameters for symmetric nuclear matter (left panel) and for neutron nuclear matter (right panel).

and as well

$$f(\vec{k}_1, \vec{k}_2) = \frac{\partial^2 \mathcal{V}}{\partial\rho(\vec{k}_1)\partial\rho(\vec{k}_2)}, \tag{3.45}$$

$$f'(\vec{k}_1, \vec{k}_2) = \frac{\partial^2 \mathcal{V}}{\partial\rho_t(\vec{k}_1)\partial\rho_t(\vec{k}_2)}, \tag{3.46}$$

$$g(\vec{k}_1, \vec{k}_2) = \frac{\partial^2 \mathcal{V}}{\partial\rho_s(\vec{k}_1)\partial\rho_s(\vec{k}_2)}, \tag{3.47}$$

$$g'(\vec{k}_1, \vec{k}_2) = \frac{\partial^2 \mathcal{V}}{\partial\rho_{st}(\vec{k}_1)\partial\rho_{st}(\vec{k}_2)}, \tag{3.48}$$

and then for the Landau parameters we have

$$f_l = \frac{2l+1}{2} N_0 \int_{-1}^{1} d(\hat{\vec{k}}_1 \cdot \hat{\vec{k}}_2) P_l(\hat{\vec{k}}_1 \cdot \hat{\vec{k}}_2) f(\vec{k}_1, \vec{k}_2) \tag{3.49}$$

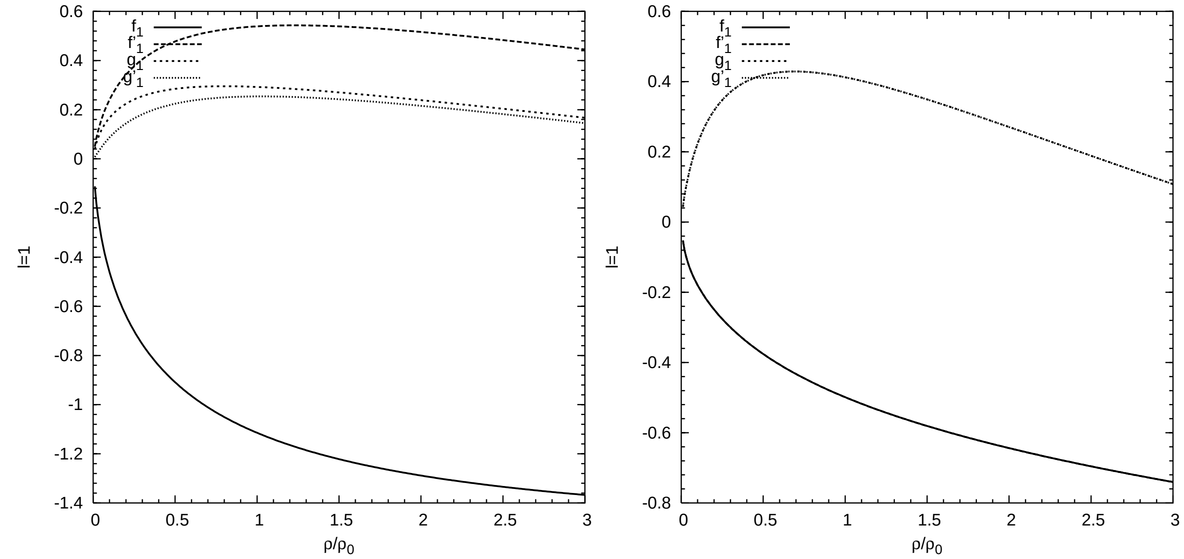

Figure 3.6: Second Landau parameters for symmetric nuclear matter (left panel) and for neutron nuclear matter (right panel).

The effective mass M^* in symmetric nuclear matter is defined by

$$\left.\frac{\partial\epsilon(\vec{k}\sigma\tau)}{\partial k}\right|_{k=k_F} = \frac{k_F}{M^*}. \tag{3.50}$$

For an isotropic system Landau, by using Galilean invariance, showed that [15]

$$\frac{M^*}{M} = 1 + \frac{1}{3}N_0 f_1 \tag{3.51}$$

where M is the free mass. The parameter f_1 is the second coefficient in the Legendre expansion of isoscalar-scalar channel of the residual interaction.

In addition to the Landau liquid parameters that we have introduced thus far here we will also introduce the Migdal parameters. It will become obvious in the next chapter why exactly we need these parameters so we will not go into it here [17].

The Migdal parameters are defined as follows

$$f_0^{\tau_\sigma \tau'_{\sigma'}}(\vec{k}_1, \vec{k}_2) = \frac{\partial^2 \mathcal{V}}{\partial\rho_{\tau_\sigma}(\vec{k}_1)\partial\rho_{\tau'_{\sigma'}}(\vec{k}_2)} \tag{3.52}$$

The connection between residual interaction channels and Migdal parameters is quite obvious and straightforward, so for the isoscalar-scalar channel we have

$$\begin{aligned} f(\vec{k}_1, \vec{k}_2) \;\; &= \;\; \frac{\partial^2\mathcal{V}}{\partial\rho_{p_\downarrow}\partial\rho_{p_\downarrow}}\frac{\partial\rho_{p_\downarrow}}{\partial\rho}\frac{\partial\rho_{p_\downarrow}}{\partial\rho} + 2\frac{\partial^2\mathcal{V}}{\partial\rho_{p_\downarrow}\partial\rho_{p_\uparrow}}\frac{\partial\rho_{p_\downarrow}}{\partial\rho}\frac{\partial\rho_{p_\uparrow}}{\partial\rho} + \frac{\partial^2\mathcal{V}}{\partial\rho_{p_\uparrow}\partial\rho_{p_\uparrow}}\frac{\partial\rho_{p_\uparrow}}{\partial\rho}\frac{\partial\rho_{p_\uparrow}}{\partial\rho} \\ &+ \;\; \frac{\partial^2\mathcal{V}}{\partial\rho_{p_\downarrow}\partial\rho_{n_\downarrow}}\frac{\partial\rho_{p_\downarrow}}{\partial\rho}\frac{\partial\rho_{n_\downarrow}}{\partial\rho} + 2\frac{\partial^2\mathcal{V}}{\partial\rho_{p_\downarrow}\partial\rho_{n_\uparrow}}\frac{\partial\rho_{p_\downarrow}}{\partial\rho}\frac{\partial\rho_{n_\uparrow}}{\partial\rho} + \frac{\partial^2\mathcal{V}}{\partial\rho_{p_\uparrow}\partial\rho_{n_\uparrow}}\frac{\partial\rho_{p_\uparrow}}{\partial\rho}\frac{\partial\rho_{n_\uparrow}}{\partial\rho} \end{aligned}$$

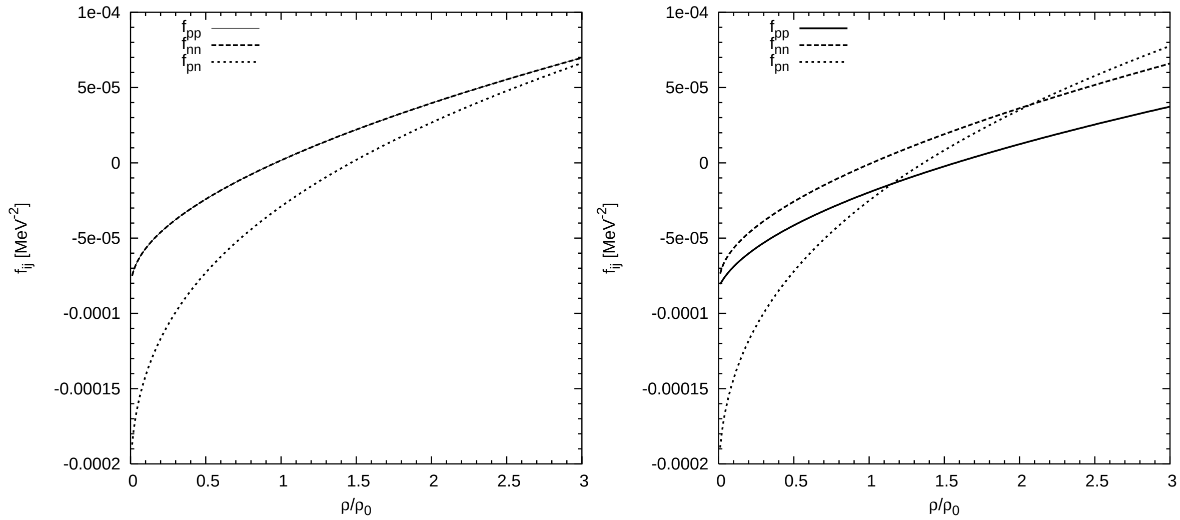

Figure 3.7: Migdal parameters with same spin states for symmetric nuclear matter (left panel) and for neutron nuclear matter (right panel).

$$+ \quad \frac{\partial^2 \mathcal{V}}{\partial \rho_{n_\downarrow} \partial \rho_{n_\downarrow}} \frac{\partial \rho_{n_\downarrow}}{\partial \rho} \frac{\partial \rho_{n_\downarrow}}{\partial \rho} + 2 \frac{\partial^2 \mathcal{V}}{\partial \rho_{n_\downarrow} \partial \rho_{n_\uparrow}} \frac{\partial \rho_{n_\downarrow}}{\partial \rho} \frac{\partial \rho_{n_\uparrow}}{\partial \rho} + \frac{\partial^2 \mathcal{V}}{\partial \rho_{n_\uparrow} \partial \rho_{n_\uparrow}} \frac{\partial \rho_{n_\uparrow}}{\partial \rho} \frac{\partial \rho_{n_\uparrow}}{\partial \rho} \tag{3.53}$$

The same connection can be established for all other channels with the aid of the inverse of the relatisnships (3.41,3.42,3.43,3.44) and the expressions (3.45,3.46,3.47,3.48).

Now the connection between Landau and Migdal parameters can easily be established (expression (3.40)). We can also define both zeroth and higher order Migdal parameters as, in the similar fashion as in (3.40)

$$f_l^{\tau_\sigma \tau'_{\sigma'}}(\vec{k}_1, \vec{k}_2) = \frac{2l+1}{2} \int_{-1}^{1} d(\hat{\vec{k}}_1 \cdot \hat{\vec{k}}_2) P_l(\hat{\vec{k}}_1 \cdot \hat{\vec{k}}_2) \frac{\partial^2 \mathcal{V}}{\partial \rho_{\tau_\sigma}(\vec{k}_1) \partial \rho_{\tau'_{\sigma'}}(\vec{k}_2)}. \tag{3.54}$$

It is common in literature for Migdal parameters in unpolarized nuclear matter to use somewhat different notation than we heve here introduced thus far, and we will also use the same convention in the next chapter. So, we have

$$f_{pp} = f^{p_\uparrow p_\uparrow} = f^{p_\downarrow p_\downarrow}; \qquad f_{pn} = f^{p_\uparrow n_\uparrow} = f^{p_\downarrow n_\downarrow}; \qquad f_{pn} = f^{n_\uparrow n_\uparrow} = f^{n_\downarrow n_\downarrow}; \tag{3.55}$$

$$g_{pp} = f^{p_\uparrow p_\downarrow} = f^{p_\uparrow p_\downarrow}; \qquad f_{pn} = f^{p_\uparrow n_\downarrow} = f^{p_\uparrow n_\downarrow}; \qquad f_{pn} = f^{n_\uparrow n_\downarrow} = f^{n_\uparrow n_\downarrow}; \tag{3.56}$$

We now once again turn to the problem of effective mass. Thus far we have only listed the connection between effective mass and Landau parameters for symmetric nuclear matter (3.51). However now with the aid of Migdal parameters we can establish a connection between effective mass of a particular species of particles and appropriate Migdal parameters in asymmetric nuclear matter.

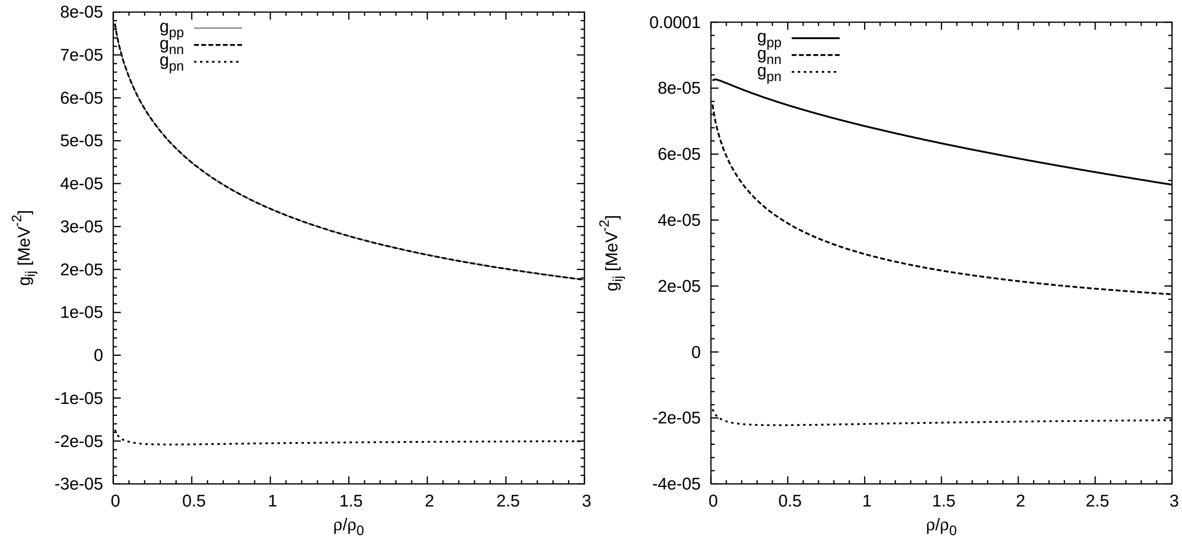

Figure 3.8: Migdal parameters with opposite spin states for symmetric nuclear matter (left panel) and for neutron nuclear matter (right panel).

In the previous section we have defined the effective mass in asymmetric but unpolarized nuclear matter (3.24). From it, just like for symmetric nuclear matter, it is possible to make a connection between Migdal parameters and effective mass as [15]:

$$\frac{M_p^*}{M} = 1 + \frac{1}{3}F_1^p \tag{3.57}$$

$$\frac{M_n^*}{M} = 1 + \frac{1}{3}F_1^n \tag{3.58}$$

where

$$F_l^p = N_0^p \left(f_l^{pp} + (k_n/k_p)^2 f_l^{pn}\right) \tag{3.59}$$

$$F_l^n = N_0^n \left(f_l^{nn} + (k_p/k_n)^2 f_l^{pn}\right) \tag{3.60}$$

Here we have introduced proton and neutron density of the state with

$$N_0^p = \frac{M_p^* k_p}{\pi^2}; \qquad and \qquad N_0^n = \frac{M_n^* k_n}{\pi^2}. \tag{3.61}$$

3.3 Polarization function in Hartree-Fock approximation

Now that we have introduced the nuclear potential and its properties we will investigate its effects on the cross section. The first and the most obvious one is that now the masses of baryons are no longer the same as before since we have introduced the effective mass concept. If we recall the expression (2.31) we can easily notice that the only place where baryon masses appear in it is the structure function, which is obvious since in fact it is constructed from the nonrelativistic propagator of baryons involved. So now the propagator will change.

Unlike the section 2.3 here we deal with the nonrelativistic but interacting baryons so single particle spectrum will now change, compared to the free gas. However we will still retain energy spectra resembling that of a free gas, as we already mentioned before,

$$E(p) = \frac{p^2}{2M^*} + U, \tag{3.62}$$

where as before M^* is the effective mass and U is the single particle potential. Because the functional dependence of the particles spectra on the momentum is identical to that of noninteracting case, the method employed earlier in section 2.3 can be easily modified to this case.

So again we start from

$$S(q_0, q) = \frac{1}{2\pi^2} \int d^3p_2 \delta(q_0 + E_2 - E_4) f_2(E_2)(1 - f_4(E_4)). \tag{3.63}$$

But now $E_4 = (\vec{p}_2 + \vec{q})^2/2M_4^* + U_4$ and the assumption of equal masses will no longer hold so we will have to distinguish between M_2^* and M_4^*. Connection with the Lindhard function is the same as before

$$S(q_0, q) = -2 \frac{Im\Pi^0(q_0, q)}{1 - \exp\left((-q_0 + \mu_2 - \mu_4)/T\right)}. \tag{3.64}$$

We will again rewrite the energy delta function in terms of angle between $\vec{p}_2$ and $\vec{q}$ as:

$$\delta(q_0 + E_2 - E_4) = \frac{M_4^*}{p_2 q} \delta(\cos\theta - \cos\theta_0) \Theta(E_2 - e_-) \Theta(e_+ - E_2), \tag{3.65}$$

where

$$\cos\theta_0 = \frac{M_4^*}{p_2 q}\left(c - \frac{\chi p_2^2}{2M_4^*}\right), \qquad p_\pm^2 = \frac{2q^2}{\chi^2}\left[\left(1 + \frac{\chi M_4^* c}{q^2}\right) \pm \sqrt{1 + \frac{2\chi M_4^* c}{q^2}}\right] \tag{3.66}$$

$$E_2 = \frac{p_2^2}{2M_2^*} + U_2; \qquad e_\pm = \frac{p_\pm}{2M_2^*}; \qquad \frac{(\vec{p}_2 + \vec{q})^2}{2M_4^2} = \frac{p_2^2}{2M_2^*} + q_0 + U_2 - U_4 \tag{3.67}$$

where the new variables are defined by the relations

$$\chi = 1 - \frac{M_4^*}{M_2^*}; \qquad c = q_0 + U_2 - U_4 - \frac{q^2}{2M_4^*}. \tag{3.68}$$

The factor $U_2 - U_4$ is the potential energy gained in converting a particle of species "2" to a particle of species "4". Substituting these results in Eq.(3.63) and performing the angular integrals we obtain

$$S(q_0, q) = \frac{M_4^*}{\pi q} \int p_2 dp_2 f_2(E_2)(1 - f_4(E_4)). \tag{3.69}$$

With the substitution $E_2 = \frac{p_2^2}{2M_2^*} + U_2$ we get

$$S(q_0, q) = \frac{M_2^* M_4^*}{\pi q} \int_{e_-}^{e_+} dE_2 f(E_2)(1 - f(E_2 + q_0)) \tag{3.70}$$

$$= \frac{M_2^* M_4^*}{\pi q} \int_{e_-}^{e_+} dE_2 \frac{1}{1 + \exp\left(\frac{E_2 - \mu_2}{T}\right)} \left(1 - \frac{1}{1 + \exp\left(\frac{E_2 + q_0 - \mu_4}{T}\right)}\right) \tag{3.71}$$

Further calculation is analogous to the section 2.3 so we will immediately go to the result, which is [4]

$$S(q_0, q) = \frac{M_2^* M_4^* T}{\pi q} \frac{\xi_- - \xi_+}{1 - \exp(-z)}. \tag{3.72}$$

where

$$z = \frac{q_0 + \mu_2 - \mu_4}{T}, \tag{3.73}$$

$$\xi_\pm = \ln \left[\frac{1 + \exp \frac{e_\pm - \mu_2 + U_2}{T}}{1 + \exp \frac{e_\pm + q_0 - \mu_4 + U_2}{T}} \right], \tag{3.74}$$

similarily as before (2.47).

For the charged current, modifications due to interactions are twofold. First the difference in neutron and proton single particle potentials appears in the response function and also in the z. Second, the response depends upon the nucleon effective mass. Since both U and M^* are strongly density dependent, the mean free paths are significantly altered from those for the noninteracting case at high density.

For neutral currents, since the initial and final state particles are identical for both leptons and baryons, we have the simplifications

$$\mu_2 = \mu_4,\ M_2^* = M_4^*,\ U_2 = U_4 \tag{3.75}$$

$$z = \frac{q_0}{T}, \qquad e_- = \frac{M_2^*}{2q^2} \left(q_0 - \frac{q^2}{2M_2^*}\right)^2, \qquad e_+ = \infty. \tag{3.76}$$

Thus, $\xi_= - z$, and one finds a result formally similar to the noninteracting expression, which is what we could have expected

$$S(q_0, q) = \frac{M_2^{*2} T}{\pi q} \left[\frac{z}{1 - \exp(-z)} \left(1 + \frac{\xi_-}{z}\right) \right]. \tag{3.77}$$

Obviously one can make an approximation from the Hartree-Fock case such to get the free gas case. It is sufficient to assume that the effective mass does not depend on density and that it is equal to the free mass. Thus we can consider a free gas as just one subcase of Hartree-Fock case.

4 RPA

In the last section of the previous chapter we introduced an improvement to the polarization function by changing the propagator of particles involved. However we still had only one loop in the polarization function. In this chapter we will consider an additional improvement of the polarization function which comes from considering higher number of loops in the polarization function such as on graph below.

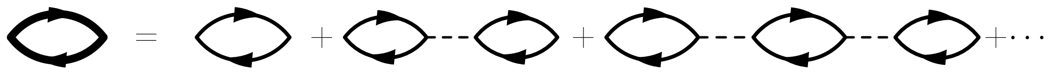

Figure 4.1: Graph representing the higher loop corrections, which we consider in this approximation. This is a better approximation then the Hartree-Fock case since the latter stops at one bubble.

The inclusion such graphs with higher number of loops represents the ring approximation or random phase approximation[1] [18]. Key point that has to be stressed out about these graphs is that there are exactly two particles participating in each loop, that is if we were to cut the graph vertically we would only cross two propagator lines. This becomes obvious if we take a look at particle-hole pair operators in random phase approximation (RPA)[2]

$$\hat{\zeta}^{\dagger}_{\alpha\beta} \equiv a^{\dagger}_{\alpha} b^{\dagger}_{\beta} \quad \hat{\zeta}_{\alpha\beta} \equiv b_{\beta} a_{\alpha}. \tag{4.1}$$

There are two of them, one is the creation and the other is the annihilation operator for particle-hole pairs. One should also note here that this is in fact quasiparticle RPA since we are using the quasipartice approximation in which we are replacing the bare mass and chemical potentials of particles with the effective ones coming from nucleon interaction.

In order to describe the graph above we need to use Dyson equation for polarization functions [4],

$$\tilde{\Pi}_{\eta\lambda\varphi\chi}(\vec{q}, q_0) = \Pi^0_{\eta\lambda\varphi\chi}(\vec{q}, q_0) + \sum_{\alpha\beta\gamma\delta} \Pi^0_{\eta\lambda\alpha\delta}(\vec{q}, q_0) K_{\alpha\delta;\beta\gamma}(\vec{q}, q_0) \tilde{\Pi}_{\beta\gamma\varphi\chi}(\vec{q}, q_0) \tag{4.2}$$

[1]This name has historic reasons and it is not very illuminating. For us case ring approximation carries much more meaning

[2]Tamm-Dancoff approximation also has the same particle-hole pair creation operator, but it does not have a particle-hole annihilation operator. So for the sake of generality we consider RPA.

where $\tilde{\Pi}(\vec{q}, q_0)$ is full polarization function, $\Pi^0(\vec{q}, q_0)$ is zeroth order polarization function, $K_{\alpha\delta;\beta\gamma}(\vec{q}, q_0)$ is kernel defined by interaction while indices

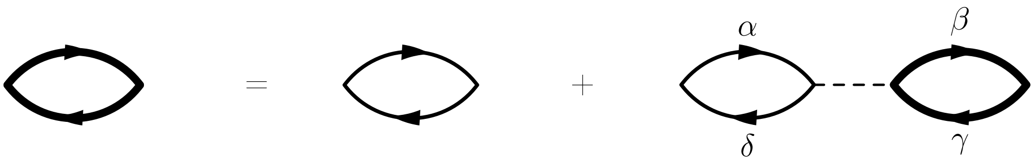

Figure 4.2: Graph representing the Dyson equation for the RPA polarization function. Thick lines bubble represents the Hartree-Fock polarization function, while the thicker bubble represents the RPA polarization function.

α, β,γ i δ only label the propagator which transmits the interaction, because of the shape of the polarization function. For fig 4.2, that is for the approximation we have made, kernel is actually just the first order kernel defined like

$$K^{(1)}_{\alpha\beta\gamma\delta} \equiv \langle \gamma\, \beta \mid V \mid \alpha\, \delta \rangle - \langle \beta\, \gamma \mid V \mid \alpha\, \delta \rangle \,, \tag{4.3}$$

where V is a potential, which defines the interaction. It has been shown [18] that this approximation indeed corresponds to the RPA because it produces the proper equation of motion.

Several things have to be noted about equations above as well as the RPA. First zeroth order polarization function is that of the previous chapter in which the participating propagator are that of Hartree-Fock approximation. Second, there is a connection between particles in one bubble, which should always be kept in mind, that while one is a particle the other is a hole. However one should also keep in mind that these holes are not antiparticles. We will not go in to further details about RPA and will just use the results about it from various references, however one should always keep in mind, when considering these results, what was the starting point of their derivation. Further details about RPA can be found in reference [18].

4.1 Polarization function in RPA approximation

If we now combine the properties of potential models that we have introduced in the previous chapter and the basic formalism of RPA which we have introduced in the previous section (here we will somewhat change the notation) we get for the polarization function [8]:

$$\Pi^{RPA}_{ij} = \frac{\Pi^0}{1 - V_{ij}\Pi^0} \tag{4.4}$$

where $V_{ij} = \delta^2 E(n)/\delta n_i \delta n_j$. Here becomes obvious why we needed the Migdal parameters in the previous chapter. Now that we have the polarization function we can also calculate the response function from it as:

$$S_{ij}(q_0, q) = -2\left[\frac{1}{1-\exp\left(-q_0+\mu_2-\mu_4\right)/T)}\right]\frac{\mathrm{Im}\Pi^0(q_0, q)}{\epsilon_{ij}(q_0, q)}, \tag{4.5}$$

$$\epsilon_{ij}(q_0, q) = \left[1 - V_{ij}Re\Pi^0(q_0, q)\right]^2 + \left[V_{ij}\mathrm{Im}\Pi^0(q_0, q)\right]. \tag{4.6}$$

In addition to the imaginary part of the polarization function, which is sufficient to evaluate the free gas nad Hartree-Fock response, the real part is also needed to evaluate the corrections due to strong interaction in RPA. At finite temperature the real part is easily evaluated numerically by using the Kramers-Kronig relation

$$Re\Pi^0(q_0, q) = -\frac{1}{\pi}\int_{-\infty}^{\infty}\frac{\mathrm{Im}\Pi(\omega, q)}{\omega - q_0}. \tag{4.7}$$

One should note here that we could have gotten the Hartree-Fock case as an approximation of Eq.(4.4) if all V_{ij} are equal zero (we have previously mentioned how to go from there to the free gas case). However it is the behaviour of these coefficients that now also influences the response function, that is, it is influenced by the interaction, which determines them. We can, depending on value of ϵ_{ij}, observe a few distinctive characteristics of response function that obviously were not there before in the other two cases. So for $\epsilon_{ij}(q_0 = 0, q) > 1$, which happens for repulsive interaction, the mediums response is suppressed. Otherwise, in for attractive interaction, the mediums response is enhanced. For strong repulsive interaction we can also have existence of collective excitations such as zero sound and spin-zero sound which could enhance the response when the energy transfer is finite and equal to the energy of collective state.

We now turn to the study of the response function in the two casees of interest to us, scattering and absorption. First for the scattering. The response function of multicomponent matter, neutrons and protons, differs in several ways from that of single-component system. At the free gas level, the neutrino cross section are influenced by compositional effects arising due to species specific neutrino matter couplings, and more importantly due to a reduction in Pauli blocking. At fixed baryon density and temperature additional baryonic components will significantly decrease the degree of particle degeneracy and enhance the scattering cross section. In neutral matter containing nucleons and leptons in β equilibrium, the proton fraction depends on dense matter EOS through the density-dependent nuclear symmetry energy.

For a two component system, the polarization function for scattering, my be written as a 2×2 matrix, with only diagonal elements, Π_p^0 and Π_n^0 (proton and neutron polarization functions). We also write the particle-hole interaction mentioned before as 2×2 matrices, in two separate channels as [8]:

$$D_V = \begin{bmatrix} f_{pp} & f_{pn} \\ f_{pn} & p_{nn} \end{bmatrix}, \qquad D_A = \begin{bmatrix} g_{pp} & g_{pn} \\ g_{pn} & g_{nn} \end{bmatrix}. \tag{4.8}$$

At this point we need, in order to interpret these coefficients, to remember the starting point of RPA. So the parameter $f_{pp}(g_{pp})$ is a measure of the matrix element between two proton and proton hole state with identical (opposite) spin projections while $f_{nn}(g_{nn})$ does the same for neutron. The parameter $f_{pn}(g_{pn})$ measures the matrix element between neutron and neutron hole and proton and proton hole states with identical (opposite) spin projections

We will first consider the vector part of the RPA polarization function and than the axial-vector part, the source of such separation will become clear later. Starting from Dyson equation

$$\Pi_V^{RPA} = \Pi^0 + \Pi_V^{RPA} D_V \Pi^0 \tag{4.9}$$

we get the same as before

$$\Pi_V^{RPA} = \frac{\Pi^0}{\mathbb{I} - D_V \Pi^0} \tag{4.10}$$

or if we use the matrix form

$$\Pi_V^{RPA} = \frac{\begin{bmatrix} \Pi_p^0 & 0 \\ 0 & \Pi_n^0 \end{bmatrix}}{\begin{bmatrix} 1 & 0 \\ 0 & 1 \end{bmatrix} - \begin{bmatrix} f_{pp} & f_{pn} \\ f_{pn} & f_{nn} \end{bmatrix} \begin{bmatrix} \Pi_p^0 & 0 \\ 0 & \Pi_n^0 \end{bmatrix}} \tag{4.11}$$

by solving this matrix equation we get

$$\Pi_V^{RPA} = \frac{1}{\Delta_V} \begin{bmatrix} (1 - f_{nn}\Pi_n^0)\Pi_p^0 & f_{pn}\Pi_p^0\Pi_n^0 \\ f_{pn}\Pi_p^0\Pi_n^0 & (1 - f_{pp}\Pi_p^0)\Pi_n^0 \end{bmatrix}, \tag{4.12}$$

where Δ_V is

$$\Delta_V = \left[1 - f_{nn}\Pi_n^0 - f_{pp}\Pi_p^0 - f_{pn}^2\Pi_p^0\Pi_n^0 + f_{pp}f_{nn}\Pi_p^0\Pi_n^0\right]. \tag{4.13}$$

Analogue to this result we can get the result for axial-vector part

$$\Pi_A^{RPA} = \frac{1}{\Delta_A} \begin{bmatrix} (1 - g_{nn}\Pi_n^0)\Pi_p^0 & g_{pn}\Pi_p^0\Pi_n^0 \\ g_{pn}\Pi_p^0\Pi_n^0 & (1 - g_{pp}\Pi_p^0)\Pi_n^0 \end{bmatrix}, \tag{4.14}$$

where Δ_A is

$$\Delta_A = \left[1 - g_{nn}\Pi_n^0 - g_{pp}\Pi_p^0 - g_{pn}^2\Pi_p^0\Pi_n^0 + g_{pp}g_{nn}\Pi_p^0\Pi_n^0\right]. \tag{4.15}$$

Multiplying the above polarization matrices by the appropriate vector and axial-vector couplings for the protons and neutrons, we arrive to the vector and axial-vector polarization functions

$$\Pi_V^{RPa} = \frac{(c_V^p)^2(1 - f_{nn}\Pi_n^0)\Pi_p^0 + (c_V^n)^2(1 - f_{pp}\Pi_p^0)\Pi_n^0 + 2c_V^p c_V^n f_{pn}\Pi_p^0\Pi_n^0}{\Delta_V}, \tag{4.16}$$

$$\Pi_A^{RPa} = \frac{(c_A^p)^2(1 - g_{nn}\Pi_n^0)\Pi_p^0 + (c_A^n)^2(1 - g_{pp}\Pi_p^0)\Pi_n^0 + 2c_A^p c_A^n g_{pn}\Pi_p^0\Pi_n^0}{\Delta_A} \tag{4.17}$$

and from there we get the response functions as

$$S_V(q_0,q) = -2\left[\frac{1}{1-\exp\left(-q_0+\mu_2-\mu_4\right)/T}\right]\mathrm{Im}\Pi_V^{RPA}(q_0,q), \tag{4.18}$$

$$S_A(q_0,q) = -2\left[\frac{1}{1-\exp\left(-q_0+\mu_2-\mu_4/T\right)}\right]\mathrm{Im}\Pi_A^{RPA}(q_0,q) \tag{4.19}$$

With these we can calculate the cross section in the RPA approximation, which will be done in the next section.

Now we turn to the calculation of response function for the case of absorption. The derivation follows in similar manner as in the case of scattering so some similar steps may be omitted. However there are several important differences. Now we only have one polarization function, combined proton and neutron, and not two separate polarization functions put together in a matrix. Also the parameters defined by interaction are different. What remains the same is that as before we will separate into two parts, vector and axial-vector, and that we start from Dyson equation and get the RPA polarization functions. So we have

$$\tilde{\Pi}_V^{RPA} = \frac{\Pi^0}{1-f_c\Pi^0}, \tag{4.20}$$

$$\tilde{\Pi}_A^{RPA} = \frac{\Pi^0}{1-g_c\Pi^0} \tag{4.21}$$

where $f_c = 2\frac{F_0'}{N_0}$ and $g_c = 2\frac{G_0'}{N_0}$. This comes from the fact that in charge current interactions both charge and isospin are transmitted, thus only the isospin changing part of the interaction is relevant. Standard separation that we have used thus far in spin aligned and spin counter aligned part also applies here. The factor 2 comes from isospin considerations.

Easily from here we get the response function as

$$\tilde{S}_V(q_0,q) = -2\left[\frac{1}{1-\exp\left(-q_0+\mu_2-\mu_4\right)/T}\right]\mathrm{Im}\frac{\Pi^0(q_0,q)}{1-f_c\Pi^0(q_0,q)}, \tag{4.22}$$

$$\tilde{S}_A(q_0,q) = -2\left[\frac{1}{1-\exp\left(-q_0+\mu_2-\mu_4\right)/T}\right]\mathrm{Im}\frac{\Pi^0(q_0,q)}{1-g_c\Pi^0(q_0,q)} \tag{4.23}$$

Similarly as in the formula (4.5) we can rewrite these response function as

$$\tilde{S}_V(q_0,q) = -2\left[\frac{1}{1-\exp\left(-q_0+\mu_2-\mu_4\right)/T}\right]\frac{\mathrm{Im}\Pi^0(q_0,q)}{\epsilon_V}, \tag{4.24}$$

$$\tilde{S}_A(q_0,q) = -2\left[\frac{1}{1-\exp\left(-q_0+\mu_2-\mu_4\right)/T}\right]\frac{\mathrm{Im}\Pi^0(q_0,q)}{\epsilon_A} \tag{4.25}$$

where

$$\epsilon_V = \left[1-f_c Re\Pi^0\right]^2+\left[f_c\mathrm{Im}\Pi^0\right]^2, \tag{4.26}$$

$$\epsilon_A = \left[1-g_c Re\Pi^0\right]^2+\left[g_c\mathrm{Im}\Pi^0\right]^2 \tag{4.27}$$

4.2 Cross section with RPA

Now that we have calculated the polarization function with RPA we turn to the calculation of the cross section for the case of RPA. In the previous section we have constantly separated the polarization function to the vector and the axial-vector part. This can be easily explained if we once again take a look at the hadron tensor and its subsequent contraction with the lepton tensor, we have calculated in the Appendix A. Just like for vector and axial-vector coupling constants we can separate the polarization function into these two components.

So now instead of coupling constants at theirs place in the cross section we have appropriate response functions as [8]

$$\frac{1}{V}\frac{d^3\sigma(E_1)}{d\Omega^2 dq_0} = \frac{G_F^2}{8\pi^3}E_3^2[1 - f(E_3)]\left[(1+\cos\theta)S_V(q_0, q) + (3-\cos\theta)S_A(q_0, q)\right] \quad (4.28)$$

In this formula response functions $S_V(q_0, q)$ and $S_A(q_0, q)$ represent both the scattering and the absorption case. The only difference between these cases, apart from the internal structure of response function, will be the function $f(E_3)$ which will in the case of scattering be the distribution function of neutrino and in the case of absorption the distribution function of a charged lepton.

5 Results and discussion

The results of our work we will present in this chapter. In the first section we will, for the sake of comparison and as a verification of our procedures, show the results for symmetric nuclear matter and in the following section we will show the results for neutron nuclear matter. The third and the fourth section will be devoted to the study of the case of β-stable nuclear matter, first without neutrinos and then with them.

Motivation for selecting exactly these cases for our study is quite obvious. First case is there because of its significance as a theoretically well know case, and because bulk of the data relating to the nuclear matter describes just this case. Also it is the simplest case because the mater is both spin and isospin symmetric so it offers a chance to test the shape of functions and expression without concentrating on the differences between particle which appear in the other cases.

The case of pure neutron matter is considered because both its practical value, it is a very good approximation to consider a cold neutron star as almost consisting solely of neutrons, and since it is also like in the case of symmetric matter a somewhat simpler case than asymmetric nuclear matter.

The other two cases are considered because those are two distinct states through which a developing proto-neutron star has to got through on hers road to becoming a neutron star, and because in fact the neutron star is in β-equilibrium for her entire existence. As mentioned in the first chapter quickly after the collapse proto-neutron star becomes opaque to neutrinos and thus begins the case of β equilibrium with the neutrinos. However as the star cools and the shock wave moves outwards star becomes transparent to neutrinos and we have the case of β equilibrium without the neutrinos, that is the chemical potential for free streaming neutrino is set to zero.

5.1 Symmetric nuclear matter

Figure 5.1 shows the neutrino differential cross section in symmetric matter. For this graph as well as for the most of other graphs of differential cross section we have chosen the transferred energy to $q = E_\nu = 30$ Mev. If we carefully look at these graphs the first thing one can notice is the broadening of the cures for Hartree-Fock and RPA compared to that of the free gas. Explanation of this effect is quite obvious if we look at the response functions we have. Obviously this increase in maximum energy transferred comes from the difference between the bare and the effective mass of the participating nucleons. The smaller the mass the larger will be the maximum energy transfer.

The previous observation came from comparing the maxima of all curves on one graph, we now compare the corresponding curves, free gas with free gas etc., between upper and lower panels. One can notice the increase in the maximum with higher density. This effect can only be assigned to also increasing chemical potential of baryons involved.

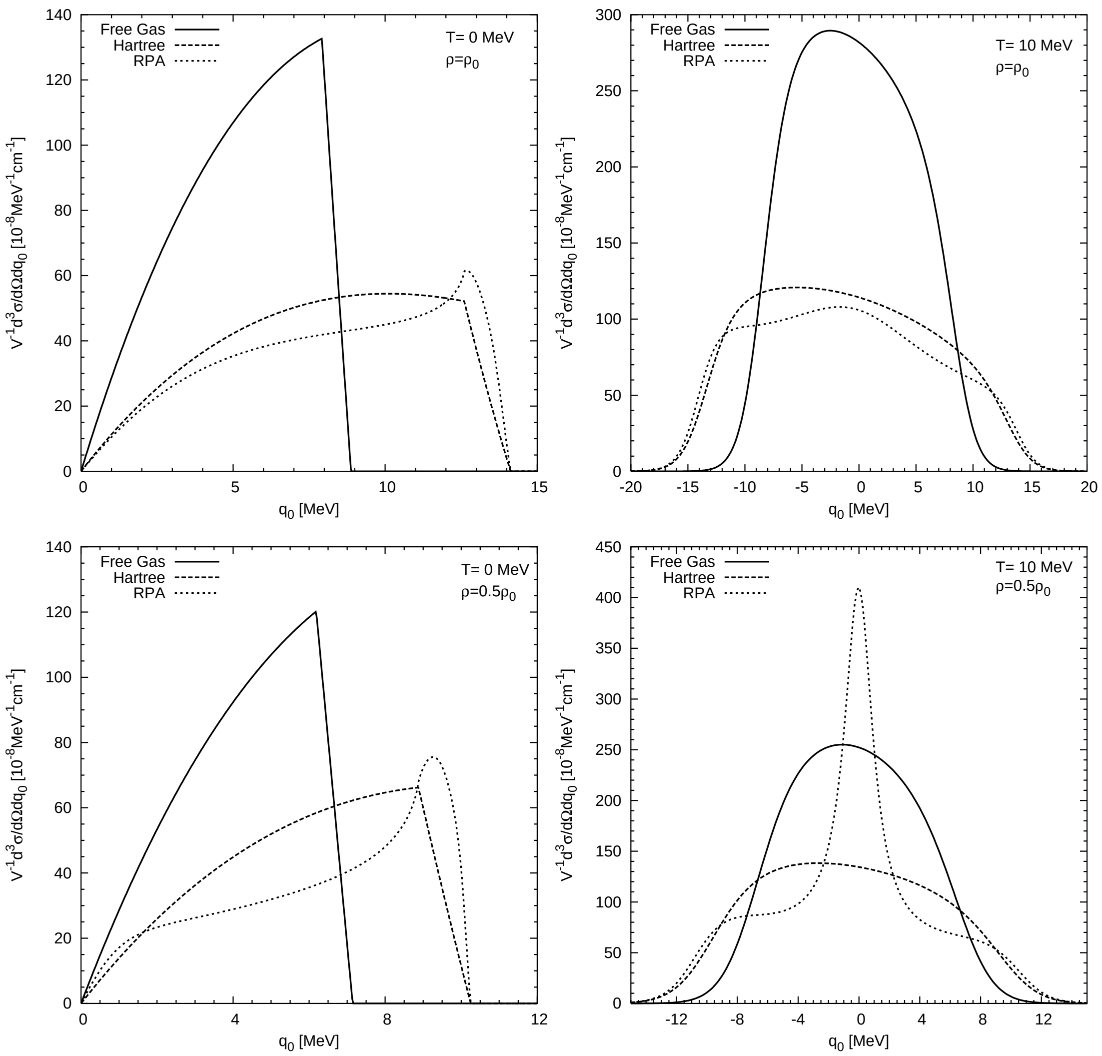

Figure 5.1: The neutrino differential cross section in symmetric matter as a function of the energy transfer for $T = 0$ Mev (left panels) and $T = 10$ Mev (right panels) at n_0 (top panels) and at $n_0/2$ (bottom panels).

In addition to appearing within the response function it self the mass or effective mass also appears as a factor in front of the response function. Keeping this in mind one can easily understand the reduction in the size of the cross section which appears if we compare the free gas curve with the curve of the Hartree-Fock and RPA. The factor 2 to

3 reduction can than partly be contributed to this difference.

If we now compare the curves for Hartree-Fock case and the curve for RPA case the biggest difference is the appearance of the peak, at the end of the curve for $T = 0$ Mev and at zero energy transfer for $T = 10$ Mev. This kind of behaviour is just what we expect because interaction is attractive so we have, as we mentioned in the chapter 4., the enhancement of mediums response. The peak is very weak for $T = 10$ Mev and $\rho = \rho_0$. But it is very strong for $T = 10$ Mev and $\rho = 0.5\rho_0$, so much that, at that point supersedes the curve for the cross section in the case of free gas. This is an important effect because if has a profound effect on the mean free path which we discuss shortly afterwards.

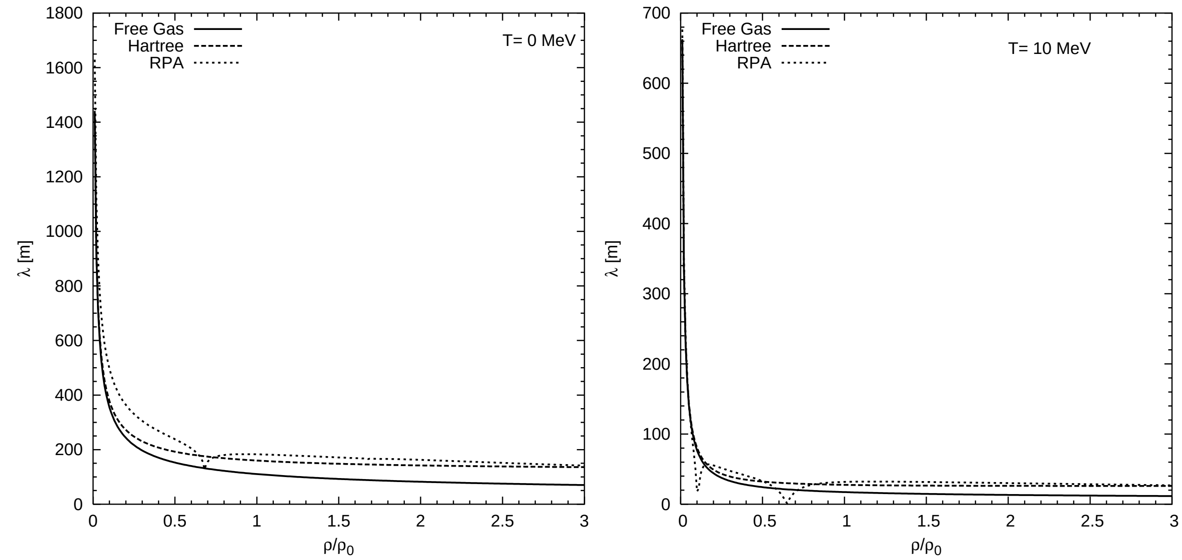

Figure 5.2: Neutrino mean free path in symmetric nuclear matter as a function of nucleon density for $T = 0$ Mev (left panel) and $T = 10$ Mev (right panel).

Figure 5.2 shows the neutrino mean free path in symmetric nuclear matter for thermalized neutrino, $E_\nu = \pi T$. The lowest densities expands all the way down to the $0.01\rho_0$ which is approximately the limit after which effects of strong interaction can no longer be observed. However, as you will be able to see, for β-equilibrium cases, we extended our calculation to much lower densities. This has been done in order to see how stable our programs are and how accurate our approach is, since it is expected that at such low densities we would get the same result for all tree approaches, free gas, Hartree-Fock and RPA.

First thing that can be noticed from these figures is that for the density range of interest to us free gas case has the shortest mean free path, Hartree-Fock case mean free path is somewhat longer and the longest mean free path belongs to the RPA case. This can be also well understood in terms of the differential cross section shown on the previous figure. The largest area under the curve belongs to the free gas case while the smallest belongs to the RPA case with Hartree-Fock case somewhere in between. From figure it is evident that as we go lower in densities the differences go smaller only to disappear completely for small enough density. This is a general observation, and an expected one as mentioned before, which will persist trough all of the cases we show.

Second thing one notices about these curves can also be linked to the behaviour that we have noticed in the differential cross section. These are the drops in the mean free path for the case of RPA, making it, for a narrow range of densities, even shorter than the free gas case. This feature has its signature in the differential cross section as an appearance of peaks for the case of RPA that goes well above the value of differential cross section for the case of free gas. As mentioned before this kind of behaviour can be contributed to the collective state which appear.

Normally what would now follow, as will have in the next sections, would be the charged current graphs. But for symmetric nuclear matter, due to the request of charge neutrality, the chemical potential of electrons is so high $\mu_e \sim 200$ Mev that it causes Pauli blocking of such magnitude that all the differential cross sections are practically zero. This in turn means that the mean free paths are practically infinite. Thus we will not show the differential cross section or the mean free path for charge currents in symmetric nuclear matter.

5.2 Neutron matter

Figure 5.3 shows the neutral current neutrino differential cross section in neutron matter. This figure is in many ways similar to the figure 5.1. As before the maximum transferred energy is 30 Mev. The main characteristic that makes this figure different is best explained on the example of the Hartree-Fock curve. The curve has two parts, one the central part is the same as for symmetric matter, but there is an additional part which appears at the end of the curve. This additional part comes from the fact that the masses, that is the effective masses, of proton and neutron are not the same. So what we have is as if two graphs have overlapped one higher in magnitude but shorter in range and the other lower in magnitude but longer in range. The same feature appears in the RPA curve, but because of the pack its origin is less obvious. And of course no such feature appears in the free gas case because the proton and neutron masses there have been made equal.

The reason that this part appears in neutron matter, although there should be no protons there, is that our entire formalism in the previous chapters has been developed for two component matter. So our pure neutron matter actually is not pure but has a very small concentration of protons. This same reason will also be the source of our program instability for mean free path and will limit us to somewhat shorter density range in some cases.

Figure 5.4 shows the neutral current neutrino mean free path in neutron nuclear matter. Here all of the features are the same as for symmetric matter. Only the differences between the mean free paths are a bit larger and for $T = 10$ Mev we have, because of

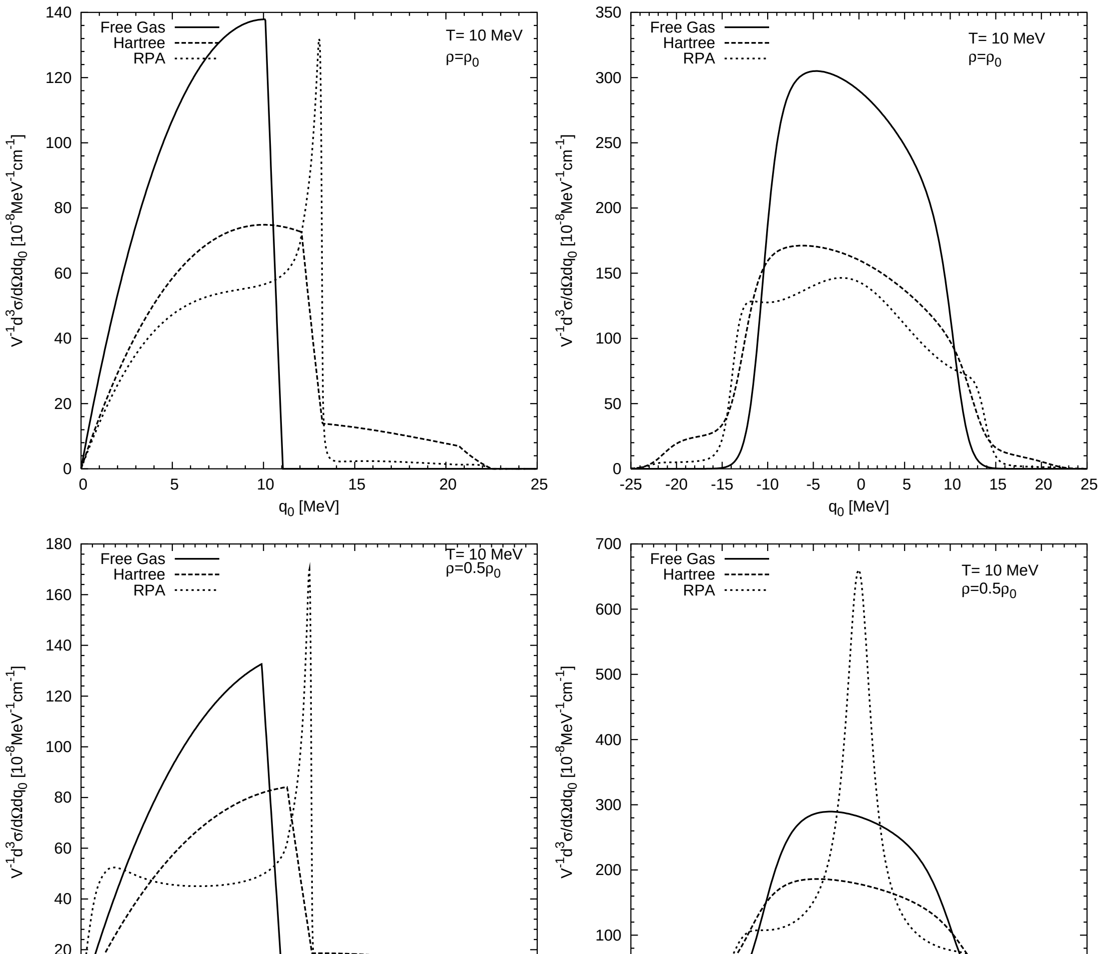

Figure 5.3: Neutral current neutrino differential cross section in neutron matter as a function of the energy transfer for $T = 0$ Mev (left panels) and $T = 10$ Mev (right panels) at n_0 (top panels) and at $n_0/2$ (bottom panels).

stability, a small density range.

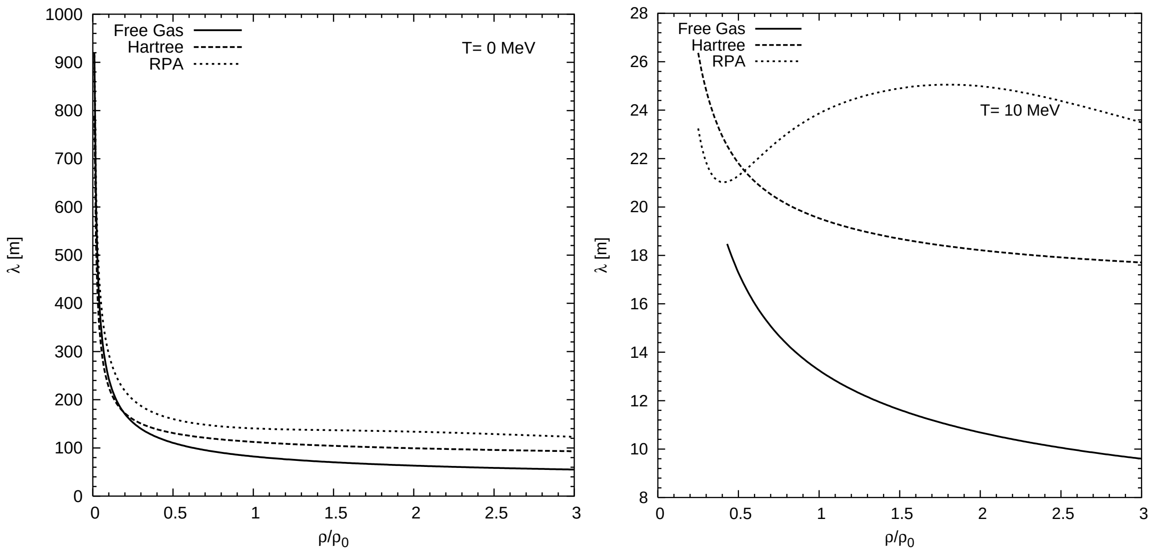

Figure 5.4: Neutral current neutrino mean free path in neutron nuclear matter as a function of nucleon density at $T = 0$ Mev (left panel) and $T = 10$ Mev (right panel).

Figure 5.5 shows the charge current neutrino differential cross section in neutron matter. As one can notice these figures for differential cross section are significantly different than those we have seen previously. This difference comes mainly from the fact that unlike before now we have different chemical potentials for two baryon particles participating in this cross section as well as different single particle potentials. This additions now significantly change the behaviour of the response function. These change manifests itself even more evidently if we now try to compare the free gas with the Hartree-Fock and RPA cases. Because no single particle potential is present in the free gas we can not even compare these two cases because they now have two different allowed ranges.

The question of allowed range now come significantly into play because of the difference between the kinematically allowed range and the allowed range of the response function. Since those two no longer overlap we have results such as in this figure where the curve for Hartree-Fock and RPA cases have an unnatural cutoff. This strange behaviour will also repeat itself in other charged current cases that will follow.

Figure 5.6 shows the charge current neutrino mean free path in neutron nuclear matter. Given a bit odd behaviour of the differential cross sections one would expect that it would have produced significantly differences between the mean free paths in the cases we have. However as one can notice several things we have expected have happened. Firstly for low densities we have no difference between the curves. Secondly at high densities all three cases give very short mean free paths. And thirdly for the intermediate density range all of the cases have different, but not to severely different, mean free paths. As in

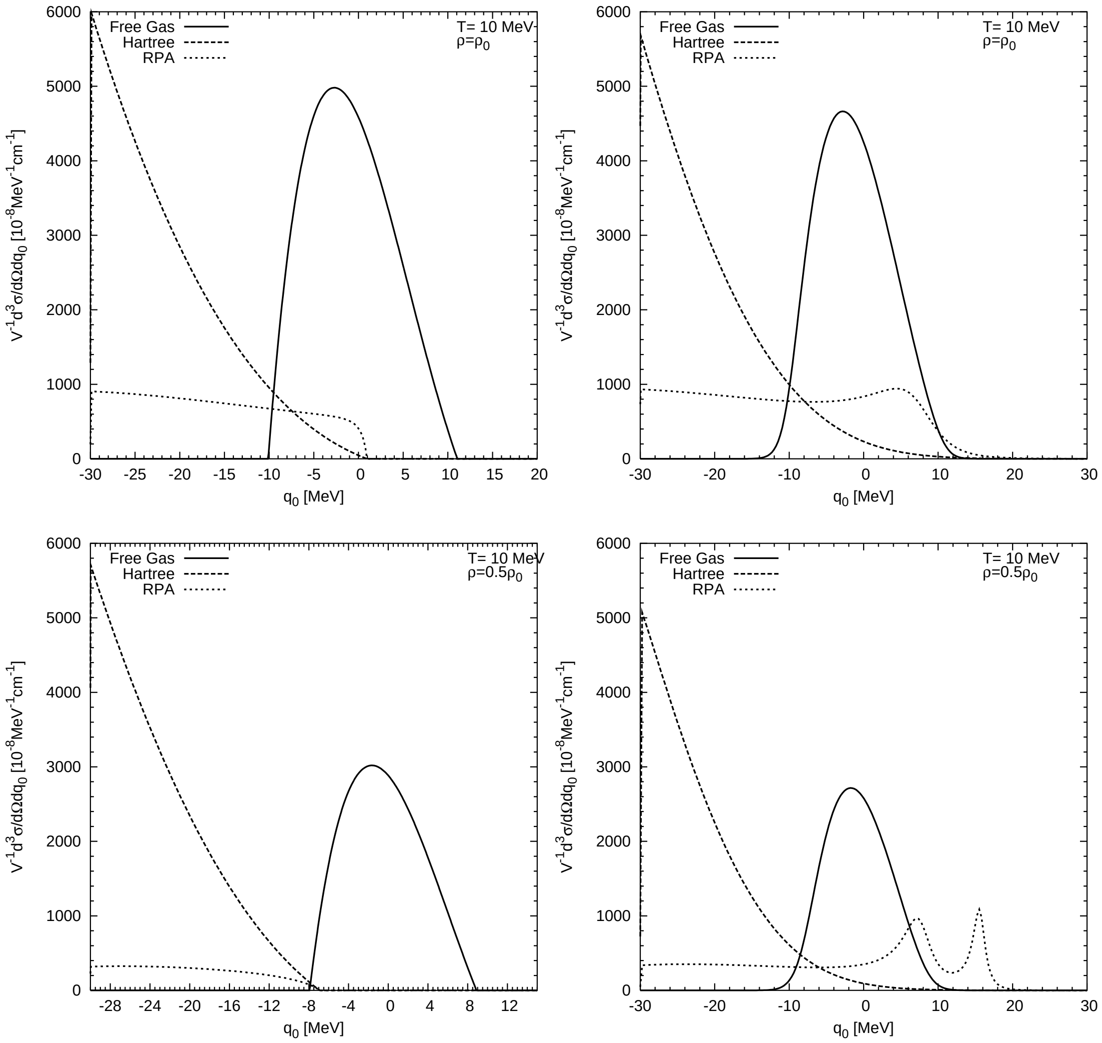

Figure 5.5: Charge current neutrino differential cross section in neutron matter as a function of the energy transfer for $T = 0$ Mev (left panels) and $T = 10$ Mev (right panels) at n_0 (top panels) and at $n_0/2$ (bottom panels).

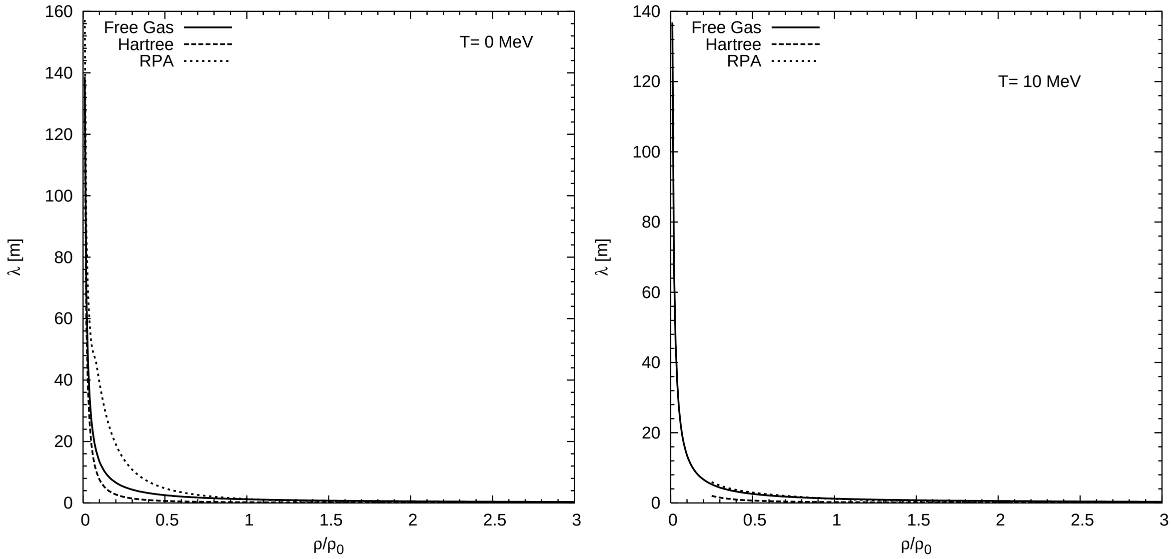

Figure 5.6: Charge current neutrino mean free path in neutron nuclear matter as a function of nucleon density at $T = 0$ Mev (left panel) and $T = 10$ Mev (right panel).

the case of neutral current for the cases of Hartree-Fock and RPA stability issues led to the termination of the calculation for the mean free path at lower densities.

5.3 β-equilibrium($\mu_\nu = 0$)

Figure 5.7 shows the neutral current neutrino differential cross section in β-stable neutrino free matter. Since we have already discussed the neutral current graphs twice we will now only point out that this graphs are no different. The small difference if that the transferred energy was now set to $q_0 = \pi * T + \mu_e$. Some of the remarks that we made earlier about strong peaks which appear in certain cases can be here observed even better.

Figure 5.8 shows the neutral current neutrino mean free path in β-stable neutrino free matter at lower temperatures. And figure 5.9 shows the neutral current neutrino mean free path in β-stable neutrino free matter at higher temperatures. As we have mentioned before for these more realistic cases of β-equilibrium we tried to extend our programs as far as the would go.

Here we have shown more temperature steps than in the previous two cases because we wanted to observe the behaviour of the mean free path with increasing temperature. As one can notice a decreasing trend can be observed which is what we expected.

Figure 5.10. shows the charge current neutrino differential cross section in β-stable neutrino free matter. This picture now is very complicated because several effects come into play and it is very difficult to distinguish which feature of the curves belongs to which effect. Especially because the different effects overlaping in some way. Here the

ρ/ρ_0	0.01	0.25	0.5	1.00	2.00
ρ_n/ρ	0.9997	0.9876	0.9758	0.9602	0.9475
μ_p(Mev)	-2.8	-41.2	-65.1	-86.3	-65.8
μ_n(Mev)	1.8	67.0	11.0	26.8	90.5
μ_e(Mev)	4.6	48.3	76.1	113.1	16.4
m_p^*(Mev)	886.11	639.75	565.56	504.02	465.92
m_n^*(Mev)	923.46	850.47	813.25	765.13	712.76
U_p(Mev)	-2.4	-43.1	-70.2	-98.9	-92.1
U_n(Mev)	-1.0	-18.4	-30.8	-43.1	-27.4
f_{pp} 10^{-5}(Mev^{-2})	-8.05	-5.16	-3.23	-0.51	3.30
f_{nn} 10^{-5}(Mev^{-2})	-7.36	-4.24	-2.56	-0.07	3.65
f_{pn} 10^{-5}(Mev^{-2})	-18.90	-10.76	-7.14	-2.50	-3.35
g_{pp} 10^{-5}(Mev^{-2})	8.22	7.48	6.63	5.36	3.78
g_{nn} 10^{-5}(Mev^{-2})	7.50	4.85	3.92	2.99	2.16
g_{pn} 10^{-5}(Mev^{-2})	-1.74	-2.19	-2.19	-2.16	-2.10

Table 5.1: Table of several parameters for the differential cross section and mean free path for some typical densities in the case of β stable neutrino free nuclear matter at $T = 0$ Mev

ρ/ρ_0	0.01	0.25	0.5	1.00	2.00
ρ_n/ρ	0.9026	0.9606	0.9619	0.9528	0.9438
μ_p(Mev)	-47.12	-60.47	-76.72	-91.93	-68.23
μ_n(Mev)	-23.87	2.27	8.05	25.00	89.50
μ_e(Mev)	23.23	62.74	84.79	116.96	157.84
m_p^*(Mev)	889.83	640.89	567.25	504.94	460.09
m_n^*(Mev)	919.48	843.62	807.48	761.54	710.91
U_p(Mev)	-2.28	-42.21	-69.84	-98.75	-92.06
U_n(Mev)	-1.11	-19.03	-31.51	-43.61	-27.78
f_{pp} 10^{-5}(Mev^{-2})	-7.80	-4.864	-3.063	-0.438	3.334
f_{nn} 10^{-5}(Mev^{-2})	-7.38	-4.238	-2.561	-0.066	3.656
f_{pn} 10^{-5}(Mev^{-2})	-18.79	-10.72	-7.131	-2.513	3.341
g_{pp} 10^{-5}(Mev^{-2})	8.04	7.170	6.412	5.250	3.731
g_{nn} 10^{-5}(Mev^{-2})	7.54	4.875	3.933	2.996	2.157
g_{pn} 10^{-5}(Mev^{-2})	-1.75	-2.179	-2.190	-2.154	-2.095

Table 5.2: Table of several parameters for the differential cross section and mean free path for some typical densities in the case of β stable neutrino free nuclear matter at $T = 10$ Mev

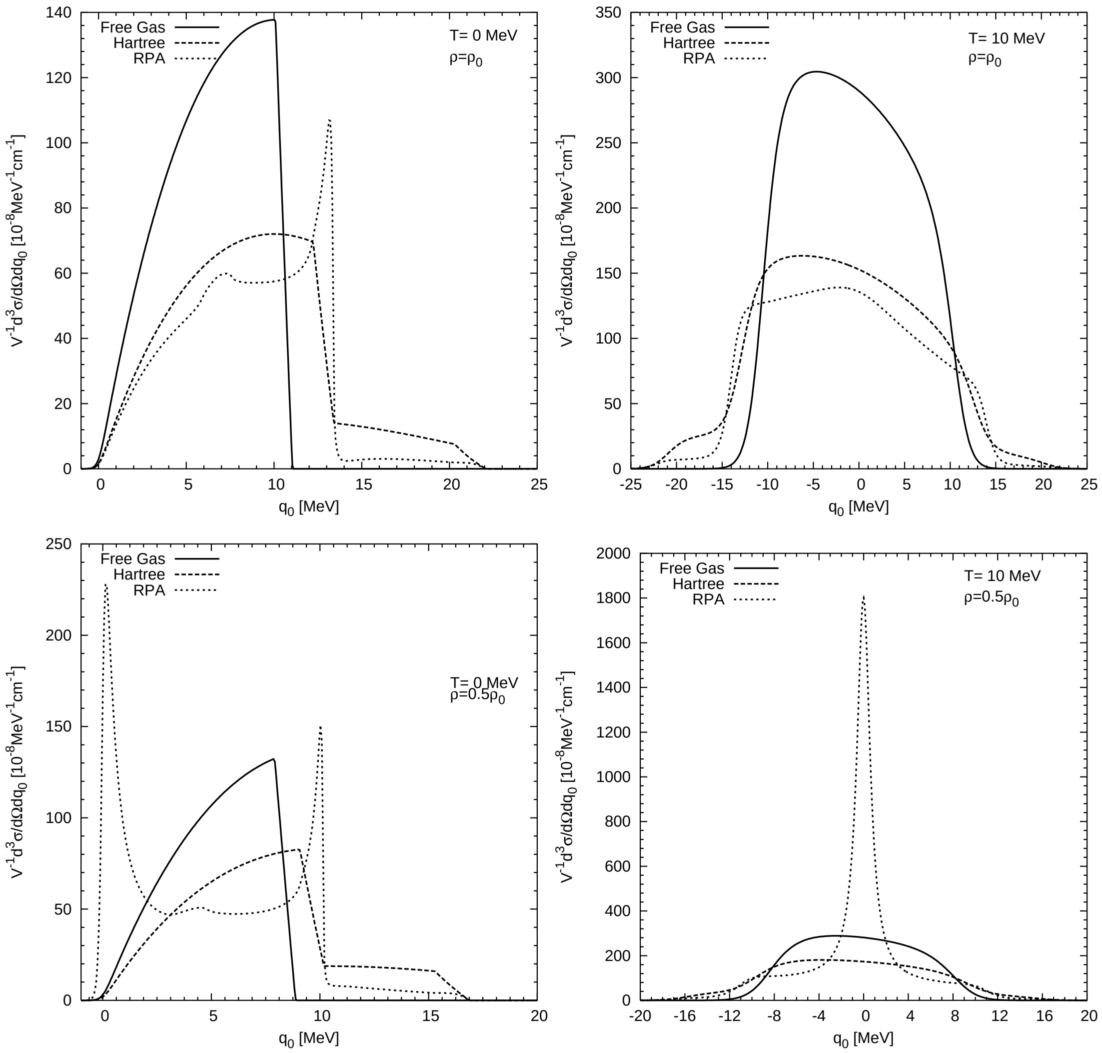

Figure 5.7: Neutral current neutrino differential cross section in β-stable neutrino free matter as a function of the energy transfer for $T = 0$ Mev (left panels) and $T = 10$ Mev (right panels) at n_0 (top panels) and at $n_0/2$ (bottom panels).

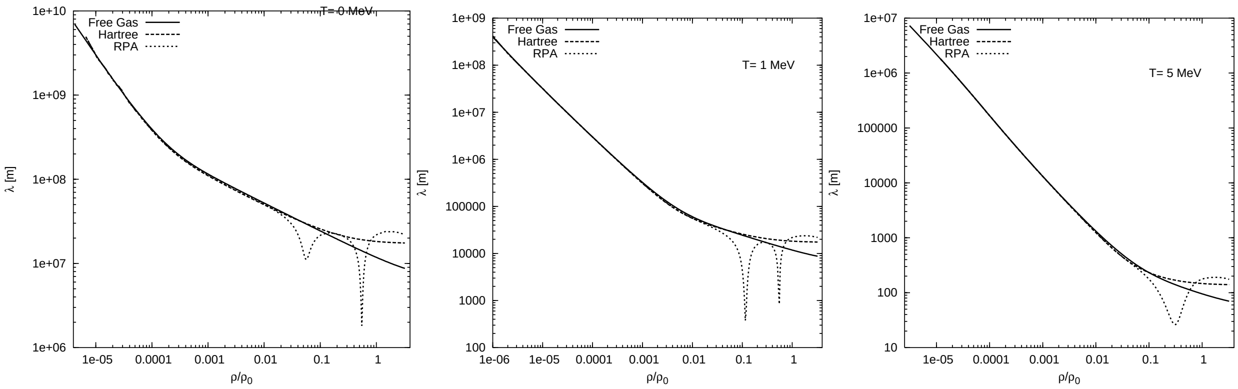

Figure 5.8: Neutral current neutrino mean free path in β-stable neutrino free matter as a function of nucleon density at $T = 0$ Mev, (left panel) $T = 1$ Mev(middle panel) and $T = 5$ Mev (right panel).

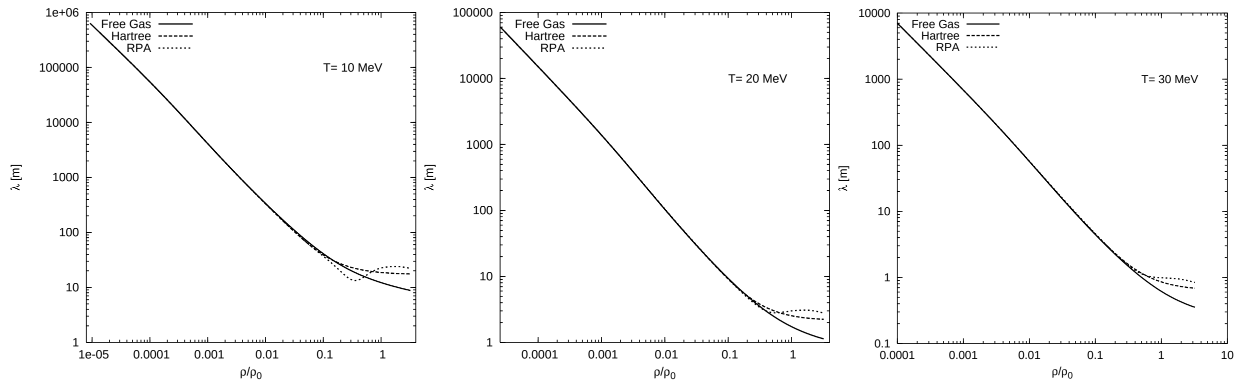

Figure 5.9: Neutral current neutrino mean free path in β-stable neutrino free matter as a function of nucleon density at $T = 10$ Mev, (left panel) $T = 20$ Mev (middle panel) and $T = 30$ Mev (right panel).

momentum was set to $|\vec{q}| = \mu_e + \pi T$.

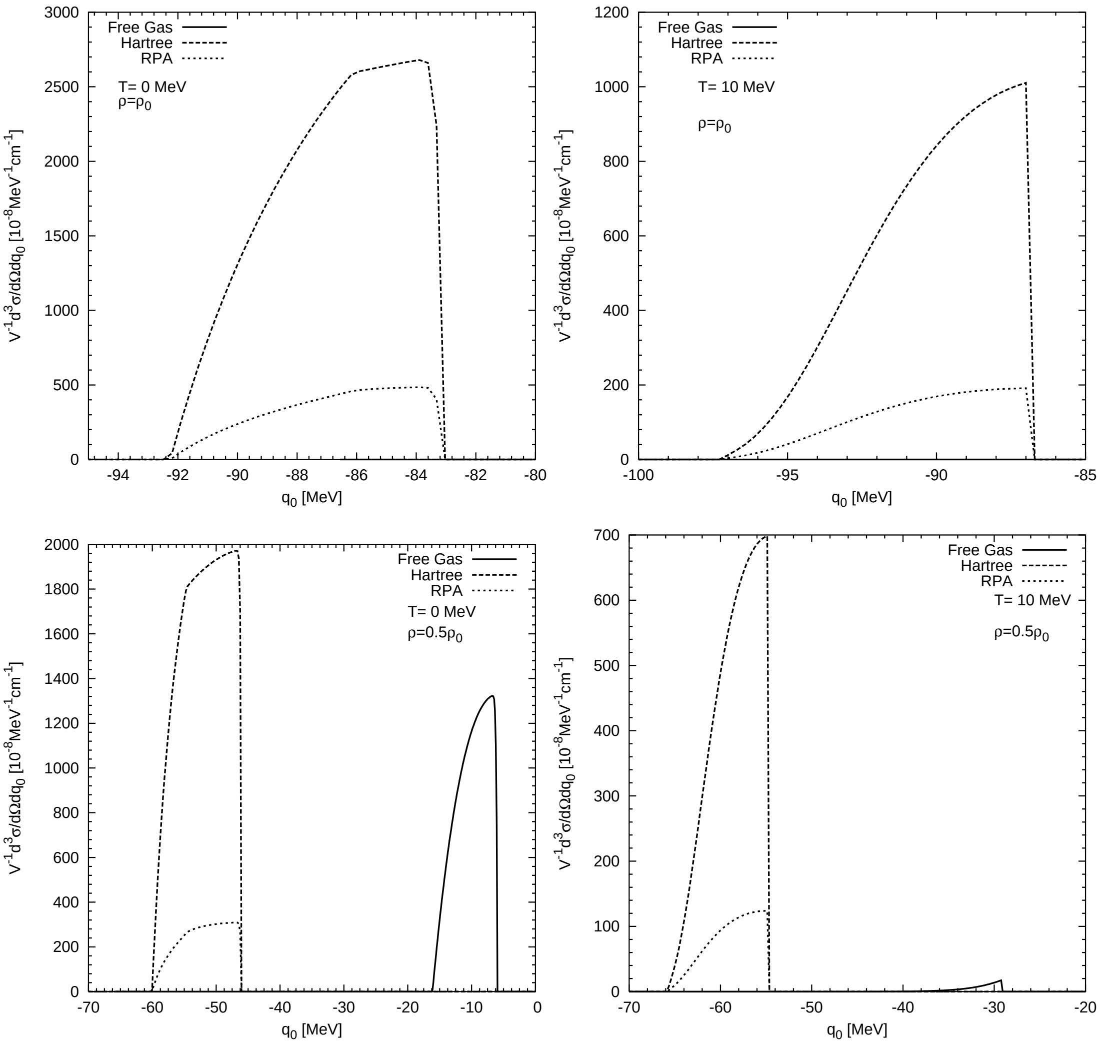

Figure 5.10: Charge current neutrino differential cross section in β-stable neutrino free matter as a function of the energy transfer for $T = 0$ Mev (left panels) and $T = 10$ Mev (right panels) at n_0 (top panels) and at $n_0/2$ (bottom panels).

These effects can be separated into three sources. First coming from the kinematics of the cross section, second coming from the Pauli blocking and third coming from the properties of the response function. The kinematics restrict allowed phase space. The Pauli blocking give us the exponential decrease for larger q_0. The properties of response function are the most complicated effect of the three. It is also the only effect by which the free gas case differs from the Hartree-Fock and RPA cases. The response function can be zero for several different set of values of exponents, which appear in it, but for us the most important one is when all of the exponents are large and thus we can neglect the contribution of the addition of one in front of the exponentials. This limiting factor as one of its parameters has, among other, the single particle potential of incoming baryons, which is zero for the case of free gas and non zero for the other cases thus giving us the different allowed ranges.

Given all of the above one can now understand why, e.g. at density equal to saturation density we have only the Hartree-Fock and RPA cases and not the free gas as well, and way are the position of the free gas case curves and other case curves so far apart.

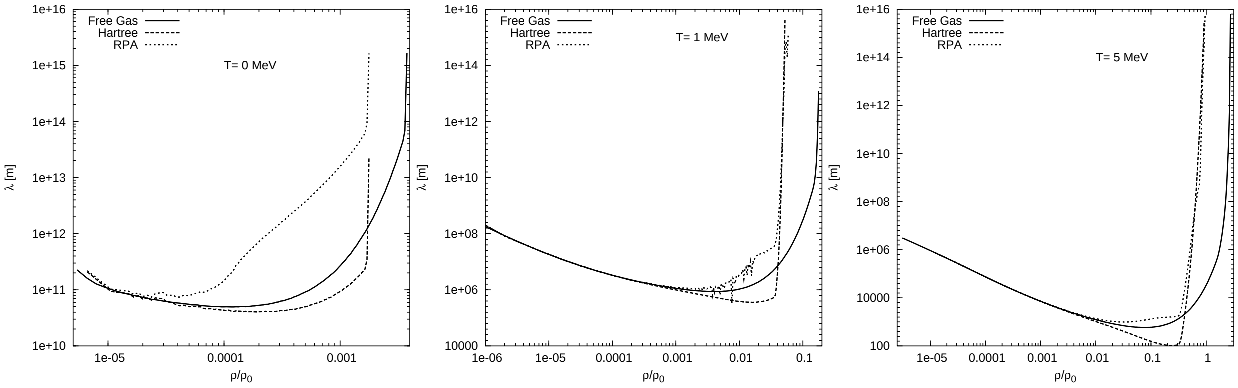

Figure 5.11: Charge current neutrino mean free path in β-stable neutrino free matter as a function of nucleon density at $T = 0$ Mev, (left panel) $T = 1$ Mev(middle panel) and $T = 5$ Mev (right panel).

Figure 5.11 shows the charge current neutrino mean free path in β-stable neutrino free matter at lower temperatures. And figure 5.12 shows charge current neutrino mean free path in β-stable neutrino free matter at higher temperatures. Discussion from above about different allowed ranges coming into play to give us very curiously looking graphs becomes even more evident here if we look at the behaviour of curves for high densities. One conclusion that can be drawn from it is that for high enough densities all of the contributions disappear giving us infinite mean free paths. As before we can notice a slow decrease in the length of the mean free path with increasing temperature for lower densities.

5.4 β-equilibrium($\mu_\nu \neq 0$)

Figure 5.13 shows the neutral current neutrino differential cross section in β-stable matter. Now that we have the neutrinos trapped we will in all cases be setting the neutrino energy to be equal to the chemical potential and the transferred momentum equal to the energy $q = E_\nu = \mu_\nu$, since only those neutrinos close to Fermi area participate.

Now that we have the neutrino chemical potential the neutral current curves will also

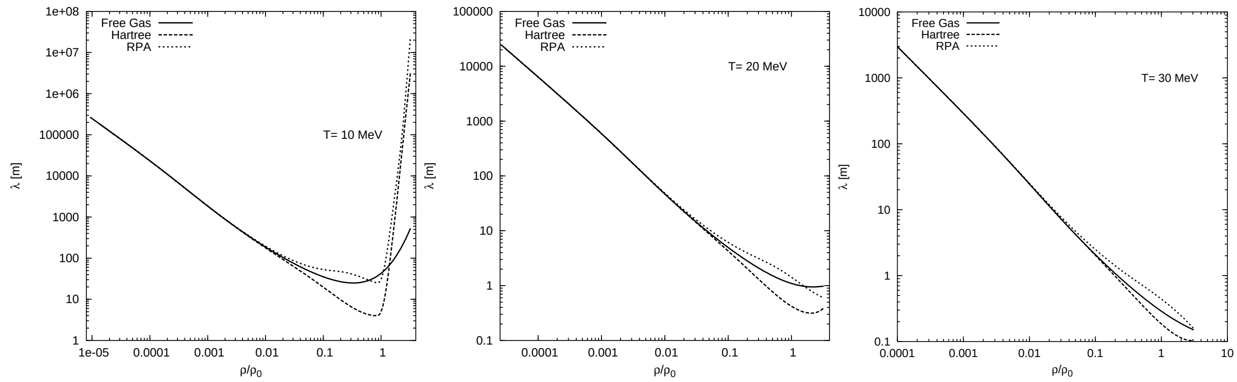

Figure 5.12: Charge current neutrino mean free path in β-stable neutrino free matter as a function of nucleon density at $T = 10$ Mev, (left panel) $T = 20$ Mev (middle panel) and $T = 10$ Mev (right panel).

ρ/ρ_0	0.01	0.25	0.5	1.00	2.00
ρ_n/ρ	0.7236	0.6984	0.6912	0.6841	0.6789
μ_p(Mev)	-0.83	-22.54	-35.00	-40.51	-31.84
μ_n(Mev)	0.87	-4.27	-6.38	2.27	59.94
μ_e(Mev)	46.51	139.92	177.79	225.71	285.90
μ_ν(Mev)	44.81	121.66	149.19	182.90	225.66
m^*_p(Mev)	895.69	680.30	611.32	546.80	495.70
m^*_p(Mev)	912.60	767.64	709.94	649.34	594.97
U_p(Mev)	-2.03	-36.92	-60.82	-87.09	-82.77
U_n(Mev)	-1.38	-26.63	-44.47	-63.39	-53.24
f_{pp} 10^{-5}(Mev^{-2})	-7.63	-4.21	-2.42	0.19	4.02
f_{nn} 10^{-5}(Mev^{-2})	-7.43	-4.19	-2.47	0.07	3.84
f_{pn} 10^{-5}(Mev^{-2})	-18.74	-10.72	-7.24	-2.82	2.79
g_{pp} 10^{-5}(Mev^{-2})	7.87	5.89	4.91	3.76	2.55
g_{nn} 10^{-5}(Mev^{-2})	7.62	5.17	4.21	3.20	2.23
g_{pn} 10^{-5}(Mev^{-2})	-1.74	-2.09	-2.10	-2.07	-2.03

Table 5.3: Table of several parameters for the differential cross section and mean free path for some typical densities in the case of β stable nuclear matter at $T = 0$ Mev

ρ/ρ_0	0.01	0.25	0.5	1.00	2.00
ρ_n/ρ	0.6929	0.6955	0.6901	0.6839	0.6789
μ_p(Mev)	-35.38	-29.57	-38.70	-42.40	-1.34
μ_n(Mev)	-26.78	-8.96	-8.89	0.94	59.21
μ_e(Mev)	41.40	138.11	176.16	224.31	284.76
μ_ν(Mev)	32.80	117.50	146.63	180.97	224.22
m_p^*(Mev)	896.72	680.91	611.55	546.87	495.73
m_p^*(Mev)	911.45	766.75	709.57	649.26	594.97
U_p(Mev)	-1.98	-36.84	-60.78	-87.08	-82.77
U_n(Mev)	-1.42	-26.73	-44.53	-63.40	-53.24
f_{pp} 10^{-5}(Mev^{-2})	-7.61	-4.21	-2.42	0.19	4.02
f_{nn} 10^{-5}(Mev^{-2})	-7.44	-4.19	-2.48	0.07	3.84
f_{pn} 10^{-5}(Mev^{-2})	-18.73	-10.72	-7.25	-2.82	-2.79
g_{pp} 10^{-5}(Mev^{-2})	7.85	5.88	4.91	3.76	2.55
g_{nn} 10^{-5}(Mev^{-2})	7.63	5.17	4.21	3.20	2.23
g_{pn} 10^{-5}(Mev^{-2})	-1.74	-2.09	-2.10	-2.07	-2.03

Table 5.4: Table of several parameters for the differential cross section and mean free path for some typical densities in the case of β stable nuclear matter at $T = 10$ Mev

feel the Pauli blocking coming from neutrinos, just like the charge current processes feel the Pauli blocking coming from electrons. Since the chemical potential of neutrinos is fairly large for these densities for zero temperature cases because of the wide kinematically allowed range we have poor resolution in the Pauli blocking allowed range.

Other than that we can here also see all of the already familiar features as in all of the previous neutral current differential cross section figures. Such as a peak for the case of RPA at $\rho = 0.5\rho_0$ and the factor of 2-3 reduction between the free gas and the Hartree-Fock cases.

Figure 5.14 shows the neutral current neutrino mean free path in β-stable matter for lower temperatures. And figure 5.15 shows the neutral current neutrino mean free path in β-stable matter for higher temperatures. Given that this is the fourth case of neutral current mean free path there is very little to be said that hasn't all ready been said. So we refer the reader to the discussions of the previous cases.

Figure 5.16 shows the charge current neutrino differential cross section in β-stable matter. As in the case of neutrino free matter we have different allowed ranges for the case of free gas and Hartree-Fock and RPA cases so it appear as if we have shifted the differential cross section between the cases. However since now we have the same values for momentum and energy transfer the cross section for the case of free gas is not destructed and is still in the picture.

One more effect, which is also common to the free gas case, becomes more evident here. That is the difference between the electron chemical potentials in the case of free gas and other two cases. This difference comes indirectly because of request for β equilibrium.

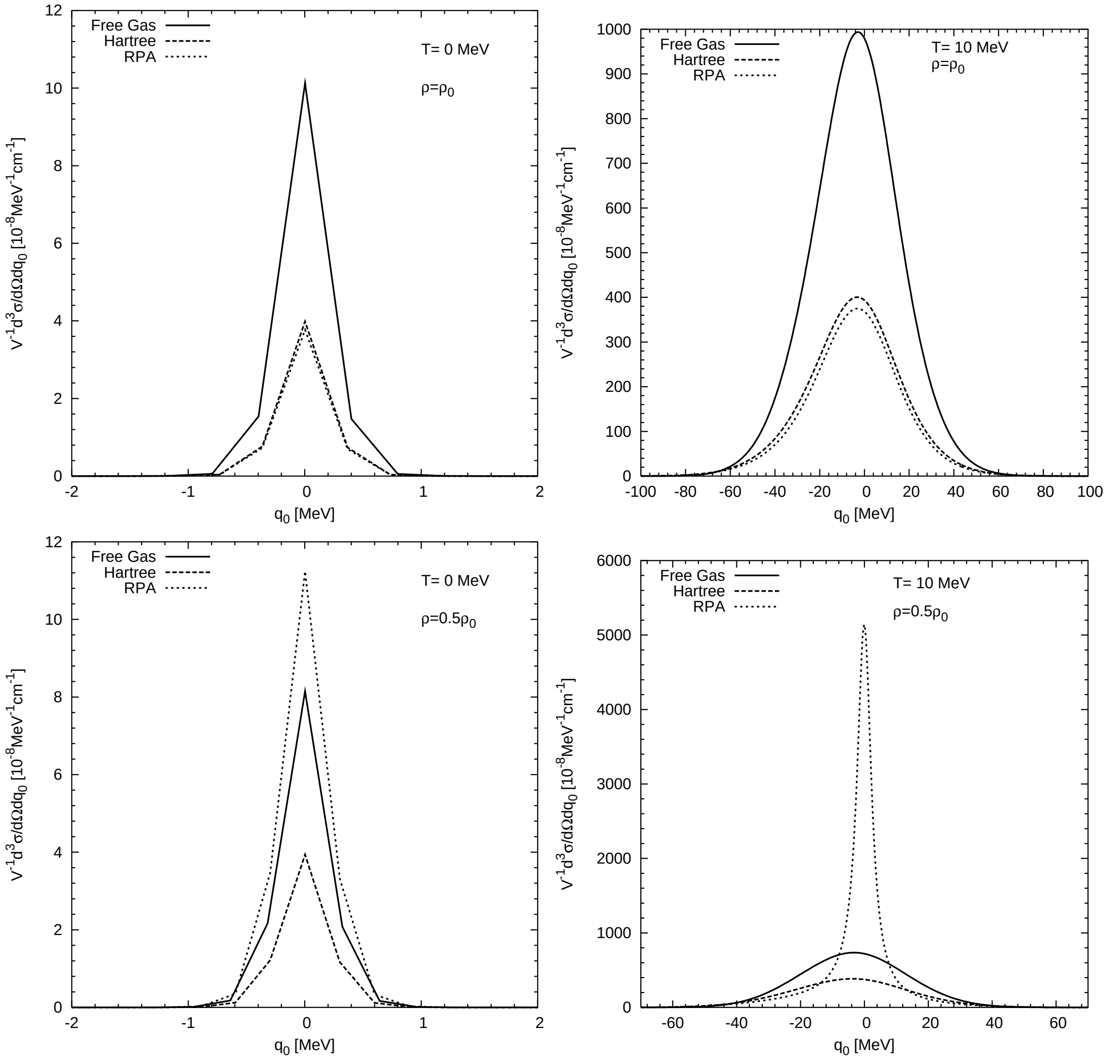

Figure 5.13: Neutral current neutrino differential cross section in β-stable matter as a function of the energy transfer for $T = 0$ Mev (left panels) and $T = 10$ Mev (right panels) at n_0 (top panels) and at $n_0/2$ (bottom panels).

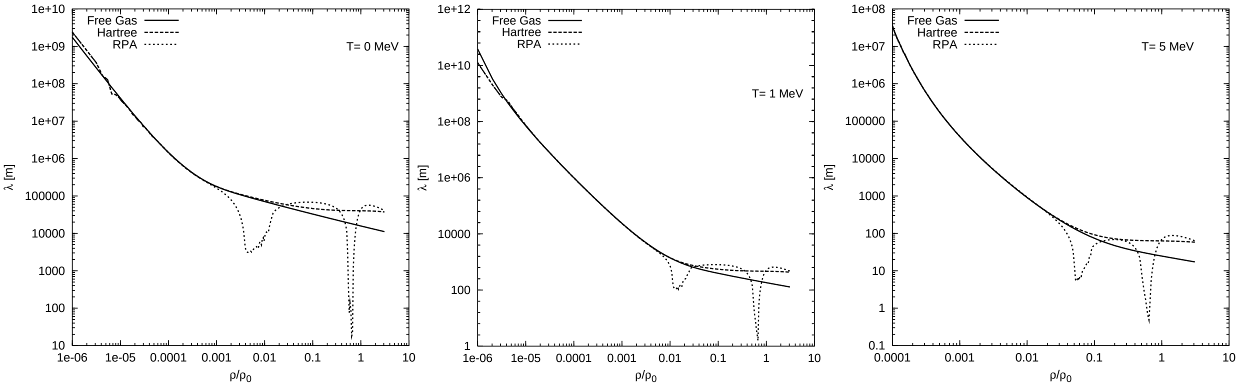

Figure 5.14: Neutral current neutrino mean free path in β-stable matter as a function of nucleon density at $T = 0$ Mev, (left panel) $T = 1$ Mev (middle panel) and $T = 10$ Mev (right panel).

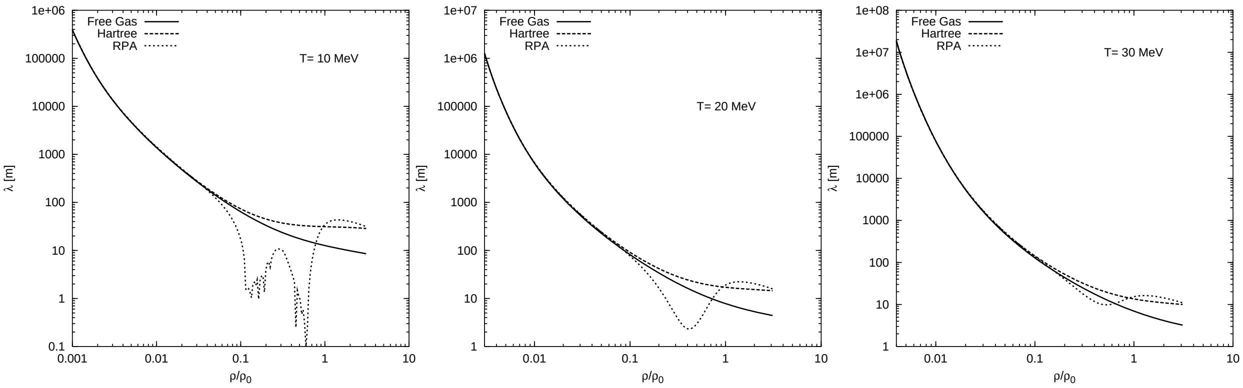

Figure 5.15: Neutral current neutrino mean free path in β-stable matter as a function of nucleon density at $T = 10$ Mev, (left panel) $T = 20$ Mev (middle panel) and $T = 30$ Mev (right panel).

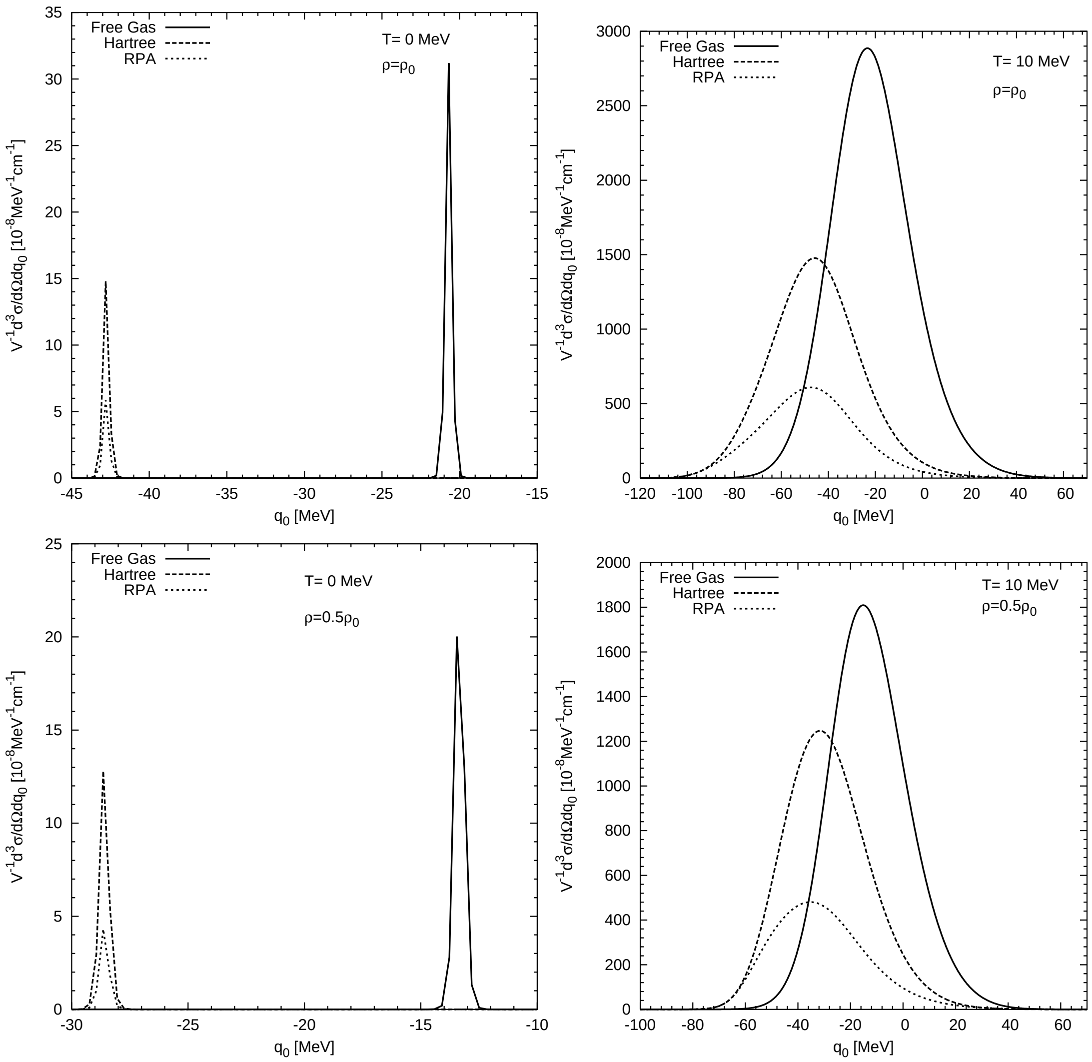

Figure 5.16: Charge current neutrino differential cross section in β-stable matter as a function of the energy transfer for $T = 0$ Mev (left panels) and $T = 10$ Mev (right panels) at n_0 (top panels) and at $n_0/2$ (bottom panels).

This is more obvious for the figures of mean free path.

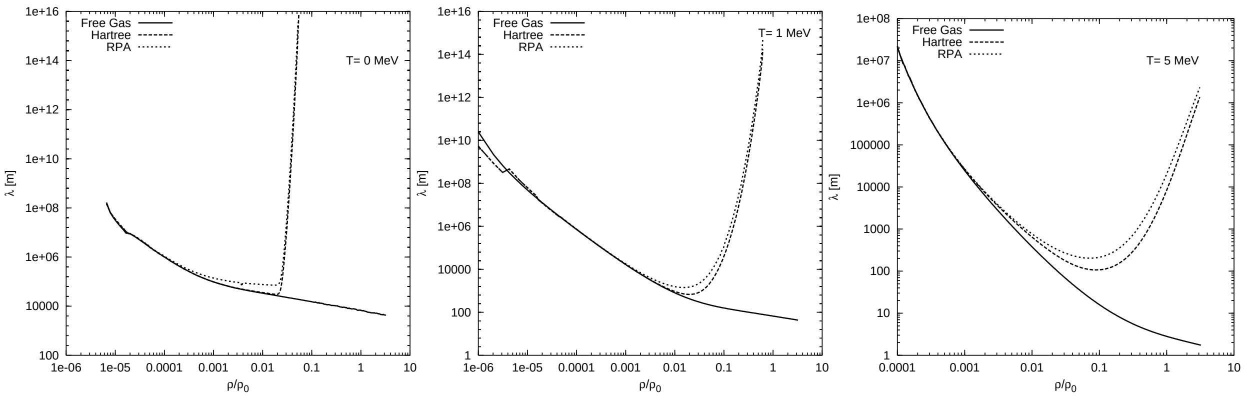

Figure 5.17: Charge current neutrino mean free path in β-stable matter as a function of nucleon density at $T = 0$ Mev, (left panel) $T = 1$ Mev (middle panel) and $T = 5$ Mev (right panel).

Figure 5.17 shows the charge current neutrino mean free path in β-stable matter for lower temperatures. And figure 5.18 shows the charge current neutrino mean free path in β-stable matter for higher temperatures. In these graphs the effect of different electron chemical potential, and thus different Pauli blocking, can be seen in the much larger mean free path for the cases of Hartree-Fock for larger densities.

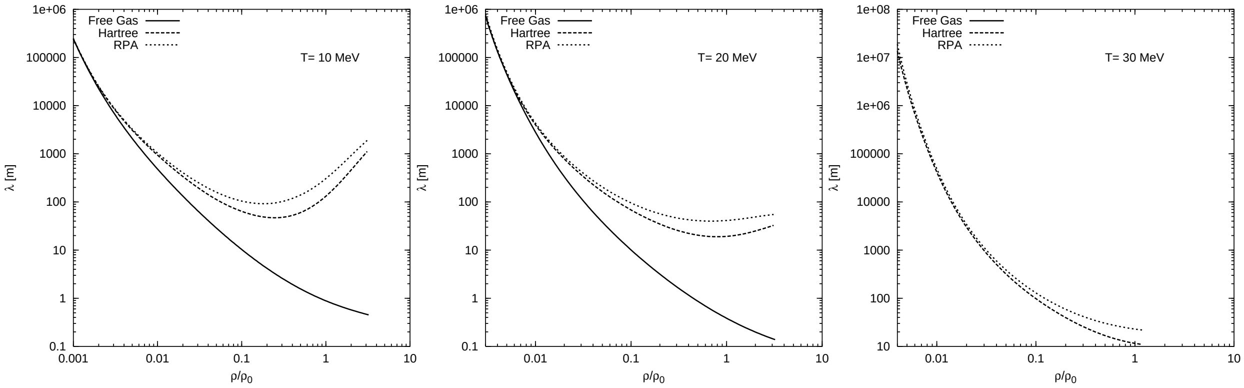

Figure 5.18: Charge current neutrino mean free path in β-stable matter as a function of nucleon density at $T = 10$ Mev, (left panel) $T = 20$ Mev (middle panel) and $T = 30$ Mev (right panel).

6 Summary

The goal of this thesis was to investigate the effects of strong interaction on behaviour of neutrinos in nuclear matter composed of protons, neutrons, electrons and sometimes neutrinos. Trough the chapters we have gradually progressed to that goal and in the previous chapter we finally reached it. We began by a description of some of the characteristics of supernova, to be more precise core collapse supernova. We described the process in which a proto-neutron star forms and explained in short what happens on the large scale of proto-neutron, and subsequent neutron, star evolution, how the cooling proceeds and why the neutrinos are so important in such an event. In some detail we described how with neutrino trapping and shock breakthrough the proto-neutron star changes significantly in those two points of its evolution. Transition between these two states is very important because that is the first signal of a supernova that we can observe, if the event is close enough to the Earth. The idea of early detection of a galactic supernova via neutrinos became the basis for **S**uper**n**ova **E**arly **W**arning **S**ystem (**SNEWS**). If this were to work a signal from several neutrino detectors would be used to detect a supernova and then warn optical observatories to an upcoming optical part of supernova signal. One additional importance of a large number of neutrino detectors is that the amount of information collected by them about a supernova, its proto-neutron star and even about the remnant would be unprecedented. The data gathered would for the first time give us information about the supernova layers structure as well as the internal proto-neutron star structure. This information would help constrain a large number of supernova numerical simulation as well as various parts of physics, which appear there in.

After the introduction we studied the neutrino interaction with the particles of interest to us within the framework of electroweak theory. However we did not use full electroweak theory but an approximation in which we considered vector bosons as if they had infinite mass. From the Lagranian with such an approximation we calculated the total and the differential cross section as well as defined the mean free path. During that calculation, since the particles are in medium, we introduced a function describing the mediums influence on the cross sections. This function is what we were mainly interested in since it describes how the strong interaction affects the cross section. In the same chapter we also defined the chemical potential and the requirements for the β equilibrium.

The next step was to introduce the nuclear potential, which defines the equation of state. This was the description of the strong interaction whose effect we wanted to study. First we introduced the basic formalism which was to help us calculate the quantities which we needed and also to compare our EOS with others (Fig. 3.1). As a step further we introduced the formalism of Landau liquid theory, which was needed to study the effects of strong interaction beyond the Hartree-Fock approximation we had at that point. One important thing that should be noted that all of our expressions, were for asymmetric nuclear matter, unless an approximation was specifically listed. Our contribution to this chapter was the introduction of a combination of two different potentials, one coming from the Brueckner G-matrix calculation [10] and the other phenomenological one [11]. In addition we also calculated the expectation value of this combined potential in as general manner as possible, because we were primarily interested in asymmetric nuclear matter. Also all of the considerations of residual interaction in the Landau liquid formalism were done keeping in mind this interest in asymmetric nuclear matter.

The final theoretical part of the thesis was the inclusion of the calculation on how the strong interaction introduces higher order correction to the response of medium. This step was done in the ring approximation. Thank to the nature of the strong interaction corrections form a geometric series, which is then easily solvable [8].

The final chapter of the thesis is the presentation of the results, which we have calculated with the aid of our programs. The results that we got were for the most part expected but there were several, which deviated from our expectations. However upon close inspection these deviation turned explainable given the parameters have been chosen. The figures we got for the cases of symmetric matter and neutron matter can be to a certain degree verified by comparison with some of the other works on this subject, such as [5] and [8]. Other cases are too specific for anything than a qualitative comparison. This comes from the fact that the strong interaction influence is twofold, both changing the β-equilibrium and the response of the matter. This chapter was our main contribution to the thesis as a result of nine months work.

However in this nice picture of the thesis, which was presented here, we did not mention several things that this thesis lacked. A careful reader can notice is the plural "paths" that we used in the title of the thesis. This is not accidental, although neutrino only has one "real" mean free path. This comes from the fact that we did not calculate the neutrino cross section on electrons that were present in the medium. Thus we could not calculate "real" total mean path, but only several separate mean free paths coming from different processes.

Several other shortcomings also appear if one takes a closer look at the thesis. One of them is the usage of Fermi weak and not full electroweak theory. Although this is a valid approximation here, if one wanted to go to higher energy this approximation would breakdown. One of the approximations that we made relates to the hadrons and leptons. We took all hadrons as nonrelativistic and all leptons as fully relativistic. For the most part this is a good approximation, especially so for hadrons. But when we go to lower densities as chemical potentials of leptons decrease this approximation worsens.

One of the more easily reparable choices in this thesis is the choice of the medium composition, which in our case is just composed of protons, neutrons, electrons and neutrinos. Although in the section 2.4 we have presented a somewhat more general approach, which included muons as well as electrons we did not consider a medium with muons later on. This has been done because initial considerations of β equilibrium that had muons showed that the percentage of muons at densities which we considered were negligible while the computational time was significantly longer. So we did not consider them later at all.

As one consider what would be the possible way to contintinue this work, apart form improving the approximations and adding some more particles to the medium, several options present them selves. First one is to try out several other set of parameters for the central part of the potentials well as to try out several other types of potentials. This could become especially important if one is to consider all pars of the calculation in a more relativistic way. This would mean that the cross section, polarisation function and the potential would be expressed in a relativistic way. This would give us a more consistent way to approach this problem. However this would make the approach to RPA trough Landau liquid theory and Migdal parameters much more complicated than it is now.

Appendix A

We begin from the invariant matrix element

$$\mathcal{M}_{fi} = \frac{G_F}{\sqrt{2}} j_\mu J^\mu \tag{6.1}$$

where the weak currents are defined as

$$j_\mu = \bar{\psi}'(x)\gamma_\mu(1-\gamma_5)\psi(x) \tag{6.2}$$

$$J^\mu = \bar{\Psi}'(x)\gamma_\mu(V - A\gamma_5)\Psi(x) \tag{6.3}$$

and the fermions functions are given by

$$\psi(x) = \sum_{sp} \left(\frac{m}{VE_p}\right)^{\frac{1}{2}} c_s(\vec{p})u_s(\vec{p})e^{-ipx} \tag{6.4}$$

We then construct the squared matrix element as

$$\sum_{s_i,s_f,S_i,S_f} |\mathcal{M}_{fi}|^2 = \frac{G_F^2}{2} L_{\mu\nu} W^{\mu\nu} \tag{6.5}$$

where the lepton tensor $L_{\mu\nu}$ is

$$L_{\mu\nu} = \sum_{s_i,s_f} j_\mu^* j_\nu = \tag{6.6}$$

$$= \sum_{s_i,s_f} [\bar{u}(k_f,s_f)(\gamma_\mu - \gamma_\mu\gamma_5)u(k_i,s_i)]^* [\bar{u}(k_f,s_f)(\gamma_\nu - \gamma_\nu\gamma_5)u(k_i,s_i)]$$

$$= \sum_{s_i,s_f} \left[\bar{u}(k_i,s_i)\gamma_0(\gamma_\mu^\dagger - \gamma_5^\dagger\gamma_\mu^\dagger)\gamma_0^\dagger u(k_f,s_f)\right] [\bar{u}(k_f,s_f)(\gamma_\nu - \gamma_\nu\gamma_5)u(k_i,s_i)] \tag{6.7}$$

With the aid of the rules for Dirac gamma matrices

$$\gamma_0^\dagger = \gamma_0, \qquad \gamma_5^\dagger = \gamma_5, \qquad \{\gamma_\mu, \gamma_5\} = 0, \qquad \gamma_0\gamma_\mu^\dagger\gamma_0 = \gamma_\mu \tag{6.8}$$

we calculate the lepton tensor:

$$L_{\mu\nu} = \sum_{s_i,s_f} [\bar{u}(k_i,s_i)(\gamma_\mu - \gamma_\mu\gamma_5)u(k_f,s_f)] [\bar{u}(k_f,s_f)(\gamma_\nu - \gamma_\nu\gamma_5)u(k_i,s_i)] \tag{6.9}$$

$$= tr\left[\sum_{s_i} u(k_i,s_i)\bar{u}(k_i,s_i)(\gamma_\mu - \gamma_\mu\gamma_5)\sum_{s_f} u(k_f,s_f)\bar{u}(k_f,s_f)(\gamma_\nu - \gamma_\nu\gamma_5)\right] \tag{6.10}$$

Give our choice of normalization we have

$$\sum_s u(k,s)\bar{u}(k,s) = \frac{k_\mu \gamma^\mu + m}{2m} \tag{6.11}$$

and with that finally we have

$$\begin{aligned} L_{\mu\nu} &= \frac{1}{4m_1 m_3}\left\{2tr\left[\hat{k}_i\gamma_\mu\hat{k}_f\gamma_\nu\right] - 2tr\left[\gamma_5\hat{k}_f\gamma_\nu\hat{k}_i\gamma_\mu\right]\right\} \\ &= \frac{2}{m_1 m_3}\left\{k_{i\mu}k_{f\nu} + k_{f\mu}k_{i\nu} - k_i k_f g_{\mu\nu} - i\epsilon_{\alpha\nu\beta\mu}k_f^\alpha k_i^\beta\right\} \end{aligned} \tag{6.12}$$

Analogues calculation can be done for the hadrons tensor $W^{\mu\nu}$ and we have

$$W^{\mu\nu} = \sum_{S_i,S_f} J*^\mu J^\nu \tag{6.13}$$

$$= \frac{1}{4M_2M_4}tr\left[(\hat{p}_i + M_2)(V\gamma^\mu - A\gamma^\mu\gamma_5)(\hat{p}_f + M_4)(V\gamma^\nu - A\gamma^\nu\gamma_5)\right] \tag{6.14}$$

$$= \frac{1}{4M_2M_4}\left\{(V^2+A^2)tr\left[\hat{p}_i\gamma^\mu\hat{p}_f\gamma^\nu\right] - 2VAtr\left[\gamma_5\hat{p}_f\gamma^\nu\hat{p}_i\gamma^\mu\right] + (V^2-A^2)M_2M_4ta\left[\gamma^\mu\gamma^\nu\right]\right\} \tag{6.15}$$

$$= \frac{1}{M_2M_4}\left\{(V^2+A^2)(p_i^\mu p_f^\nu + p_f^\mu p_i^\nu - p_i p_f g^{\mu\nu}) + 2iVA\epsilon^{\gamma\delta\mu\nu}p_{i\gamma}p_{f\delta} + (V^2-A^2)M_2M_4 g^{\mu\nu}\right\} \tag{6.16}$$

If we now combine these two result, and use the property of Levi-Civita tensor $\epsilon_{\alpha\beta\mu\nu}\epsilon^{\gamma\delta\mu\nu} = -2(g_\alpha^\gamma g_\beta^\delta - g_\alpha^\delta g_\beta^\gamma)$ we get

$$\begin{aligned} L_{\mu\nu}W^{\mu\nu} &= \frac{4}{m_1m_3M_2M_4}\left\{V^2(k_i\cdot p_i k_f\cdot p_f + k_i\cdot p_f k_f\cdot p_i - M_2M_4 k_i\cdot k_f)\right. \\ &\quad +A^2(k_i\cdot p_i k_f\cdot p_f + k_i\cdot p_f k_f\cdot p_i + M_2M_4 k_i\cdot k_f) \\ &\quad \left.+2VA(k_i\cdot p_i k_f\cdot p_f - k_i\cdot p_f k_f\cdot p_i)\right\} \end{aligned} \tag{6.17}$$

Our approximations mentioned in section 2.2, which give us

$$k_i\cdot k_f = \epsilon_i\epsilon_f(1-\cos\theta) \tag{6.18}$$

So we can with this expression and by using the other approximations from the section 2.2 simplify our result so we have

$$L_{\mu\nu}W^{\mu\nu} = \frac{4}{m_1m_3M_2M_4}\left\{V^2\epsilon_i\epsilon_f M_2M_4(1+\cos\theta) + A^2\epsilon_i\epsilon_f M_2M_4(3-\cos\theta)\right\} \tag{6.19}$$

And at the end we finally calculate our squared matrix element as

$$\sum_{s_i,s_f,S_i,S_f}|\mathcal{M}_{fi}|^2 = \frac{2G_F^2}{m_1m_3M_2M_4}\left\{V^2\epsilon_i\epsilon_f M_2M_4(1+\cos\theta) + A^2\epsilon_i\epsilon_f M_2M_4(3-\cos\theta)\right\} \tag{6.20}$$

Appendix B

Here we perform the Hartree-Fock calculation on the two particle states.

$$|\Psi_1\Psi_2\rangle = \left[|k_1\rangle \otimes \left|\frac{1}{2}, m_{s_1}\right\rangle \otimes \left|\frac{1}{2}, m_{t_1}\right\rangle\right] \otimes \left[|k_2\rangle \otimes \left|\frac{1}{2}, m_{s_2}\right\rangle \otimes \left|\frac{1}{2}, m_{t_2}\right\rangle\right] \tag{6.21}$$

So we have, as usual, the direct and the exchange term

$$\langle V(q)\rangle = \frac{1}{2}\sum_{k_1,m_{s_1},m_{t_1}}\sum_{k_2,m_{s_2},m_{t_2}} \left(\langle\Psi_2\Psi_1|\, v\,|\Psi_2\Psi_1\rangle - \langle\Psi_1\Psi_2|\, v\,|\Psi_2\Psi_1\rangle\right) \tag{6.22}$$

Where the potential $V(q)$ has the form

$$V(q) = const. \times O_\sigma O_\tau \frac{m^2}{q^2+m^2} \tag{6.23}$$

where the momentum transfer is defined as $\vec{q} = \vec{k}_2 - \vec{k}_1$. We now procede to the calculation of the expectation values for the various spin and isospin operators which appear in our potential as defined by eq (3.3,3.4,3.5)

First the direct case

$$\begin{aligned}
\left[\left\langle\frac{1}{2},\frac{1}{2}\right| \otimes \left\langle\frac{1}{2},\frac{1}{2}\right|\right] \mathbb{I}\otimes\mathbb{I} \left[\left|\frac{1}{2},\frac{1}{2}\right\rangle \otimes \left|\frac{1}{2},\frac{1}{2}\right\rangle\right] &= 1\\
\left[\left\langle\frac{1}{2},-\frac{1}{2}\right| \otimes \left\langle\frac{1}{2},-\frac{1}{2}\right|\right] \mathbb{I}\otimes\mathbb{I} \left[\left|\frac{1}{2},-\frac{1}{2}\right\rangle \otimes \left|\frac{1}{2},-\frac{1}{2}\right\rangle\right] &= 1\\
\left[\left\langle\frac{1}{2},\frac{1}{2}\right| \otimes \left\langle\frac{1}{2},-\frac{1}{2}\right|\right] \mathbb{I}\otimes\mathbb{I} \left[\left|\frac{1}{2},\frac{1}{2}\right\rangle \otimes \left|\frac{1}{2},-\frac{1}{2}\right\rangle\right] &= 1\\
\left[\left\langle\frac{1}{2},-\frac{1}{2}\right| \otimes \left\langle\frac{1}{2},\frac{1}{2}\right|\right] \mathbb{I}\otimes\mathbb{I} \left[\left|\frac{1}{2},-\frac{1}{2}\right\rangle \otimes \left|\frac{1}{2},\frac{1}{2}\right\rangle\right] &= 1
\end{aligned} \tag{6.24}$$

$$\begin{aligned}
\left[\left\langle\frac{1}{2},\frac{1}{2}\right| \otimes \left\langle\frac{1}{2},\frac{1}{2}\right|\right] \vec{\sigma}_1\otimes\vec{\sigma}_2 \left[\left|\frac{1}{2},\frac{1}{2}\right\rangle \otimes \left|\frac{1}{2},\frac{1}{2}\right\rangle\right] &= \left[\left\langle\frac{1}{2},\frac{1}{2}\right| \otimes \left\langle\frac{1}{2},\frac{1}{2}\right|\right] \vec{\tau_1}\otimes\vec{\tau_2} \left[\left|\frac{1}{2},\frac{1}{2}\right\rangle \otimes \left|\frac{1}{2},\frac{1}{2}\right\rangle\right] = 1\\
\left[\left\langle\frac{1}{2},-\frac{1}{2}\right| \otimes \left\langle\frac{1}{2},-\frac{1}{2}\right|\right] \vec{\sigma}_1\otimes\vec{\sigma}_2 \left[\left|\frac{1}{2},-\frac{1}{2}\right\rangle \otimes \left|\frac{1}{2},-\frac{1}{2}\right\rangle\right] &= \left[\left\langle\frac{1}{2},-\frac{1}{2}\right| \otimes \left\langle\frac{1}{2},-\frac{1}{2}\right|\right] \vec{\tau_1}\otimes\vec{\tau_2} \left[\left|\frac{1}{2},-\frac{1}{2}\right\rangle \otimes \left|\frac{1}{2},-\frac{1}{2}\right\rangle\right] = 1\\
\left[\left\langle\frac{1}{2},\frac{1}{2}\right| \otimes \left\langle\frac{1}{2},-\frac{1}{2}\right|\right] \vec{\sigma}_1\otimes\vec{\sigma}_2 \left[\left|\frac{1}{2},\frac{1}{2}\right\rangle \otimes \left|\frac{1}{2},-\frac{1}{2}\right\rangle\right] &= \left[\left\langle\frac{1}{2},\frac{1}{2}\right| \otimes \left\langle\frac{1}{2},-\frac{1}{2}\right|\right] \vec{\tau_1}\otimes\vec{\tau_2} \left[\left|\frac{1}{2},\frac{1}{2}\right\rangle \otimes \left|\frac{1}{2},-\frac{1}{2}\right\rangle\right] = -1\\
\left[\left\langle\frac{1}{2},-\frac{1}{2}\right| \otimes \left\langle\frac{1}{2},\frac{1}{2}\right|\right] \vec{\sigma}_1\otimes\vec{\sigma}_2 \left[\left|\frac{1}{2},-\frac{1}{2}\right\rangle \otimes \left|\frac{1}{2},\frac{1}{2}\right\rangle\right] &= \left[\left\langle\frac{1}{2},-\frac{1}{2}\right| \otimes \left\langle\frac{1}{2},\frac{1}{2}\right|\right] \vec{\tau_1}\otimes\vec{\tau_2} \left[\left|\frac{1}{2},-\frac{1}{2}\right\rangle \otimes \left|\frac{1}{2},\frac{1}{2}\right\rangle\right] = -1
\end{aligned} \tag{6.25}$$

And then the exchange part

$$
\begin{aligned}
\left[\left\langle\frac{1}{2},\frac{1}{2}\right|\otimes\left\langle\frac{1}{2},\frac{1}{2}\right|\right]\mathbb{I}\otimes\mathbb{I}\left[\left|\frac{1}{2},\frac{1}{2}\right\rangle\otimes\left|\frac{1}{2},\frac{1}{2}\right\rangle\right]&=1\\
\left[\left\langle\frac{1}{2},-\frac{1}{2}\right|\otimes\left\langle\frac{1}{2},-\frac{1}{2}\right|\right]\mathbb{I}\otimes\mathbb{I}\left[\left|\frac{1}{2},-\frac{1}{2}\right\rangle\otimes\left|\frac{1}{2},-\frac{1}{2}\right\rangle\right]&=1\\
\left[\left\langle\frac{1}{2},\frac{1}{2}\right|\otimes\left\langle\frac{1}{2},-\frac{1}{2}\right|\right]\mathbb{I}\otimes\mathbb{I}\left[\left|\frac{1}{2},-\frac{1}{2}\right\rangle\otimes\left|\frac{1}{2},\frac{1}{2}\right\rangle\right]&=0\\
\left[\left\langle\frac{1}{2},-\frac{1}{2}\right|\otimes\left\langle\frac{1}{2},\frac{1}{2}\right|\right]\mathbb{I}\otimes\mathbb{I}\left[\left|\frac{1}{2},\frac{1}{2}\right\rangle\otimes\left|\frac{1}{2},-\frac{1}{2}\right\rangle\right]&=0
\end{aligned}
\tag{6.26}
$$

$$
\begin{aligned}
\left[\left\langle\frac{1}{2},\frac{1}{2}\right|\otimes\left\langle\frac{1}{2},\frac{1}{2}\right|\right]\vec{\sigma}_1\otimes\vec{\sigma}_2\left[\left|\frac{1}{2},\frac{1}{2}\right\rangle\otimes\left|\frac{1}{2},\frac{1}{2}\right\rangle\right]=\left[\left\langle\frac{1}{2},\frac{1}{2}\right|\otimes\left\langle\frac{1}{2},\frac{1}{2}\right|\right]\vec{\tau_1}\otimes\vec{\tau_2}\left[\left|\frac{1}{2},\frac{1}{2}\right\rangle\otimes\left|\frac{1}{2},\frac{1}{2}\right\rangle\right]&=1\\
\left[\left\langle\frac{1}{2},-\frac{1}{2}\right|\otimes\left\langle\frac{1}{2},-\frac{1}{2}\right|\right]\vec{\sigma}_1\otimes\vec{\sigma}_2\left[\left|\frac{1}{2},-\frac{1}{2}\right\rangle\otimes\left|\frac{1}{2},-\frac{1}{2}\right\rangle\right]=\left[\left\langle\frac{1}{2},-\frac{1}{2}\right|\otimes\left\langle\frac{1}{2},-\frac{1}{2}\right|\right]\vec{\tau_1}\otimes\vec{\tau_2}\left[\left|\frac{1}{2},-\frac{1}{2}\right\rangle\otimes\left|\frac{1}{2},-\frac{1}{2}\right\rangle\right]&=1\\
\left[\left\langle\frac{1}{2},\frac{1}{2}\right|\otimes\left\langle\frac{1}{2},-\frac{1}{2}\right|\right]\vec{\sigma}_1\otimes\vec{\sigma}_2\left[\left|\frac{1}{2},-\frac{1}{2}\right\rangle\otimes\left|\frac{1}{2},\frac{1}{2}\right\rangle\right]=\left[\left\langle\frac{1}{2},\frac{1}{2}\right|\otimes\left\langle\frac{1}{2},-\frac{1}{2}\right|\right]\vec{\tau_1}\otimes\vec{\tau_2}\left[\left|\frac{1}{2},-\frac{1}{2}\right\rangle\otimes\left|\frac{1}{2},\frac{1}{2}\right\rangle\right]&=2\\
\left[\left\langle\frac{1}{2},-\frac{1}{2}\right|\otimes\left\langle\frac{1}{2},\frac{1}{2}\right|\right]\vec{\sigma}_1\otimes\vec{\sigma}_2\left[\left|\frac{1}{2},\frac{1}{2}\right\rangle\otimes\left|\frac{1}{2},-\frac{1}{2}\right\rangle\right]=\left[\left\langle\frac{1}{2},-\frac{1}{2}\right|\otimes\left\langle\frac{1}{2},\frac{1}{2}\right|\right]\vec{\tau_1}\otimes\vec{\tau_2}\left[\left|\frac{1}{2},\frac{1}{2}\right\rangle\otimes\left|\frac{1}{2},-\frac{1}{2}\right\rangle\right]&=2
\end{aligned}
\tag{6.27}
$$

We now combine these result together with the momentum part (we will not write out the constant value in front because it is always there) to get. For the direct part

$$
\begin{aligned}
&\frac{1}{2}\sum_{k_1,m_{s_1},m_{t_1}}\sum_{k_2,m_{s_2},m_{t_2}}\langle\Psi_2\Psi_1|\,\mathbb{I}_\sigma\otimes\mathbb{I}_\sigma\mathbb{I}_\tau\otimes\mathbb{I}_\tau\frac{m^2}{q^2+m^2}\,|\Psi_2\Psi_1\rangle=\\
&\frac{1}{2}\Bigg[\sum_{k_1,k_2}^{k_{F_{p\uparrow}},k_{F_{p\uparrow}}}1+2\sum_{k_1,k_2}^{k_{F_{p\uparrow}},k_{F_{p\downarrow}}}1+\sum_{k_1,k_2}^{k_{F_{p\downarrow}},k_{F_{p\downarrow}}}1+\sum_{k_1,k_2}^{k_{F_{n\uparrow}},k_{F_{n\uparrow}}}1+2\sum_{k_1,k_2}^{k_{F_{n\uparrow}},k_{F_{n\downarrow}}}1+\sum_{k_1,k_2}^{k_{F_{n\downarrow}},k_{F_{n\downarrow}}}1+\\
&2\sum_{k_1,k_2}^{k_{F_{p\uparrow}},k_{F_{n\uparrow}}}1+2\sum_{k_1,k_2}^{k_{F_{p\downarrow}},k_{F_{n\downarrow}}}1+2\sum_{k_1,k_2}^{k_{F_{p\uparrow}},k_{F_{n\downarrow}}}1+2\sum_{k_1,k_2}^{k_{F_{p\downarrow}},k_{F_{n\uparrow}}}1\Bigg]
\end{aligned}
\tag{6.28}
$$

$$
\begin{aligned}
&\frac{1}{2}\sum_{k_1,m_{s_1},m_{t_1}}\sum_{k_2,m_{s_2},m_{t_2}}\langle\Psi_2\Psi_1|\,\vec{\sigma}_1\otimes\vec{\sigma}_2\mathbb{I}_\tau\otimes\mathbb{I}_\tau\frac{m^2}{q^2+m^2}\,|\Psi_2\Psi_1\rangle=\\
&\frac{1}{2}\Bigg[\sum_{k_1,k_2}^{k_{F_{p\uparrow}},k_{F_{p\uparrow}}}1-2\sum_{k_1,k_2}^{k_{F_{p\uparrow}},k_{F_{p\downarrow}}}1+\sum_{k_1,k_2}^{k_{F_{p\downarrow}},k_{F_{p\downarrow}}}1+\sum_{k_1,k_2}^{k_{F_{n\uparrow}},k_{F_{n\uparrow}}}1-2\sum_{k_1,k_2}^{k_{F_{n\uparrow}},k_{F_{n\downarrow}}}1+\sum_{k_1,k_2}^{k_{F_{n\downarrow}},k_{F_{n\downarrow}}}1+\\
&2\sum_{k_1,k_2}^{k_{F_{p\uparrow}},k_{F_{n\uparrow}}}1+2\sum_{k_1,k_2}^{k_{F_{p\downarrow}},k_{F_{n\downarrow}}}1-2\sum_{k_1,k_2}^{k_{F_{p\uparrow}},k_{F_{n\downarrow}}}1-2\sum_{k_1,k_2}^{k_{F_{p\downarrow}},k_{F_{n\uparrow}}}1\Bigg]
\end{aligned}
\tag{6.29}
$$

$$\frac{1}{2}\sum_{k_1,m_{s_1},m_{t_1}}\sum_{k_2,m_{s_2},m_{t_2}}\langle\Psi_2\Psi_1|\,\mathbb{I}_\sigma\otimes\mathbb{I}_\sigma\vec{\tau}_1\otimes\vec{\tau}_2\frac{m^2}{q^2+m^2}\,|\Psi_2\Psi_1\rangle =$$

$$\frac{1}{2}\left[\sum_{k_1,k_2}^{k_{F_{p\uparrow}},k_{F_{p\uparrow}}}1+2\sum_{k_1,k_2}^{k_{F_{p\uparrow}},k_{F_{p\downarrow}}}1+\sum_{k_1,k_2}^{k_{F_{p\downarrow}},k_{F_{p\downarrow}}}1+\sum_{k_1,k_2}^{k_{F_{n\uparrow}},k_{F_{n\uparrow}}}1+2\sum_{k_1,k_2}^{k_{F_{n\uparrow}},k_{F_{n\downarrow}}}1+\sum_{k_1,k_2}^{k_{F_{n\downarrow}},k_{F_{n\downarrow}}}1-\right.$$
$$\left.2\sum_{k_1,k_2}^{k_{F_{p\uparrow}},k_{F_{n\uparrow}}}1-2\sum_{k_1,k_2}^{k_{F_{p\downarrow}},k_{F_{n\downarrow}}}1-2\sum_{k_1,k_2}^{k_{F_{p\uparrow}},k_{F_{n\downarrow}}}1-2\sum_{k_1,k_2}^{k_{F_{p\downarrow}},k_{F_{n\uparrow}}}1\right] \tag{6.30}$$

$$\frac{1}{2}\sum_{k_1,m_{s_1},m_{t_1}}\sum_{k_2,m_{s_2},m_{t_2}}\langle\Psi_2\Psi_1|\,\vec{\sigma}_1\otimes\vec{\sigma}_2\;\vec{\tau}_1\otimes\vec{\tau}_2\frac{m^2}{q^2+m^2}\,|\Psi_2\Psi_1\rangle =$$

$$\frac{1}{2}\left[\sum_{k_1,k_2}^{k_{F_{p\uparrow}},k_{F_{p\uparrow}}}1-2\sum_{k_1,k_2}^{k_{F_{p\uparrow}},k_{F_{p\downarrow}}}1+\sum_{k_1,k_2}^{k_{F_{p\downarrow}},k_{F_{p\downarrow}}}1+\sum_{k_1,k_2}^{k_{F_{n\uparrow}},k_{F_{n\uparrow}}}1-2\sum_{k_1,k_2}^{k_{F_{n\uparrow}},k_{F_{n\downarrow}}}1+\sum_{k_1,k_2}^{k_{F_{n\downarrow}},k_{F_{n\downarrow}}}1-\right.$$
$$\left.2\sum_{k_1,k_2}^{k_{F_{p\uparrow}},k_{F_{n\uparrow}}}1-2\sum_{k_1,k_2}^{k_{F_{p\downarrow}},k_{F_{n\downarrow}}}1+2\sum_{k_1,k_2}^{k_{F_{p\uparrow}},k_{F_{n\downarrow}}}1+2\sum_{k_1,k_2}^{k_{F_{p\downarrow}},k_{F_{n\uparrow}}}1\right] \tag{6.31}$$

And for the exchange part:

$$-\frac{1}{2}\sum_{k_1,m_{s_1},m_{t_1}}\sum_{k_2,m_{s_2},m_{t_2}}\langle\Psi_1\Psi_2|\,\mathbb{I}_\sigma\otimes\mathbb{I}_\sigma\mathbb{I}_\tau\otimes\mathbb{I}_\tau\frac{m^2}{q^2+m^2}\,|\Psi_2\Psi_1\rangle =$$

$$-\frac{1}{2}\left[\sum_{k_1,k_2}^{k_{F_{p\uparrow}},k_{F_{p\uparrow}}}\frac{m^2}{q^2+m^2}+\sum_{k_1,k_2}^{k_{F_{p\downarrow}},k_{F_{p\downarrow}}}\frac{m^2}{q^2+m^2}+\sum_{k_1,k_2}^{k_{F_{n\uparrow}},k_{F_{n\uparrow}}}\frac{m^2}{q^2+m^2}+\sum_{k_1,k_2}^{k_{F_{n\downarrow}},k_{F_{n\downarrow}}}\frac{m^2}{q^2+m^2}\right] \tag{6.32}$$

$$-\frac{1}{2}\sum_{k_1,m_{s_1},m_{t_1}}\sum_{k_2,m_{s_2},m_{t_2}}\langle\Psi_1\Psi_2|\,\vec{\sigma}_1\otimes\vec{\sigma}_2\mathbb{I}_\tau\otimes\mathbb{I}_\tau\frac{m^2}{q^2+m^2}\,|\Psi_2\Psi_1\rangle =$$

$$-\frac{1}{2}\left[\sum_{k_1,k_2}^{k_{F_{p\uparrow}},k_{F_{p\uparrow}}}\frac{m^2}{q^2+m^2}+4\sum_{k_1,k_2}^{k_{F_{p\uparrow}},k_{F_{p\downarrow}}}\frac{m^2}{q^2+m^2}+\sum_{k_1,k_2}^{k_{F_{p\downarrow}},k_{F_{p\downarrow}}}\frac{m^2}{q^2+m^2}+\sum_{k_1,k_2}^{k_{F_{n\uparrow}},k_{F_{n\uparrow}}}\frac{m^2}{q^2+m^2}+4\sum_{k_1,k_2}^{k_{F_{n\uparrow}},k_{F_{n\downarrow}}}\frac{m^2}{q^2+m^2}+\right.$$
$$\left.\sum_{k_1,k_2}^{k_{F_{n\downarrow}},k_{F_{n\downarrow}}}\frac{m^2}{q^2+m^2}\right] \tag{6.33}$$

$$-\frac{1}{2}\sum_{k_1,m_{s_1},m_{t_1}}\sum_{k_2,m_{s_2},m_{t_2}}\langle\Psi_1\Psi_2|\,\mathbb{I}_\sigma\otimes\mathbb{I}_\sigma\vec{\tau}_1\otimes\vec{\tau}_2\frac{m^2}{q^2+m^2}\,|\Psi_2\Psi_1\rangle =$$

$$-\frac{1}{2}\left[\sum_{k_1,k_2}^{k_{F_{p\uparrow}},k_{F_{p\uparrow}}}\frac{m^2}{q^2+m^2}+\sum_{k_1,k_2}^{k_{F_{p\downarrow}},k_{F_{p\downarrow}}}\frac{m^2}{q^2+m^2}+\sum_{k_1,k_2}^{k_{F_{n\uparrow}},k_{F_{n\uparrow}}}\frac{m^2}{q^2+m^2}+\sum_{k_1,k_2}^{k_{F_{n\downarrow}},k_{F_{n\downarrow}}}\frac{m^2}{q^2+m^2}+\right.$$
$$\left.4\sum_{k_1,k_2}^{k_{F_{p\uparrow}},k_{F_{n\uparrow}}}\frac{m^2}{q^2+m^2}+4\sum_{k_1,k_2}^{k_{F_{p\downarrow}},k_{F_{n\downarrow}}}\frac{m^2}{q^2+m^2}\right] \tag{6.34}$$

$$
-\frac{1}{2}\sum_{k_1,m_{s_1},m_{t_1}}\ \sum_{k_2,m_{s_2},m_{t_2}}\langle\Psi_1\Psi_2|\,\vec{\sigma}_1\otimes\vec{\sigma}_2\vec{\tau}_1\otimes\vec{\tau}_2\frac{m^2}{q^2+m^2}\,|\Psi_2\Psi_1\rangle =
$$

$$
-\frac{1}{2}\left[\sum_{k_1,k_2}^{k_{F_{p\uparrow}},k_{F_{p\uparrow}}}\frac{m^2}{q^2+m^2}+4\sum_{k_1,k_2}^{k_{F_{p\uparrow}},k_{F_{p\downarrow}}}\frac{m^2}{q^2+m^2}+\sum_{k_1,k_2}^{k_{F_{p\downarrow}},k_{F_{p\downarrow}}}\frac{m^2}{q^2+m^2}+\sum_{k_1,k_2}^{k_{F_{n\uparrow}},k_{F_{n\uparrow}}}\frac{m^2}{q^2+m^2}+4\sum_{k_1,k_2}^{k_{F_{n\uparrow}},k_{F_{n\downarrow}}}\frac{m^2}{q^2+m^2}+\right.
$$

$$
\left.\sum_{k_1,k_2}^{k_{F_{n\downarrow}},k_{F_{n\downarrow}}}\frac{m^2}{q^2+m^2}+4\sum_{k_1,k_2}^{k_{F_{p\uparrow}},k_{F_{n\uparrow}}}\frac{m^2}{q^2+m^2}+4\sum_{k_1,k_2}^{k_{F_{p\downarrow}},k_{F_{n\downarrow}}}\frac{m^2}{q^2+m^2}+8\sum_{k_1,k_2}^{k_{F_{p\uparrow}},k_{F_{n\downarrow}}}\frac{m^2}{q^2+m^2}+8\sum_{k_1,k_2}^{k_{F_{p\downarrow}},k_{F_{n\uparrow}}}\frac{m^2}{q^2+m^2}\right] \tag{6.35}
$$

where

$$
\begin{aligned}
k_{F_1} &= (6\pi^2\rho_1)^{\frac{1}{3}} && (6.36)\\
k_{F_2} &= (6\pi^2\rho_2)^{\frac{1}{3}} && (6.37)
\end{aligned}
$$

In order to complete the calculation we need to evaluate the sums in the previous expressions.

$$
\begin{aligned}
\sum_{k_1,k_2}^{k_{F_1},k_{F_2}} 1 &= \frac{1}{(2\pi)^6}\frac{4}{9}\pi^2 k_{F_1}^3 k_{F_2}^3 = \rho_1\rho_2 && (6.38)\\
\sum_{k_1,k_2}^{k_{F_1},k_{F_2}}\frac{m^2}{q^2+m^2} &= \frac{m^2}{8\pi^4}\frac{1}{48}\left\{\left(m^4+6m^2(k_{F_2}^2+k_{F_1}^2)-3(k_{F_2}^2-k_{F_1}^2)^2\right) log\left(\frac{m^2+(k_{F_2}+k_{F_1})^2}{m^2+(k_{F_2}-k_{F_1})^2}\right)\right.\\
&- 16m\left[atan\left(\frac{k_{F_1}-k_{F_2}}{m}\right)(k_{F_2}^3-k_{F_1}^3)+atan\left(\frac{k_{F_2}+k_{F_1}}{m}\right)(k_{F_2}^3+k_{F_1}^3)\right]\\
&- \left.4k_{F_2}k_{F_1}(m^2-3k_{F_2}^2-3k_{F_1}^2)\right\} && (6.39)
\end{aligned}
$$

Appendix C

If we start from the definition of polarisation function (2.37), here we have used somewhat different notation to be in agreement with our reference, but the transition is quite obvious,

$$\Pi^0(q_0, q) \quad = \quad \frac{2}{(2\pi)^3} \int d^3p \left[\frac{f(E_p)\left[1 - f(E_{|\vec{p}+\vec{q}|})\right]}{q_0 + E_p - E_{|\vec{p}+\vec{q}|} + i\epsilon} - \frac{\left[1 - f(E_p)\right] f(E_{|\vec{p}+\vec{q}|})}{q_0 + E_p - E_{|\vec{p}+\vec{q}|} - i\epsilon} \right] \tag{6.40}$$

And calculate the imaginary part of the polarisation function

$$Im\ \Pi^0(q_0, q) = -\frac{2\pi}{(2\pi)^3} \int d^3p \delta(q_0 + E_p - E_{|\vec{p}+\vec{q}|}) \left[f(E_p) - f(E_{|\vec{p}+\vec{q}|}\right]. \tag{6.41}$$

We can rewrite the difference between the nucleon distribution functions as

$$\begin{aligned} f(E_p) - f(E_{|\vec{p}+\vec{q}|}) = & \frac{1}{\exp\left((E_p - \mu_p)/T\right) + 1} - \frac{1}{\exp\left((E_{|\vec{p}+\vec{q}|} - \mu_{|\vec{p}+\vec{q}|})/T\right) + 1} \\ & = \left(1 - \exp\left(E_p - E_{|\vec{p}+\vec{q}|} + \mu_{|\vec{p}+\vec{q}|} - \mu_p\right)/T\right)\right) \\ & \frac{1}{\exp\left((E_p - \mu_p)/T\right) + 1} \left(1 - \frac{1}{\exp\left((E_{|\vec{p}+\vec{q}|} - \mu_{|\vec{p}+\vec{q}|})/T\right) + 1}\right) \\ = & \left(1 - \exp\left(E_p - E_{|\vec{p}+\vec{q}|} + \mu_{|\vec{p}+\vec{q}|} - \mu_p\right)/T\right)\right) f(E_p) \left(1 - f(E_{|\vec{p}+\vec{q}|}\right) \end{aligned} \tag{6.42}$$

So we write the imaginary pert of the polarisation function in a more convenient form for comparison with the response function

$$\begin{aligned} Im\ \Pi^0(q_0, q) = & -\frac{1}{4\pi^2} \left(1 - \exp -(q_0 + \mu_p - \mu_{|\vec{p}+\vec{q}|})/T)\right) \\ & \int d^3p \delta(q_0 + E_p - E_{|\vec{p}+\vec{q}|}) f(E_p) \left(1 - f(E_{|\vec{p}+\vec{q}|}\right) \end{aligned} \tag{6.43}$$

To remind our self we rewrite the response function from equation (2.35) as:

$$S(q_0, q) = \frac{1}{2\pi^2} \int d^3p \delta(q_0 + E_p - E_{|\vec{p}+\vec{q}|}) \left(1 - f(E_{|\vec{p}+\vec{q}|}\right) \tag{6.44}$$

If we compare these two equation we can easily get the connection between them as

$$Im\ \Pi^0(q_0, \vec{q}) = -\frac{1}{2} \left(1 - \exp\left(-(q_0 + \mu_p - \mu_{|\vec{p}+\vec{q}|})/T\right)\right) S(q_0, \vec{q}) \tag{6.45}$$

Bibliography

[1] M. Prakash, et. al., Phys. Rep. **280**, (1997),1.

[2] F.Cei, hep-ex/0202043

[3] K.Langake, GMartinez-Pinedo,nucl-th/0203071

[4] S.Raddy, J.M. Prakash, J. M. Lattimer, Phys. Rev. **D58**, (1998), 013009.

[5] N. Radde, *Neutrino Transport in Proto-Neutronen Sternen*, Diplomarbait (1996) TUD, Darmstadt

[6] G.W. Carter, M. Prakash, Phys. Lett. **525B**, (2002), 249ff

[7] F. Mandl, G. Shaw, *Quantum Field Theory*, (A Wiley-Interscience Publication, New York,1993)

[8] S.Raddy, J.M. Prakash, J. M. Lattimer, J.A. Pons, Phys. Rev. **C59**, (1999), 2888ff.

[9] H. Nakada, nucl-th/0304021

[10] G.F. Bertsch and I. Hammamoto, Phys. Rev. **C26**, (1982), 1323

[11] K. Nakayama, W.G. Love, Phys. Rev. **C38**, (1988), 51

[12] A. Akmal, V. R. Pandharipand, D.G. Ravenhall, Phys. Rev. **C58**, (1998), 1804.

[13] S. L. Schapiro, S. A. Teukolsky, *Black Holes, White Dwarfs, and Neutron Stars: The Phyisics of Compact Objects*, (Wiley, New York, 1983)

[14] N. K. Glendenning, *Compact Stars*, (Springer, New York, 1997)

[15] O. Sjöberg, Nucl. Phys. **A265** (1976) 511

[16] M. Bender, J. Dobaczewski, J. Engel, W. Nazarewicz, nucl-th/0112056

[17] A.B. Migdal, *Theory of Finite Fermi Systems and Application to Atomic Nuclei*, (Interscience, New York, 1962)

[18] A.L. Fetter, J.D. Walecka, *Quantum Theory of Many Particle Systems*, (McGraw-Hill, New York,1971)

[19] A. Burows, T.A. Thompson, astro-ph/0211404

[20] E.N.E. van Dalen, at al., nucl-th/0303037